Preforming Process for Out-of-Autoclave Composite Manufacturing

Louis GROU
Department of Mechanical Engineering
McGill University, Montreal

June 2019

A thesis submitted to McGill University in partial fulfillment of the requirements of the degree of Master of Engineering

Abstract

The aerospace industry is continuously looking for economical alternative to the expensive state-of-the art autoclave manufacturing process. Recent development in Out-of-Autoclave (OOA) processes like Liquid Composite Moulding (LCM) have made it more than ever a serious candidate to fill that task. However, manipulation of dry fabric reinforcement is challenging and may lead to manufacturing inefficiencies and defect generations. These issues are handled in other composite industries, like automotive for instance, by including preforming techniques in the manufacturing process. The goal of the present work is to develop, optimize and evaluate, while respecting the standards of the aerospace industry, a tailored preforming technique for dry fabric reinforcement using polymeric binders.

First the thermochemical characterization of four binder materials with different chemical composition is performed to determine the appropriate application and preforming process parameters adapted to each chemistry. Next, the resin-binder interactions are investigated through various thermo-mechanical characterization mostly to ensure compatibility between the composite polymer matrix and the four different binders. The binder miscibility behaviour in epoxy resin is evaluated by modulated differential scanning calorimetry (MDSC), rheology and microscopy experiments. The thermo-mechanical influence of the binders is studied through dynamic mechanical analysis (DMA) and mechanical tensile test performed on resin-binder mixtures. The results reveal that the resin-binder interactions are highly different for each binder chemistry. The impact of different preforms configuration on the mechanical properties of a reinforced composite laminate is demonstrated through the characterization of the short-beam interlaminar shear strength. Furthermore, permeability characterization (in-plane and out-of-plane) is performed to analyze the impact of several preforming techniques on the mould filling process.

The potential influence of the preforming parameters on the liquid resin injection process and resulting mechanical performance of the manufactured reinforced composite laminate are revealed by this methodology. Hence, the outcomes of this whole experimental characterization process provide practical guidelines for the development, optimization and evaluation processes of a preforming process using a tailored binder application.

Sommaire

L’industrie aérospatiale est constamment à la recherche d’alternatives économiques aux coûteux procédés fabrication en autoclave traditionnellement utilisés. Les récentes avancées technologiques des procédés hors autoclave, mais particulièrement ceux au niveau des procédés de moulage par injection de résine liquide, font désormais d’eux de sérieux candidats pour remplir ce rôle. Cependant, la manipulation des renforts textiles secs représente des défis techniques considérables pouvant entre autres réduire l‘efficacité du procédé manufacturier et causer la génération de défauts de fabrication. Ce problème est généralement pris en charge en incluant une étape de préformage dans le procédé de fabrication. L’objectif du travail présenté dans ce mémoire est de développer, d’optimiser et d’évaluer, tout en respectant respect les normes de l’industrie aérospatiale, une technique de préformage sur mesure des renforts textiles secs à l’aide de liants polymériques.

Tout d'abord, la caractérisation thermochimique de quatre liants de composition chimique différente est effectuée dans le but de déterminer les paramètres d’application et de préformage adaptés à chaque chimie. Ensuite, les interactions entre une résine époxy et les liants étudiées sont évaluées au moyen de diverses caractérisations thermomécaniques, principalement dans le but d’assurer la compatibilité des matériaux étudiés. Le niveau de miscibilité des liants dans la résine époxy est évalué par des expériences de calorimétrie différentielle à balayage, de rhéologie et de microscopie. L'influence thermomécanique des liants est étudiée par la réalisation d’essais d’analyse mécanique dynamique (AMD) et test de traction mécanique réalisés sur des mélanges de résine-liant. Les résultats révèlent que les interactions résine-liants sont propres à chaque combinaison de matières. L'impact de différentes configurations de préformes sur les propriétés mécaniques d'un stratifié composite renforcé est démontré par la caractérisation de la résistance au cisaillement interlaminaire. De plus, une caractérisation expérimentale des perméabilités dans le plan et hors plan est réalisée à fin analyser l'impact de plusieurs techniques de préformage sur le processus d’injection de résine liquide.

L'influence ainsi que l’étendue potentielle des paramètres de préformage sur le processus d'injection de résine liquide ainsi que sur les performances mécaniques du laminé composite fabriqué sont mises de l’avant par cette méthodologie. Par conséquent, l’ensemble des résultats récoltés grâce à ce processus de caractérisation expérimentale permettent d’établir des

recommandations techniques qui serviront à guider le développement, l'optimisation et l'évaluation du procédé de préformage misant sur l'application locale de liant polymérique.

Acknowledgements

I would like to express my very great appreciation to Professor Pascal Hubert for is assistance, guidance and support throughout this project. It was an honour and a privilege to have him as my supervisor. I'm also very grateful of the opportunity to be a part of the McGill Structures and Composite Material Laboratory.

I would like to thank Martin Lévesque from Hutchinson Aerospace and Industry for providing not only the opportunity to be a part of this project but also access to all the resources needed. His expertise in research and development were highly valuable to the realization of this project but also for my professional experience. I would like to offer my special thanks to Antonin-Leclair-Marechal also from Hutchinson Aerospace and Industry who did tremendous work synchronizing my research project with the other research project going on at Hutchinson. His support throughout this project was always highly appreciated. I would also like to thank everyone else from the Hutchinson R&D team who helped me with my work and made my stay very enjoyable.

I am particularly grateful that I had the chance to work with Linus Lehnert and Derek Harvey and to count them as good friends now. They were always reliable sources for any type of advice and always ready to help when needed.

I would also like to thank all the members of the McGill Structure from which I had the chance to meet very interesting and skilled people. I am particularly grateful for the assistance given by Lucie Riffard and Adam Smith who also provided me very valuable advice for my research. I would also like to acknowledge the help provided by Dr. Cristian Demaria with the transverse permeability experiments.

Finally, I would like to greatly acknowledge the financial support provided by the Consortium for Aerospace Research and Innovation in Canada (CARIC), the Consortium for Research and Innovation in Aerospace in Quebec (CRIAQ), the Research Centre for High Performance Polymer and Composite Systems (CREPEC), and industrial partners such as Hutchinson Aerospace & Industry Ltd.

Table of Contents

List of Tables

Page

List of Figures

Page

1. Introduction

1.1 Background and Motivations

In aerospace industry, it is frequent to see metallic parts or even assemblies redesigned to consider the use of composite materials for weight and cost saving objectives. However, the aerospace industry is continuously looking for more economical alternative to the expensive state-of-the art autoclave manufacturing process. Hutchinson Aerospace & Industry is specialized in the thermoplastic and composite manufacturing of aircraft parts such as air ducting, cockpit panels and aesthetic interior panels. In 2016, Hutchinson has initiated a research project (COMP1601) to develop an out-of-autoclave (OOA) manufacturing process for complex aerospace composite structures. The project targets identified for the structure attributes are presented in Table 1. A schematic of a typical business jet cockpit presented in Figure 1 demonstrates the type of complex geometry considered in this project. This type of component often has specific geometric features such as hollow structures for rigidity, net-shape features for functionality and double curvatures for aestheticism, which all represent manufacturing challenges.

Table 1: Project COMP1601 targets for the structure attributes [1]

Attribute	Unit	Target
Weight	[kg]	-30%
Operation time	[min/in^2]	-30%
Material cost	[$/kg]	-25%
Manufacturing cost	[$/in^2]	-30%
Tooling cost	[$]	-25%
Number of assembled components	[# of assemblies]	-50%
Dimensional tolerance (fit)	[in]	Equivalent or better than reference
Mechanical properties	[MPa]	
Aesthetic and functional integrity (form and function)	[# of visual defaults per part]	

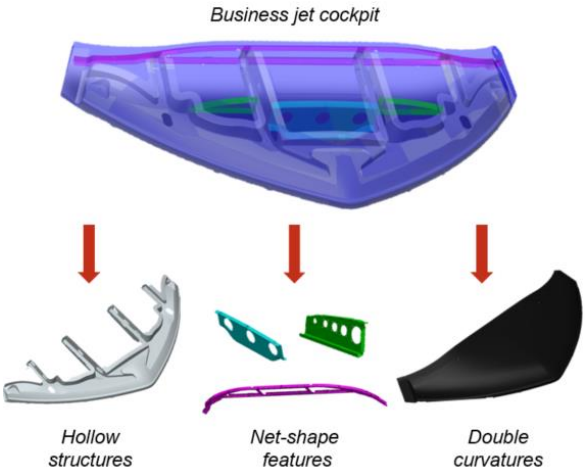

Figure 1: Example of a business jet cockpit complex structure

The process development methodology followed in project COMP1601 was based on the development of specific manufacturing technology also referred as ‘’technological bricks’’. The development of each technological bricks such as resin transfer moulding, hollow cores/inserts manufacturing, smart tooling and preforming process for example, was orientated to overcome

specific technical challenges of manufacturing complex geometries with OOA processes. More specifically, this thesis mostly focuses on the development, optimization and evaluation process of a tailored near-net-shape preforming technique for dry fabric reinforcement.

1.2 Challenges of Dry Fabric Reinforcement Manipulations

Manipulation of dry reinforcement fabric material is still nowadays one of the biggest challenges of OOA composite manufacturing in terms of quality stability and production rate [2, 3]. Even if a lot of efforts are deployed to bring more automatization in this process [4, 5], most of the fabric draping and positioning operations still involve manual labour especially in the context of low volume production. This usually results in a lack of repeatability and productivity [6]. Dry fabric reinforcement can have high drapeability behaviour (ability to conform to complex shapes) which is an advantage when complex geometries are manufactured but can also become an important source of process variations [7, 8]. Defects generated by the draping of the fabric plies such as fibre misalignment, wrinkles[9] or fabric fraying[10] may modify the preform permeability or generate resin flow variations that could lead to failed injection process [3, 11]. Draping defects may also lead to a reduction of the composite mechanical properties [12, 13]. Also, unlike prepreg materials, dry fabric textiles are non-tacky hence they may be difficult to hold in place on previously draped plies or on vertical surfaces. Hence, in order to achieve a certain level of quality, the dry fabric draping operations usually require a lot care and manual skills, thus reducing the production rate and increasing the labour cost.

1.3 Liquid Composite Moulding

The possibility of producing complex geometries, incorporation of moulded-in inserts and the selection of low-cost materials compared to prepreg materials are examples of the numerous advantages of Liquid Composite Moulding (LCM). LCM regroups many variations of closed mould manufacturing process that all comprise on the same key steps [6, 14, 15] (Figure 2). First layers of dry fabric reinforcement are assembled in a preform through a preforming process. Next the preform is laid down in a rigid mould that will provide the shape of the moulded part. Then, a liquid resin is injected in the mould cavity by the application of a pressure gradient and flows through the preform until the cavity is filled. Hence, a second tooling is required to allow the

application of the pressure gradient (ΔP). It can either be second rigid tool or a flexible tooling such as a vacuum bag or rubber membrane.

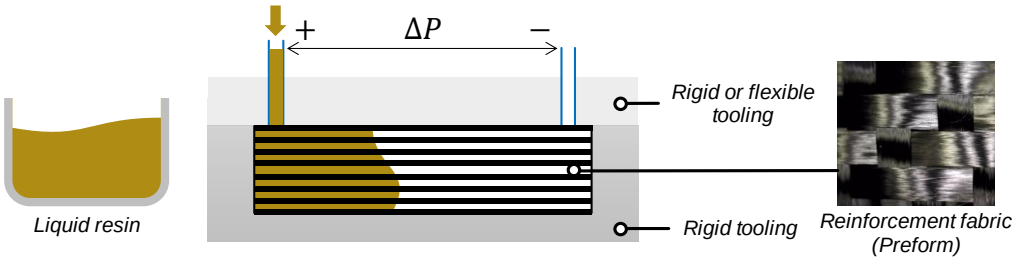

Figure 2: Schematic of the basic principle of LCM processes

The differences among LCM processes are mostly defined by the selection of the injection and tooling strategies. Utilization of positive pressure only, vacuum only or combination of both are the common injection strategies used. Tooling strategies can be divided into two main categories, combination of rigid and flexible tooling or a combination of two rigid tooling (matched mould). A summary of the most common LCM processes and their characteristic is presented in Table 2.

Table 2: Summary of common LCM processes [6, 14, 16].

Acronym(s)	Name	Injection strategy	Tooling strategy	Key Features
RTM	Resin transfer moulding	Positive (low) pressure	Matched mould	-Structural and cosmetic part -High initial investments
VARI	Vacuum assisted resin injection	Positive (low) pressure combined with vacuum	Matched mould	-Same as RTM - Increased pressure gradient
SRIM	Structural reaction injection moulding	Derived RTM process for reactive processing and technique (e.g. polyurethane)	Matched mould	-High capital costs -High throughput
VI, VARTM, RIFT, SCRIMP	Vacuum infusion	Resin flow (through the preform) enabled using a vacuum source	One rigid tool plus a flexible tool	-Elimination of prepregging stage -High consumable cost
RFI	Resin film infusion	Though the thickness impregnation by resin films placed between fabric layers	Matched mould or rigid-flexible tools	-B-stage resins -Low throughput
C-RTM	Compression RTM	Combination of RTM and compression moulding processes	Matched mould	- High capital costs - High throughput

The quality and production rate of the LCM process mostly depend on the outcome of the mould filling operation. The concept of permeability describes the flow behaviour of a liquid (e.g. resin) through a porous media (e.g. preforms) is the starting point of LCM process modelling.

1.3.1 Flow Behaviour Modelling

Darcy's law governs the resin flow during the LCM process. It was first introduce by Darcy's in 1862 in his studies of the underground flow[17].

$$\vec{v} = -\frac{[K]}{\mu} \cdot \Delta P \tag{1.1}$$

where $\vec{v}$ is the fluid superficial velocity (observable flow velocity) flowing through the porous media, $[K]$ is the permeability of the porous media in tensor form, ΔP is the pressure gradient and μ is the dynamic viscosity of the fluid. The fluid superficial velocity is often represented in its unidirectional form.

$$v_x = -\frac{K_x}{\mu} \cdot \left(\frac{\partial p}{\partial x}\right), v_y = -\frac{K_y}{\mu} \cdot \left(\frac{\partial p}{\partial y}\right), v_z = -\frac{K_z}{\mu} \cdot \left(\frac{\partial p}{\partial z}\right) \tag{1.2}$$

Further derivation of the unidirectional form of Darcy's law allows to show the relation with other parameters that are usually monitored or known during LCM processing. These parameters are the volumetric flow rate Q, the cross-section area A and the length of the injected cavity L.

$$v = \frac{Q}{A} = \frac{K}{\mu} \cdot \frac{-\Delta P}{L} \tag{1.3}$$

1.3.1.1 Porous media

The concept of porous media is an important aspect in the characterization of permeability behaviour of reinforcement textiles. Porosity describes the empty spaces distributed within a given material. The areal porosity ϕ_A describes the ratio between the pores surfaces A_p and the total surface of the studied volume A_0. Porosity is a tridimensional concept, but areal porosity is assumed to be equivalent to the volume porosity ϕ_V when the media is considered homogeneous [18].

$$\phi_V = \frac{pores\ volume}{total\ volume} = \frac{V_p}{V_0} = \phi_A = \frac{pores\ area}{total\ area} = \frac{A_p}{A_0} \tag{1.4}$$

Applied to composite material, the concept of porosity is directly related to the fibre volume fraction as the fibre represents the solid part of the porous volume and can be described by equation (1.5). The preform fibre volume fraction V_f can be evaluated using equation (1.6). where Aw_f is the preform areal weight (g/m^2); N_L, is the number of layers constituting the preform, ρ_f the density of the fibre and h the preform thickness.

$$\phi + V_f = 1 \tag{1.5}$$

$$V_f = \frac{volume\ of\ fibres}{total\ volume} = \frac{Aw_f\, N_L}{\rho_f\, h} \tag{1.6}$$

1.3.1.2 One Dimensional Mould Filling Analysis

One dimensional analysis is useful to quickly predict or evaluate different parameters involved in the mould filling process. Such analytical methods allow to show the relation between the mould filling time, material ($\mu, K\ \&\ \phi$) and process parameters ($Q, \Delta P\ \&\ A$). To include the time factor in to the derivation of equation (1.3) we first need to introduce the concept of interstitial velocity ($v_{i,x}$). Darcy's law describes the superficial velocity of the fluid (v_x) which is the velocity apparent to the eye. However, during the injection process, the liquid resin does not actually follow a linear path inside the porous media as illustrated in Figure 3. Hence, the movement of the resin particles would be best described by the interstitial velocity ($v_{i,x}$) and its relation to the superficial velocity (v_x) is described by equation (1.7).

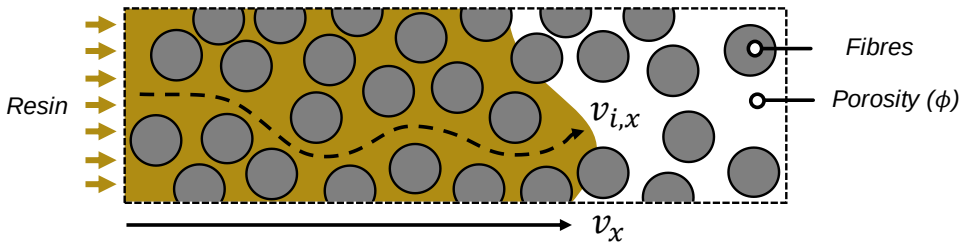

Figure 3: Superficial (v_x) versus interstitial velocity ($v_{i,x}$)

$$v_x = v_{i,x}\frac{A_{flow}}{A_{total}} = v_{i,x}\phi = \frac{dx}{dt}\phi \tag{1.7}$$

For longitudinal injection at constant pressure, equation (1.3) can be derived to equation (1.8) to evaluate the filling time t_f. Where P_i is the applied injection pressure, P_f is the flow front pressure and x_f is the length of the injected cavity.

$$When, P_0 - P_b = cte \rightarrow t_f = \frac{x_f^2 \cdot \mu \cdot \phi}{2K_x \cdot (P_i - P_f)} \tag{1.8}$$

For longitudinal injection at constant flow rate Q, the filling time can easily be evaluated using equation (1.9) since the injection rate and the cavity section A are known. Hence the fluid superficial velocity is constant throughout the entire injection process. For this type of injection, it is often important to evaluate the pressure that will be developed inside the mould. Considering these assumptions, equation (1.3) can be derived to equation (1.10).

$$t = \frac{\phi \cdot A}{Q} \tag{1.9}$$

$$P_i(t) = P_f + \frac{\mu \cdot Q^2}{\phi \cdot A^2 \cdot K} \tag{1.10}$$

1.3.1.3 Double Scale Flow

The concept of permeability describes the displacement of the resin happening at the macroscopic scale. During the injection process, the pressurized resin firstly fills the gap between the fibre bundles at a rate proportional to the resin viscosity, applied pressure and preform permeability. In parallel, the resin infiltrates a different rate the fibre bundles and until every single fibre of the preform is impregnated. This second flow behaviour happening at the microscopic scale mostly depends on the capillary flow and wetting behaviour between the resin and the fibres[19]. Figure 4 illustrates the evolution of the fibre bundle impregnation (saturation) level the during the injection process.

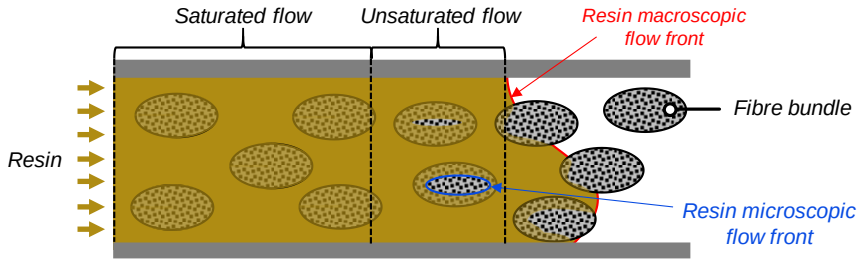

Figure 4: Dual flow scale behaviour

In general, the complete saturation of the fibre bundle is reached a few millimetres behind the macroscopic resin flow front. Unsaturated fibre bundles create a ‘’pressure well’’ effect reducing the available portion of the pressure gradient effective on the macroscopic flow front

slowing down its velocity. Hence, the apparent permeability of a porous media will be higher in the presence of saturated flow regime and lower in the presence of an unsaturated flow regime. Furthermore, an imbalance between the macroscopic and microscopic flow rate may impact the quality of the moulded component. If the difference between in the micro and macro flow rate is too important, this could lead to void generation either at the macroscale (air trapped between the fibre bundles) or at the microscale (air trapped within the fibre bundle) [19]. It is possible to reduce the number of voids by matching the macroscopic and microscopic flow rates [20].

1.4 Preforming Processes for Dry Fabric Reinforcement

Preforming processes are usually included in the overall composite manufacturing process (prior to the resin injection step) to overcome the challenges of the dry fabric manipulation and increase the process repeatability and production rate. In general, preforming processes can be classified between mechanical or chemical technologies.

1.4.1 Introduction to Mechanical Preforming

Mechanical preforming processes regroup mostly techniques from the textile industries and can be categorized into three scales. The one-dimensional scale (1D) is the textile yarn (also fibre bundle or tows) which consist of a bundle of many fibres (either hold by a sizing or twisted together) usually define by their linear density, twist and dimensions. Common materials for fibres are fibreglass, carbon and aramid. These textile yarns are usually coated with a sizing material during their manufacturing process to increase the adhesive interactions with the resin [21].

The two-dimensional (2D) scale refers to woven fabrics manufactured by interlacing textile yarn. Various types of weaving technique are used to produce dry fabric reinforcement material from the textile yarn. Woven fabrics are usually defined by the weave pattern (e.g. plain, satin or twill), the amount of warp and weft yarn per unit of width and length respectively, yarn size and finally by an areal density [22]. The fabric areal density is usually in units of g/m^2 sometimes referred as ‘’*gsm*’’ which stands for gram per square metre. An important characteristic of woven material is their drapeability behaviour which is mainly the results of their ability to deform under in-plane shear and bending [9, 23]. Simply put, the drapeability behaviour is an indication of the ability of a woven fabric to be conformed to 3D geometries and will differ depending on the fabric characteristic (weave pattern, yarn density, areal weight, etc.) [7].

The last scale corresponds to the manufacturing of 2.5D and 3D dry preforms. Techniques such as stitching, or tufting allow to assemble several layers of fabric material. Other techniques like braiding (multi-axial) weaving, knitting or TFP (tailored fibre placement) allow directly produce 2.5D and 3D preforms [6, 24-26]. All these textile processes have high levels of automation but also the drawback of representing high level of capital investment. Also, each textile processes are usually restricted to certain types of geometries which make their utilization less versatile. A summary of the key features of most common preforming textiles techniques is presented in Table 3.

Table 3: Summary of textile process used for the preforming of dry fabric reinforcements. Adapted from [6]

Textile process	Advantages	Disadvantages
2-D Woven fabric	- Good drapeability and in-plane properties - Widely commercially available and relatively cheap - No investment required	- Off-axis tailorability limitation - Manual preform fabrication process - Low out-of-plane properties
3D Woven fabric	- Automated preform fabrication process - Moderate in-plane and out-of-plane properties	- Limited to flat fabrics or simple profiles - High capital investment (specialized equipment) - Slow and expensive process
2D braiding	- Automated preform fabrication process - Well suited for complex curved part - Good balance of off-axis properties	- Limited to profile geometries and machine size limitations - High capital investment (specialized equipment)
3D braiding	- Good balance of in-plane and out-of-plane - Well suited for complex shapes - Automated preform fabrication	- Slow and expensive process - Limited to profile geometries and machine size limitations - High capital investment (specialized equipment)
Knitting	- Highly automated preform fabrication - Good tailorability for balanced in-plane properties	- High capital investment (specialized equipment) - Low design flexibility
Stitching/Tufting	- Complex preforms possible through preforms consolidation - Automated process	- Requires manual draping of individual layers - High capital investment (robot, stitching/tufting equipment, tooling)
Tailored fibre placement (TFP)	- Complex fibre orientation - Net-shape preforms - Automated process	- High capital investment (specialized equipment) - Machine size limitations

1.4.2 Introduction to Preforming Using Binder Material

Preforming process using binder material relies on the adhesive bonding of a stack of dry fabric reinforcement. The result of this process is a handleable semi-rigid, pre-shaped fibrous semi-product also called bindered preform or 3D preform. The bonding agents used are usually

thermally activated polymers, also called binder or tackifier, placed between the reinforcement fabric layers of the preform. These binder materials are usually solid and non-tacky at room temperature. A simplified representation of the preforming process using thermally activated binder is presented in Figure 5. First the binder material is applied on the surface of the dry fabric reinforcement to produce a ‘’bindered fabric’’. Fabrics pre-coated with binder are commercially available and some are even qualified for aerospace applications. However, the bindered version of a fabric can be twice the cost of the same fabric without binder material. Next, several layers of bindered fabric are laid-up ply by ply in a preforming tool. Then the binder material is activated, usually by a thermoforming process (application of heat and pressure), to bond the stack of fabrics and produce the 3D preform. The binder activation by thermoforming is also called consolidation or debulking operations [3, 8, 27-30].

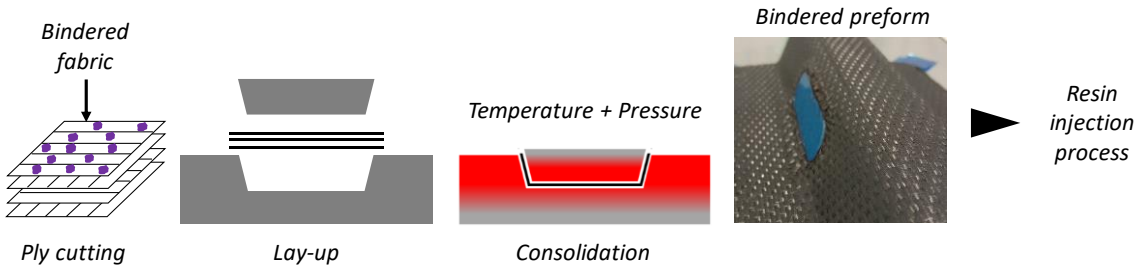

Figure 5: Preforming process using binder material

Binders may have different function other than shaping and bonding layers of reinforcement fabric such acting as a fabric stabilizer. In most of the cases, the presence of binder material limits the deformation of the fabric (shear) but also prevent the edge of the cut plies to fray [10]. The pictures presented in Figure 6 illustrate the ability of binder to limit the fraying of the edges of the plies.

(a) (b)

Figure 6: (a) Examples of cut ply without binder showing signs of frayed edges (b) and fabric with binder showing no signs of frayed edges.

A different variation of binder sometimes referred as ‘’tackifier’’ are material that is tacky at room temperature. These products are often used in hand layup process to temporarily stick the plies to the mould surface or on previously laid-up plies. Such tackifiers are commercially available in various forms like aerosol spay (e.g. Airtack 2 from Airtech Advanced Material Group), adhesive web (e.g. Searfix from SAERTEX GmbH & Co. KG) or liquified resin design for projection applications. In summary, binder material can be grouped in four different categories: thermal softening (non-reactive), curing (reactive) solid binder, fabric stabilizers and tackifier [3, 8, 27].

1.5 Preforming Technology Preselection

An evaluation process was performed as preliminary work for this thesis and revealed that the bindered preform technology would best answer the technological (LCM, complex geometry) and commercial (low-volume production) requirements of the project. The stabilization of dry fabric as shown on Figure 6 and the ability to form complex 3D geometries are the main technical advantage of using binder material. Furthermore, it was estimated that this type of process would better fit the business case of the project as it usually requires fewer investments compared to mechanical preforming which often requires expensive equipment. Furthermore, it was evaluated that a tailored (localized) application of binder material would bring many technical advantages and potential material savings. However, the development of a tailored manufacturing process comes with a certain amount technical challenges and uncertainties.

1.6 Challenges and Motivations

The challenges and motivations of this thesis mainly come from the selection of tailored (localized) application of binder as preforming process, considering the controlled and measured parameters of project COMP1601 previously presented in Table 1.

- **Operation time:** A tailored binder application process will allow to improve the dry fabric reinforcement draping process hence reducing the labour time associated with this operation
- **Material cost:** Bindered fabrics available on the market are usually expensive (up to twice the price of the same non-bindered fabric). Localized binder application implies that less material will be needed. Also, the process is developed to be performed within Hutchinson's facilities. Hence, the local application of binder material is expected to provide substantial material savings compared to commercial bindered fabric.
- **Manufacturing cost:** Improve fabric drapability would minimize the risk of defect cause by bad fabric dapping. Also, tailored binder applications can be achieved with less investment compared to mechanical preforming technology like stitching and tufting that requires a robot or TFP and 3D weaving that requires specialized equipment.
- **Dimensional tolerance:** The presence of binder minimizes the fraying effect of the fabric hence increase the contour precision of the fabric placement.
- **Mechanical properties:** Usually resin and fabric suppliers will suggest compatible binder material ensuring a minimal impact the composite thermo-mechanical properties. However, no compatible binder is suggested with the resin used in project COMP1601, hence a compatible binder needs to be identified. Furthermore, since the binder material will be applied by a tailored application, the impact of different binder concentration needs to be evaluated. Mainly to identify the safe concentration of binder material that can be used.
- **Aesthetic and functional integrity:** The presence of binder on the fabric is invisible after the parts have been injected, which is not the case with stitching technique where the stitch yarns are visible. This needs to be considered as carbon aesthetic finish look are sometimes required.

1.7 Thesis Objectives and Organization

This thesis presents the workflow carried out to achieve the development, optimization & evaluation process of the tailored preforming technology. The main objective is to understand the effect of binder material on LCM processing and on the thermo-mechanical properties of reinforced composite laminates to guide the preforming process development and optimization.

Chapter 2: Both a technological and literature review of the preforming process using binder material are covered in this chapter. The objective is to identify the key parameters of the preforming process as well as the most efficient methodology that led to those meaningful results. The conclusions of this chapter are used to guide the development, optimization & evaluation process presented in the following chapters.

Chapter 3: This chapter presents the thermochemical characterization of four binder materials with different chemical composition. The objective is to measure the melting and glass transition temperature to define the binder processing (application and preforming) guidelines tailored to each material chemistry. Identification of the polymer chemistry (reactive or non-reactive) is also crucial in the definition of the overall process as it indicates if the material can undergo multiple heating cycle.

Chapter 4: This chapter presents the efforts made to characterize and understand the interactions between binder materials (the same as presented in Chapter 3) and an epoxy resin designed for LCM. It is generally agreed that the utilization of bindered preform should not reduce the composite material mechanical properties. The expected outcomes of the work presented in this chapter are summarized by the following objectives:

- Identify the ‘’compatible’’ binder concentration for each binder for which the impact on the resin properties is minimized.
- Comment the efficiency of each resin-binder evaluation strategy used in this thesis.

Chapter 5: The work presented in this chapter investigates the influence of different preforming methods on in-plane and out-of-plane preform permeability. The expected conclusions from this experimental work are guidelines for preforming process development and optimization to achieve best mould filling results.

Chapter 6: This chapter presents the recommendation for the development & optimization process of the tailored preforming technology based on the conclusion of Chapters 2, 3, 4 and 5.

1.8 Presentation of Measured Material Properties

All the presented results from experimental characterization in this these is carried out using the following equations. A sample average measured properties ($\bar{x}$) will be calculated using equation (1.11) where n is the number of specimens tested and x_i the measured value for each specimen. The sample standard deviation (S_{n-1}) and coefficient of variation (CV) are calculated using equation and (1.13) respectively (1.12).

$$\bar{x} = \frac{(\sum_{i=1}^{n} x_i)}{n} \tag{1.11}$$

$$S_{n-1} = \sqrt{\frac{(\sum_{i=1}^{n} x_i^2 - n(\bar{x})^2)}{(n-1)}} \tag{1.12}$$

$$CV = 100 \times \frac{S_{n-1}}{\bar{x}} \tag{1.13}$$

The main purpose in performing several material characterization experiments is to assess the impact of binder on a reference material (matrix, fabric reinforced polymer, etc.). Hence, the impact of binder on material properties is often presented in terms of percentage of reduction or increase (Δ_{REF}) calculated using equation (1.14)

$$\Delta_{REF} = \frac{\bar{x}_{sample} - \bar{x}_{ref}}{\bar{x}_{ref}} \tag{1.14}$$

The properties measured on a sample with representative condition (manufacturing method and material selection) of a selected standard material configuration ($\bar{x}_{ref}$) serves as the baseline reference. Details of the reference sample configurations used are presented in the methodology sections of each characterization experiments.

2. Review of Preforming Using Binder Material

This chapter presents a technological and literature review of the preforming process using binder material. First the characteristics defining the type of binder material, the chemical composition and physical forms, are presented. Next, a review of the key characteristics of the thermally activated powdered binder type such as material concentration, particle size and resin-binder interaction is detailed. Then, a description of the binder application and preforming process are covered revealing the key parameters for each process. Finally, a literature review of the impact of binder material on fabric reinforced composite laminate processing and thermo-mechanical properties is presented.

2.1 Binder Chemical Compositions

2.1.1 Non-Reactive Binder

Thermoplastic based binders gets their binding and shaping ability through the reversible melting-solidification transition which is why they are usually identified as ‘’non-reactive’’ binders. Hence, multiple forming cycles are possible when processed in the appropriate temperature range. Examples of commonly used thermoplastic polymer are polyamide, polyester, phenoxy, etc. For high performance applications like aerospace components, engineered thermoplastic like polyetheretherketone (PEEK) and polyphenylene sulphide (PPS) are usually preferred [3].

2.1.2 Reactive Binder

Thermoset based binder relies on the cure of the material provide the bonding and shaping abilities. This chemical reaction which is usually triggered by an external source of energy such as heat or UV radiation. Hence, this type of binder material is usually identified as ‘’reactive binder’’. The resulted highly cross-linked polymer structure following the chemical reaction prevent from performing multiple forming cycle [3, 8, 27]. Most common type of polymer for reactive binders are epoxy, unsaturated polyester and phenolic [31, 32].

It is important to point out that the definition of a binder reactivity is based on their processing requirement (melting-solidification versus chemical reaction) and not on their ability to react with the resin injected during the LCM process.

2.2 Binder Physical Forms

Most binder material commercially available either in webs liquified or powdered form (Figure 7). This could potentially influence the some of the fabric properties such as the drapeability behaviour, compaction and permeability behaviour. The type of binder material will mostly influence the development of the binder coating process as liquid, webs and powdered material usually requires application process.

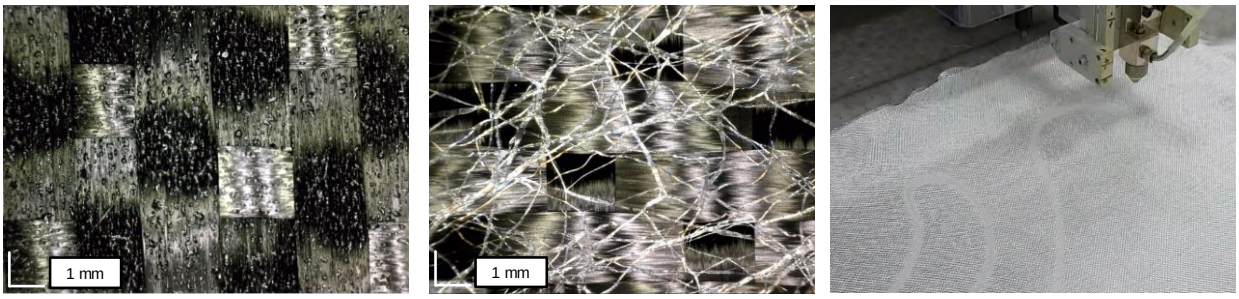

(a) (b) (c)

Figure 7: Example of (a) powdered, (b) adhesive web and (c) liquified binder

2.2.1 Powdered

Powdered polymer is the most frequent physical form used for the manufacturing of bindered fabric. They can be applied manually using devices like sifter, sieve or shaker. However, for aerospace applications, material coating process using industrial equipment is preferred as it yields more uniform and controlled material deposition. This type of binder material is usually applied using a process used with hot-melt adhesives [33] or by curtain coating process [34]. Precoated fabrics are commercially available with singled or doubled coated face. Single-sided fabric may lead to preforms manufacturing defects if two non-bindered sides are facing in the preforms stack up leading to the non-bonding of these two faces. Two-sided bindered fabrics have the advantage to eliminate this manufacturing risk but their price is usually higher as they need to go twice in the binder coating process [27].

2.2.2 Adhesive Web

Adhesive webs are usually produced by applying molten material with a fibril gun either on a backing film or directly the reinforcement fabric cloth. When coated on a backing film, they can be subsequently coated on a fabric using industrial pressure laminating process. Rolls of

material can also be bought to be applied between the reinforcement fabric layers during the layup process [27].

2.2.3 Liquified Binder

Liquified binders can be grouped in two main categories, emulsions and solutions. The advantage of using liquid binder is mainly their ability to be applied using projection processes. Binder solid particles can be mixed with a liquid (often water) to create a dual phase mixture called an emulsion. For emulsified binder a drying step is required after the application to evaporate the liquid phase and keep only the binder solid phase. Binder material can also be solubilized a solvent. The main disadvantage with solutions binder is the health and safety risk from the uses of chemical solvents. Also, this type binder is reported to produce a high ratio of scrap material and to reduce the production rate caused by need of solvent evaporation [3, 27, 33].

2.3 Binder Material Concentration

The amount of binder material coated on the fabric (w_b $[g]$ or Aw_b $[g/m^2]$) should be high enough to preserve the preformed shape and keep bonding of the layers. However, increasing the amount of material also increases the fabric shear and bending stiffness hence reducing its drapeability behaviour [9, 23]. Furthermore, the presence of binder shall not reduce the mechanical properties of the composite laminate. To avoid any negative impact on the matrix properties the binder material concentration should not represent more than 14% of the final laminate resin mass content (w_b/w_r) [3]. Fabric suppliers regularly express the amount of binder material as a percent of the dry fabric nominal mass (fabric mass without binder). Standard binder concentration usually ranges from 2% to 10% percent of the fabric mass (w_b/w_f) [3, 21, 35]. However, the specific amount of binder needed to achieve the desired preform properties in functions of the reinforcement fabric characteristics like the type of weave, tow size, type of fabric material, fabric areal weight. Also, the compatible binder to resin ratio depends on the specific material involved. Hence, the specific required amount of binder material should be determined on a case-by-case basis [27].

2.4 Powdered Binder Particles Size

Small particles (diameter < 100 μm) have a reduced spread area of when molten thus increasing the risk of being completely absorbed within the fibre which would ultimately reduce bonding strength. Large particles (diameter > 400 μm) are harder to melt and may induce deformation of the fabric or increase the risk of being a contaminant, both phenomena resulting in a reduction of the composite laminate mechanical properties. The general range of recommended binder size is 100 to 400 μm [3, 27].

2.5 Resin-Binder Interactions

Since the binder material will be a part of the manufactured composite laminate, its presence should not be neglected [3, 27]. Many researches have concluded that the presence of binder material may generate positives and or negative impact on the laminate thermo-mechanical properties (a review is presented in Section 2.8). In general, resin-binder combinations will be considered compatible if no diminution of the manufactured composite laminate thermo-mechanical properties is observed. Kruckenberg and Paton [32], define binder compatibility in the book *Resin Transfer Moulding for Aerospace Structures* as :

‘*’The ability of two or more substances to combine to form a homogeneous composition having useful properties. In particular, the ability of one resin (e.g. tackifier) to bond to another resin (e.g. matrix resin) without significant loss of properties at the interface.*’’

The interactions between the resin and the binder have found to be highly dependent of the specific material combinations and of concentrations involved [36, 37]. Hence it is often recommended that these interactions should be investigated on a case-by-case basis. Evaluation of mechanical properties of composite laminate (manufactured with the method intended for production) is usually considered as the ultimate criteria to assess the compatibility of binder material [27].

The next sections present an overview of polymer blends (2.5.1) and thermoplastic-thermoset interfacial adhesion (2.5.2) theoretical backgrounds which may help better understanding the principle of resin-binder compatibility.

2.5.1 Polymer Blends Theory

The physical interactions between the resin and binder in a composite laminate may be considered, to some extent, equivalent to those present in a polymer blend if we make abstraction of the reinforcement fabric. The miscibility (or immiscibility) of polymers is reported as a key characteristic for polymer blend in [38]**.** Polymers are considered compatible if they show complete miscibility, characterized by the absence of separate phases in the blend, when mixed in any ratio [39]. However, the most common result of mixing polymers is a blend showing phase separation, suggesting the incompatibility between the constituent. This usually lead to the reduction of the blend mechanical properties like impact resistance and elongation at break. However, immiscibility of polymers can be desired when the objective of blending polymer is to benefit from physical properties of the different constituents [40]. A good example is the addition of thermoplastic toughening agent in epoxy resin to improve their fracture toughness characteristics [41-46]. Hodgkin have concluded that ‘’*thermoplastic … should be soluble in the uncured epoxy, but must phase separate during cure to form a multiphase morphology*’’ [46]. Hence, a more practical definition of polymer compatibility can be introduced, ‘’technological compatibility’’, which defines a blend of polymers presenting an ensemble of desired properties without the polymers being completely miscible. The drawback of immiscible polymers can be overcome by a chemical strategy called ‘’compatibilization’’ which modifies the chemical or physical bonding interactions between the blended phases through the use of components called ‘’compatibilizer’’. The compatibilization strategy relies on three main mechanisms, the reduction of the interfacial tension (physical absorption, ‘’wetting’’), stabilization of the morphology (mechanical interlocking) and enhancement of the adhesion properties (primary versus secondary bonds) of the solid phases. This is usually achieved using two methods, either by introducing block copolymer or by inducing reactive blending [40, 47].

2.5.2 Thermoplastic-Thermoset Interfacial Adhesion

Deng *et al*. [47] have presented the theoretical background of thermoplastic-thermoset interfacial adhesion in a review paper. They reported that interfacial interactions among polymers are usually the result of a mixed contribution of five phenomena, physical absorption, mechanical interlocking, chemical bonding, diffusion and electrostatic theories. The physical absorption

theory, also known as the ‘’wetting’’, states that the bonding of material interfaces is the result of attraction forces happening at the molecular level (secondary or Van der Waals forces) between the materials. The mechanical interlocking theory suggests that the adhesion force is the result of the adhesive infiltrating the adherent surface roughness (surface microscopic scale peaks and valleys, porosities, etc.). After solidification, the adhesive is trapped in the adherent (substrate) surface topography, hence providing a mechanical locking forces. However, for this adhesion mechanism to be effective, the adhesive viscosity needs to be low enough to efficiently wet the surface rugosity. The chemical bonding theory suggests that bonding forces are the result of a chemical reaction involved between the adhesive and the adherent. Strong covalent primary bonds can be achieved in the interfacial region by using adhesive that react (co-cure) with the adherent. The reactivity can be increased with surface treatment or by using coupling agents. The diffusion theory affirms that interdifussion between polymer showing good miscibility and diffusibility properties (compatible polymer) will lead to the creation of adhesive forces. Finally, Deng *et al*., suggest that chemical bonding and diffusion are the mechanisms provides the strongest interfacial interactions.

2.5.3 Binder Processing Compatibility

The resin-binder interaction may also impact the manufacturing process of the composite laminate. If the binder is found to be soluble in the resin, then potential dissolution of binder during the injection process could influence the resin flow behaviour. Migration of the binder may also occur hence leading to material accumulation in certain areas. This can potentially lead to a deterioration of laminate properties if the concentration of binder material exceeds the materials compatible ratio [48]. The ideal scenario is to have a binder material that is solid and non-soluble at injection temperature to avoid any unwanted binder material dissolution or displacement. But, in order to increase the resin-binder blend homogeneity, the melting or softening point of the binder material should be lower than the resin cure temperature [27]. Hence, the binder material could be melted during the cure process thus being easily diffused (minimizing phase dissociation) within the resin while avoiding the risk of binder displacement. Also, Potter [49] has reported that premature gelation of the resin during the injection process may be induced by chemical interaction with the binder material.

2.6 Powdered Binder Application Process

The present section addresses more specific requirements of the powdered binder application previously introduced in Section 2.2.1. The binder application process is presented in Figure 8(a).

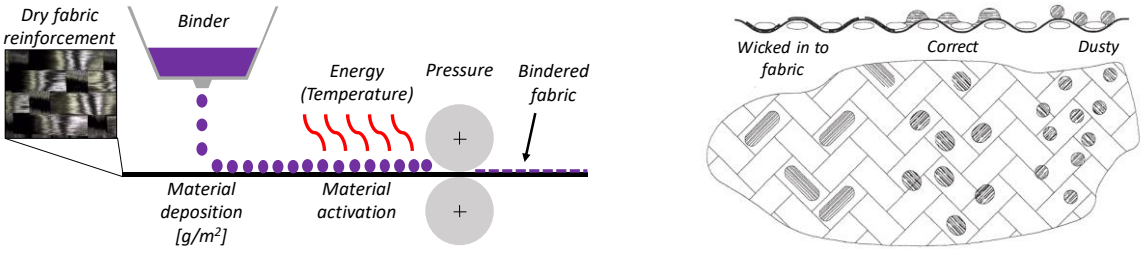

(a) (b)

Figure 8: (a) Binder application process and (b) ideal (powder) material distribution on the fabric surface schematic from [3]

The first step of the process is the deposition of the binder material on one or both surfaces of the dry fabric reinforcement. Next, the material is activated so that it bonds to the surface of the fabric. The application of pressure can be included in the process to increase the consolidation of the material.

The definition of the binder application process parameters (activation temperature and activation time) is generally guided by the material thermochemical properties (reactive versus non-reactive, melting/softening point and melt viscosity) and physical characteristic (particles size) [50]. Figure 8(b) illustrates the ideal binder material distribution on the fabric surface. The application process parameters should be adjusted so that the binder reach the ideal viscosity level that will provide maximum bonding forces during the preforming operation. Overheating would result in a significant reduction of the material viscosity causing the binder to be wicked into the fabric tow (reduction of the bonding area), hence reducing the bonding forces between the layers. On the other hand, insufficient heating would limit the reduction viscosity thus preventing the spreading of the material and ultimately leading to poor bonding between the plies as the material [3, 27]. The recommended amount of binder material (to 2% to 10% percent of the fabric mass (w_b/w_f) [3, 21, 35]) was already addressed in Section 2.3. Basically, the amount of binder material must be high enough to provide the preforming capabilities but must also respect the materials compatible ratio to prevent any reduction of the composite laminate mechanical properties. Hence,

the binder distribution on the fabric must be uniform and precisely controlled to ensure the preforming and compatibility characteristics of the binder fabric [51].

2.7 Preforming Process Key Parameters

Wu *et al*. [52] studied the effect of preforming parameters on the final fibre volume fraction (V_f) and final thickness (h) of bindered preform and concluded that the binder activation temperature, binder activation time, compaction temperature and binder concentration (fabric wt.%) are the key parameters of the preforming process. They showed that these parameters have a significant impact on the preform compaction behaviour and allow to control the final compaction level (V_f & h) and even reach higher compaction level. They suggest that the melting of the binder during the preforming process results in a lubrication effect thus increasing the nesting of the fabric. They demonstrated that the compaction temperature parameter, which corresponds to the consolidation step presented in Figure 5, have the most important impact on the preform compaction behaviour.

S. van Oosterom *et al*. [53] showed that the preform compaction resistance is greatly influenced by the thickness applied during the consolidation process. They have also reported that compaction resistance (during the closure of a rigid match tool) may influence the filling time and flow behaviour during the subsequent injection process.

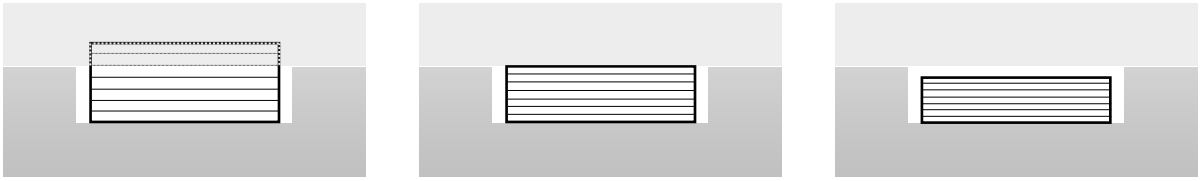

Under pre-compaction ($h_p >> h_m$) | Targeted thickness ($h_p \geq h_m$) | Over pre-compaction ($h_p < h_m$)

Figure 9: Preform compaction level

Many researchers have measured the interply adhesion of bindered preform through T-peeling tests to evaluate the influence of certain preforming parameters. Schmidt *et al*. [36] have concluded that the resulting interply peel strength is mostly influenced by the type of binder material used and that the binder loading would have an impact only under a certain range. They showed that increasing the binder loading past the point where it has fully covered the surface between the plies wouldn't lead to an augmentation of the interply adhesion properties. Tanoglu

[54] came to the same conclusion regarding the binder loading. However, they have shown that an increase of the preform consolidation temperature would increase the interply adhesion when a thermoplastic binder is used (higher infiltration of the binder within the fabrics tows). Brody [50] has shown that reactive binder would provide stronger interply adhesion than non-reactive (thermoplastic) binder. They suggest that this increase of interplay adhesion observed is caused by a chemical interaction between the fabric sizing and the reactive binder.

2.8 Impact of Binder on Composite Thermo-Mechanical Properties

Henne [43] have studied epoxy toughening strategies based on the utilization of thermoplastic binder for LCM carbon reinforced composite part. Polyhydroxy ehter (phenoxy) and copolyamide (CoPA) binder chemistry were studied in three different forms, powder, veils and grid. Results of compression after impact (CAI) tests showed that CoPA binder improved the CRFP impact resistance by minimally 50%, using small binder amount (6-12 g/m^2). The melting of the CoPA during the laminate curing process is suggested to be the cause of toughening improvement. The interlaminar shear strength (ILSS) results showed that the CoPA binder is significantly affected by elevated temperature in powder form but have shown overall improvement in veil form. Phenoxy led to an improvement of the CAI behaviour and to the highest results of ILSS. However, phenoxy have shown complete dissolution during infusion (potential binder rich resin front) causing manufacturing problems (presence of air bubbles). Beier [55] has studied the mechanical properties of stitched and bindered (phenoxy and polyamide) carbon fabric preform. They showed that nonwoven (adhesive webs) phenoxy binder have almost no impact on the apparent interlaminar shear strength while polyamide binder would lead to a reduction of the property. They also showed that both binder has increased the laminate fracture toughness (G_{Ic} & G_{IIc}) but no significant improvement of the CAI behaviour.

Brody *et al*. [50] have compared the impact of reactive (epoxide, PRETEX 110) versus non-reactive (thermoplastic polyester ATLAC 363E) binders mechanical properties of glass reinforced vinyl ester composite. They showed that the thermoplastic polyester binder had reduced both the Mode I (G_{Ic}) interlaminar fracture toughness and propagation while the reactive epoxy binder a showed a significative improvement. They also showed that the extent of the impact of depends on the material concentration and preforming process. Tanoglu *et al*. [54] have studied

the effect of thermoplastic polyester binder on the thermophysical (DMA) and mechanical properties of glass fibre/epoxy laminates. They reported that the presence of the thermoplastic binder lead to a reduction of the Mode I interlaminar fracture toughness (65%), interlaminar shear strength (25%) and a reduction of 6 °C of the matrix glass transition temperature. Daelemans *et al*. [41] have also studied the impact of polyester based thermoplastic binder on thermophysical properties (DSC & DMA) of a glass/epoxy laminate. They revealed that the glass transition behaviour of the resin may be affected if the polyester binder concentration reaches a certain limit. DSC scan of resin-binder mixture has revealed the presence of the binder glass transition temperature when it was representing 16.7% of the weight mixture as shown on Figure 10. However, they showed that the thermoplastic binder can act as an efficient interlaminar toughener (increased mode I interlaminar fracture toughness) for specific resin-binder ratio.

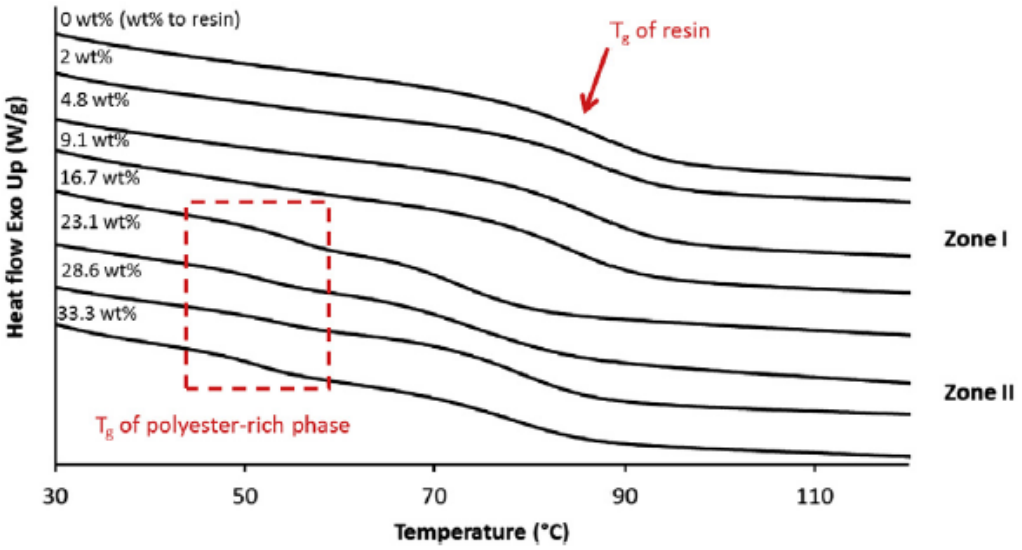

Figure 10: DSC thermograms of epoxy resin/polyester binder mixture from [41] with different binder concentration showing the presence second glass transition for high binder concentration suggesting a phase separation.

Lionetto *et al*. [56] have studied the effect of a reactive binder (HP03 from Hexcel) on the chemoreology of the RTM6 epoxy resin. They revealed that the presence of the reactive binder affects the cure reaction kinetics and that the binder presence is required to complete the stochiometric balance of the resin-hardener mixture. Thus, the presence of the binder is required to get the optimal performances from the RTM6 resin.

The different conclusions of Beier [55] and Henne [43] on the polyamide and phenoxy binder, and from Brody *et al*. [50], Tanoglu *et al*. [54] and Daelemans *et al*. [41] on the polyester binder show that resin-binder compatibility needs to be evaluated on a case-by-case basis. Schmidt *et al*. [36] have studied various binder material (phenoxy, polyester, copolyamide, copolyester and one epoxide) thought different characterization methods (DSC, Tensile test and DMA) and have highlighted the complexity of resin-binder interactions. In conclusion, this review shows that the specific combination of resin-binder, preforming parameters (e.g. binder physical form and concentration), injection and cure process temperature surely influence the resulting impact (mostly negative) of binder material on the composite laminate mechanical properties. A summary of the impact of binder on composite thermo-mechanical properties review is presented in Table 4.

Table 4: Summary of the impact of binder on composite thermo-mechanical properties review

Material	CAI	ILSS	GIc & GIIc	T_g	Tensile
Phenoxy	↑[43], ○[55], ↑[42]	↑[43] ,○[55], ↑[42]	↑[55], ↑[42]	↓[36]	↑[36]
(Co)PA	↑[43], ○[55],	↑&↓[43], ↓[55], ↓[50]	↑[55], ↓[41]	↓[36]	↓[36]
(Co)PET	/	↓[50]	↓[50], ↓[54],↑[41]	↓[54],↓[41],↓[36]	↓[36]
Epoxide		↑[50]	↑[50]		

General trend observed, increase (↑), decrease (↓), (○) no clear influence

2.9 Impact of Binder on Flow Behaviour in Liquid Composite Moulding

Equation (1.8) describing the filling time for a longitudinal injection at constant pressure is a good starting point to understand how the presence of binder may affect the mould filling behaviour. Briefly, the presence of binder may change the preform porosity ϕ, the resin viscosity μ , the preform permeability K and the shape of flow front (linear versus distorted behaviour). The modification of one or many of these parameters will ultimately influence either the final filling time t_f or the required pressure (ΔP). In general, thermosetting resins used in composite manufacturing have a limited working life hence inaccurate estimation of the mould filling time may lead to incomplete injection. A change in the required pressure may also compromise the injection process it may be limited due to mould and or the injection equipment capabilities.

2.9.1 Binder Morphology on Preform Porosity

The addition of binder on the surface of the reinforcement textile should theoretically fill some of these empty spaces and reduce the preform porosity. However, it should not modify the fibre volume fraction of the preform. The classic equation for fibre volume ratio (1.6) considers only the density of the fibres and does not account for the density of the binder. From a mechanical properties estimation point of view it is accepted to evaluate the fibre volume fraction excluding all non-fibre solids such as binder or stitching yarn in a non-crimp fabric (NCF) [57]. From the mould filling perspective, it is unclear whether binder material should be included or not in the fibre volume fraction estimation. Furthermore, the preforming process, which is generally a combination of applied temperature and pressure, will define the final distribution of the binder material within the preform [3, 27]. The binder distribution can be defined as inter-layer or intra-layer as shown Figure 11. Intra-layer defines binder material that has penetrated inside the fibre tows while inter-layer location defines the case where the binder remains on the surface of the fabric. It has been suggested that the inter-layer presence of binder material may reduce the unsaturated permeability of a preform more than the intra-layer location [58, 59].

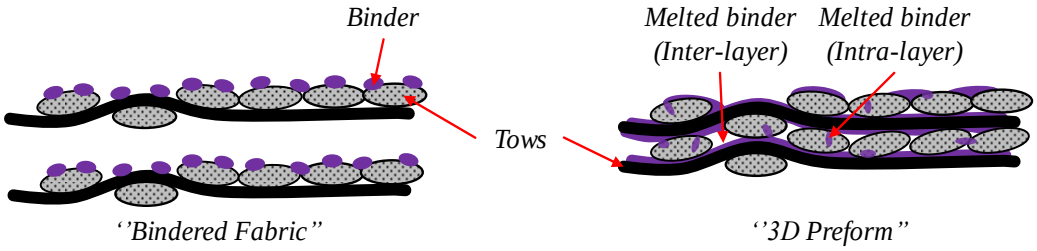

Figure 11: Binder Inter-layer (a) and Intra-layer distribution (b)

2.9.2 Induce Variation in the Filling Process

Gokce and Advani [60] have reported that an accurate control of the filling time and flow pattern is crucial to achieve a successful liquid resin injection. Combined variations of resin viscosity and preform permeability may have significant impact on the mould filling time and required injection pressure, but won't necessarily lead to a failed injection. On the other hand, the accuracy of mould filling simulations can be significantly diminished if the variations in the flow pattern becomes too important as the mould design often relies these simulations to determine the location of resin vents and gates. Hence, they suggest that variation of the flow pattern is more

critical than variation in the permeability behaviour as it would directly lead to a failed injection. The potential ‘’disturbance’’ reported by Gokce and Advani [60] that may cause variations in the filling time and or filling behaviour are presented in the following subsections.

2.9.2.1 Resin Viscosity

The impact of the resin-binder interaction on the resin injection process was previously presented in Section 2.5.3. Chen *et al*. [48] have shown that washout and dissolution effect of polyester binder in a vinyl ester resin could lead to variations into the resin viscosity. Schmidt *et al*. [36] has studied the impact of different binder material on initial viscosity of an epoxy resin. They have found that the solubility of the binder and the scale of its impact on the resin viscosity depends on the type of polymer and on the injection temperature. Lionetto *et al*. [56] have shown that binder material could impact the cure reaction kinetics of a resin. The presence of binder has shortens the working time of the resin by reducing the time to reach gelation but have also lowered of the gelation temperature compared to the neat resin.

2.9.2.2 Preforms Manufacturing Defects

Defects generated during the preform manufacturing or textile impurities may lead to local permeability variation, thus leading to variation in the flow pattern. However, major preform defects can easily be detected before the injection process, thus mostly minor defects are more likely to be present in the preform hence leading to minor impact on the injection process. S. van Oosterom *et al*. [53] have shown local defects in preform manufacturing like missing an extra tow or variation into preform areal weight could lead to moderate effect on the overall mould filling time or flow front shape.

2.9.2.3 Textile Preform Compaction During Mould Closing

In closed mould processes like RTM, the textile preform is compressed between two rigid walls. Further, in application where a high fibre volume fraction is required a high compaction level of the fibre bed can be developed. On the other hand, in processes that rely on atmospheric pressure only, like infusion and light-RTM, the level of fibre bed compaction possible is much lower. The fabric architecture is expected to change accordingly to the intensity of the compaction pressure applied. A global change in permeability is expected, leading to variation in terms of

filling time but not in terms of in-plan flow pattern. S. van Oosterom *et al*. [53] have confirmed that the filling time was highly affected by the compaction resistance of the preform. They have also observed modifications of the flow behaviour as the ratio of in-plane and out-of-plane flow was changing in function of the preform compaction resistance.

2.9.2.4 Interaction of Textile Layers Under Compaction

Most of the textile fabrics used to manufacture preform are made of woven fabric where the fibre tows are overlapping at different intervals depending on the weave pattern used. Under compaction, the textile layers are packed one into another, this phenomenon is also called the nesting effect (Figure 12). The type of weave pattern, the intensity of the applied pressure and the condition (dry compaction versus wet compaction) are parameters influencing the nesting effect**.**

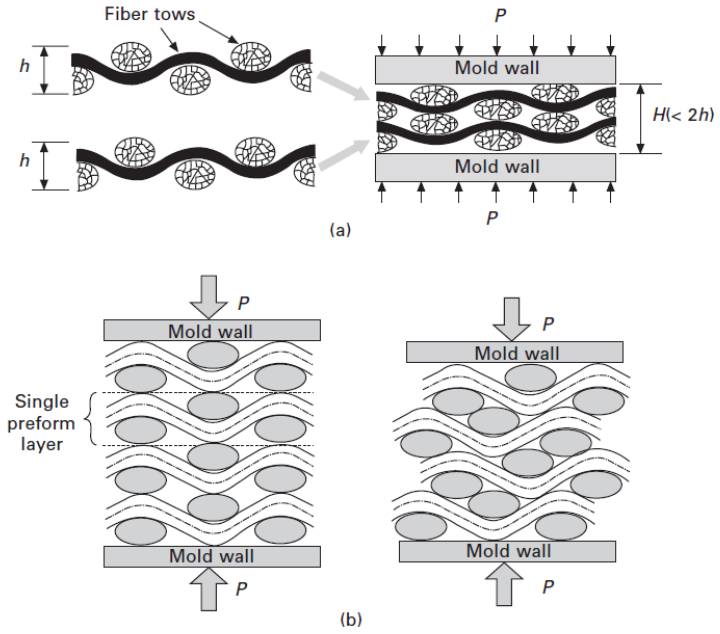

Figure 12: Preform layers interaction under compaction. The reduction of overall thickness caused by single layer compression(a) or by the nesting of the layers(b) [60]

The nesting phenomena may influence the global permeability of the preform as it influences the shape of the channels flow within the preform. Grujicic *et al*. [61] have used a computational approach to validate that the nesting effect in a multi-layer preform lead to a reduction of the preform permeability caused by an increase of fibre density within the laminate space. Lomov *et al*. [62] have studied the nesting behaviour of a reinforcement textile using a 3D geometrical model. They concluded that the nesting behaviour increase as the tightness of the

fabric is reduced. They also reported that the nesting effect is decreased when the fabric is pre-sheared. In a pre-sheared state, the fabric can sustain less deformation before reaching its buckling point as it is already closer to its locking angle. The addition of certain types of binder, especially webs that are often used to stabilize fabrics, may greatly reduce the shear deformation of a fabric and could possibly have the same effect as a pre-sheared fabric or tighter fabric on nesting behaviour. George [57] has shown in his work that the presence of binder may cause fabric to wrinkle under compaction during mould closure causing a ‘’channelling’’ effect that may potentially lead to flow pattern instabilities.

Wu *et al*. [52] has shown that the presence of binder and the preforming temperature will lead to different compaction behaviour. Higher preforming temperature will lead to a reduction of resulting preform thickness for a same amount of ply and binder concentration. The hypothesis is that as the preforming temperature rises, the viscosity of the binder decreases and play the role of a lubricant between the layers. Becker *et al*. [16] have studied the impact of a low areal weight web binder on the transverse permeability. They have found that inactivated binder web placed between each layer impede the nesting effect.

2.9.2.5 Accidental Flow Paths

Often referred as "racetracking" this mould filling disturbance is mostly encountered in match mould application like RTM. Racetracks are unintentional gaps in the mould cavity generated from different factors such as inaccurate preform joints, missing fabric tow or gaps between the mould cavity walls and the preform caused by imprecise fabric draping. Simply put, they are oversized open channels generating high resin flow yielding critical filling pattern variation. It is the most common disturbance in mould filling behaviour as it is difficult to prevent technically. Once the preform is placed in the mould and the mould closed, they become practically impossible to detect. Its severity and lack of detection methods make it one the most critical disturbance that can be potentially encountered. To ease the preform manufacturing process of large complex parts, the preform is often decomposed into smaller components as shown in Figure 13. This technique brings the advantage of simplifying the manufacturing process of each preform sub components. However, the management of the joints between the preform can be challenging. Steenkamer *et al*. [63] have presented the effect of preforming joints on the flow pattern and

showed that if not managed properly it can lead to flow pattern variation as presented on Figure 14.

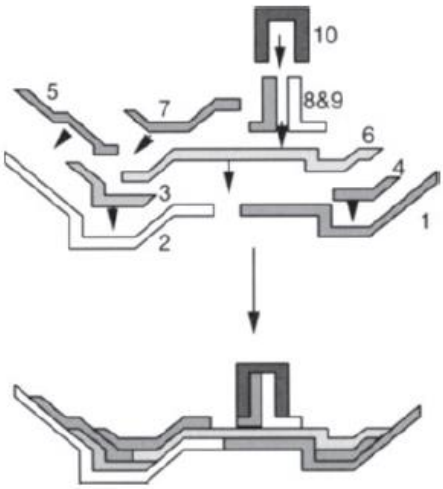

Figure 13: Exploded view of a complex preform made of multi-sub components from [8]

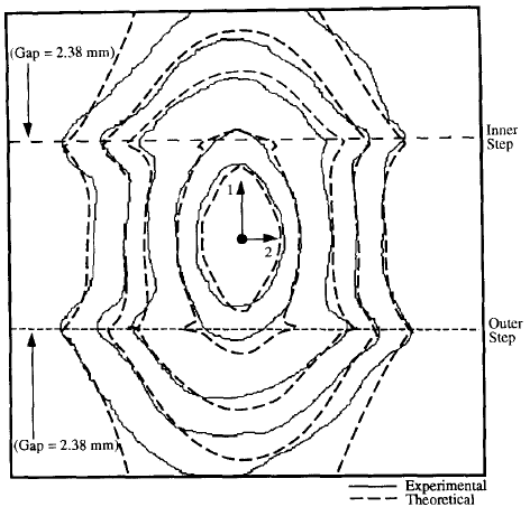

Figure 14: Effect of preforming joints on flow behaviour from [63]

2.9.3 Improvement of Mould Filling From Using Bindered Preform

Some studies have shown the interesting potential of binder material as a solution to tailor the flow pattern during the injection. Depending on the preforming process, utilization of binder material could be a way to reduce anisotropic permeability behaviour of certain fabric type as reported by Sommerlot [59]. Also, a local application of the binder material could minimize its impact on the bulk permeability properties and potentially create ‘’channels’’ or flow ‘’buffer’’ to guide the flow during the injection as reported by Magagnato [64]. Snape *et al*. [10] have shown that the use of bindered preform is an efficient solution to minimize the recurrent loss of accuracy in the cutting process of dry fabric. Inaccurate ply cutting could lead a variety of defects including unwanted gap within the preform potentially generating ‘’racetracking’’ effect [28, 60, 63]. ‘’Fibre wash out’’ is a process generated defect resulting in a distortion of the fibre bed cause by the washing force generated the flow of resin. The use of bindered preform is a known solution to that problem [28, 65].

2.10 Summary

The technological and literature review presented in this chapter revealed the influence of the binder material thermochemical behaviour on the preforming [27, 36, 52, 53], application [3, 21, 27] and liquid injection process [27, 36, 48]. It also showed that understanding the thermochemical behaviour is crucial to develop processing methods (application and preforming) appropriate to each binder chemical composition.

This review also showed that that the presence of binder lead, in most of the cases, to a negative impact on the composite thermo-mechanical properties [36, 41, 50, 54, 55]. The properties dominated by the resin behaviour such as the glass transition temperature (T_g), interlaminar shear strength (ILSS) and fracture toughness for example, are more likely to be affected by the presence of binder material. Moreover, it was presented that resin-binder interactions (binder solubility) may hinder the resin injection process or the resin cure kinetics. This review also revealed that the resin-binder compatibility interactions are unique to each combination. Hence, even if all the studied binder in this thesis were reported epoxy compatible (either by published work or by the supplier), the compatibility of each binder needs to be experimentally validated. The three main factors of resin-binder interaction are the material chemistry used, the manufacturing process (from the binder application to the resin cure step) and the concentration of binder material used.

This review also demonstrates that both in-plane permeability [48, 53, 58, 59, 64, 66] and transverse permeability [16] are affected by the addition of binder material in the preform. The material concentration used for the preform manufacturing, the type preforming process used, the type of polymer (thermoplastic or thermoset) and its physical form (powder, liquid, veils, web, powdered, etc.) are different factors that will determine the impact on permeability. Since the injection process is the crucial step in LCM, there is now doubt that understanding the impacts of preforming technologies on the preform permeability characteristic is mandatory.

3. Binder Application Process Development

This chapter presents the thermochemical characterization of four binder materials with different chemical composition. The influence of the material thermochemical behaviour on the preforming, binder application and liquid injection process have been previously presented in Chapter 2. First, the thermal degradation behaviour of the different binder is characterized by thermogravimetric analysis (TGA). Next the thermochemical behaviour of the studied binder material is characterized through differential scanning calorimetry (DSC). Finally, the binder material thermal behaviour is validated by performing hot-stage microscopy experiments. The measured melting (crystalline polymer) temperature T_m and glass transition temperature T_g are used to define the binder processing (application and preforming) guidelines.

3.1 Studied Binder Material

The preselection of binder material was done following two main requirements. The first one is compatibility with the other constituent of the composite material such as the liquid epoxy resin and reinforcement fabric (carbon, fibreglass, etc.). The extended evaluation of compatibility between the binders and the epoxy resin is presented further in Chapter 4. Secondly, since the localized application of binder material is the key feature of developed preforming process, the access to the raw material form is required. The preselected binder material and some of their properties obtained from technical documentation are presented in Table 5.

Table 5: General properties of studied binder materials

Material	**Physical form**	**Chemical composition**	**Particle Size** [µm] (%)	**Thermochemical Properties** T_g [°C]	T_m [°C]
CoPET	Powder	Copolyester	80-160	18	98-107
EB	Powder	Epoxy-based	12-200, $\bar{x} = 69$	NA	75-105
ME	Powder	Bisphenol-A based, high molecular weight epoxy resin	160-400 (46.6%) 32-160 (50.1%) < 32 (3.3%)	80	ca. 150
PH	Powder	Phenoxy (poly hydroxyl ethers)	$\bar{x} = 110$ (100% </= 212)	92	NA

Powdered binder was preferred to liquid binder as the latter presents some safety (often used with solvent) and handling concerns. Veil materials were discarded because of their limited ability of local applications compared to powders. All binder products are reported to be non-

reactive by the manufacturers. As previously explained in Section 2.1, this appellation refers to the material processing behaviour as thermoplastic are considered ‘’non-reactive’’ and thermosets are considered ‘’reactive’’. The following thermochemical characterization experiments will validate the non-reactive behaviour of the studied binder materials.

3.2 Thermochemical Characterization Methodology

The first step of thermochemical characterization process was to measure the binder materials thermal decomposition temperature (T_d) by thermogravimetric analysis (TGA). Secondly, differential scanning calorimetry (DSC) was used to identify thermal transitions and reactions. Thirdly, modulated differential scanning calorimetry (MDSC) was performed to better define the thermal transitions and reactions. Standard DSC was performed before MDSC as it allows to use faster heating ramp thus leading faster to preliminary results. Finally, the melting/softening point (T_m) of each binder material was visually accessed by hot-stage microscopy (HSM).

3.3 Thermogravimetric Analysis

During thermogravimetric analysis a sample is placed inside a furnace where its weight is measured as a function of time and temperature. Weight change in a material caused by the application of temperature includes phenomena like evaporation of volatile constituents, oxidation, thermal decomposition, heterogeneous reaction, etc. [67]. Most common generated results from thermogravimetric analysis is the weight-loss ratio (%) as a function of temperature or time.

The thermal degradation temperature T_d of each binder material was evaluated using a thermogravimetric analyzer TGA Q500 from TA Instrument. Heating experiments (20°C per minute up to 950°C) were performed in inert nitrogen atmosphere. One experiment per material was performed. The experiment raw data were exported in text files format using the TA Instrument Universal Analysis 2000 software. Then, using Excel the curves of weight loss and its first derivative, the loss rate (mg/°C), were plotted.

The degradation temperature T_d was associated as the onset temperature of the first increase of the mass loss rate. The maximal loss rate temperature ($T_{d,peak}$) of each binder material is presented for comparison purposes only.

3.3.1 Results

Mass loss rate curves presented in Figure 15 illustrate the difference in the thermal degradation behaviours which can be explained by the binder different chemical compositions. The copolyester binder (*CoPET*) shows a wider and shorter peak compared to the other materials. The two epoxy chemistries, *EB* & *ME*, show similar thermal behaviour. The phenoxy binder (*PH*) shows a narrow peak like the epoxy chemistries but with a significantly lower peak signal. The degradation temperature of each binder samples is labelled on Figure 15 (dash line boxes). Unlike the maximal loss rate temperature, the difference of onset degradation temperature between samples is more significative. The onset temperature for *EB* material is evaluated at 250°C, which significantly lower compared to the other material evaluated at 391°C, 351°C and 350°C for the *PH*, *CoPET* and *ME* binder respectively.

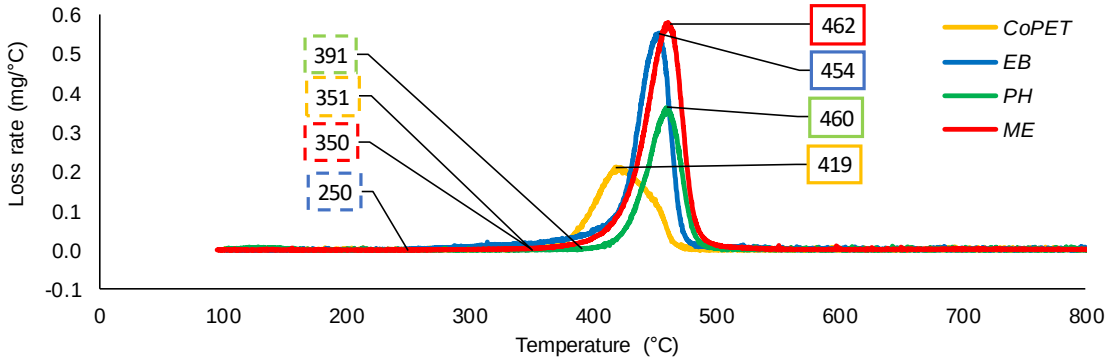

Figure 15: Mass loss rate curves of binder materials. The maximal and onset loss rate temperatures are labelled with solid line boxes and dash line boxes respectively.

The original weight loss curves are presented on Figure 16(a) and a zoomed section of the weight loss for the temperature from 25°C to 400°C is presented on Figure 16(b).

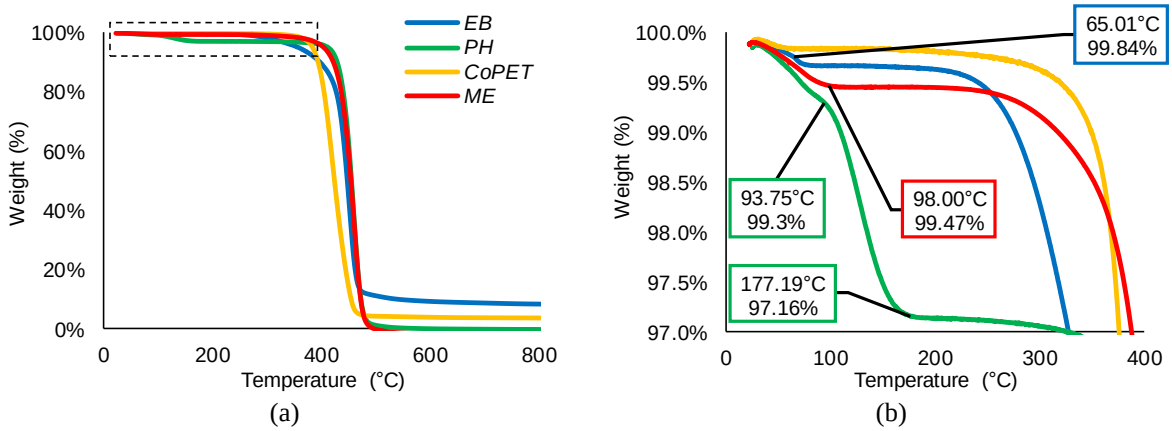

(a) (b)

Figure 16: Complete weight loss (a) and zoomed section for temperature range 25°C to 400°C (b)

All binders showed a very small weight loss (<1%) from 25°C to 100°C or less which could be caused by the drying of the sample or the evaporation of water or other volatile. The phenoxy sample shows an additional 2% weight loss between 93°C and 177°C. The *EB* binder shows a change in the slope of the weight loss at 65°C. A summary of the thermogravimetric results is presented in Table 6. The weight loss results were measured from the weight difference at the degradation temperature T_d of each sample and 700°C using the ''Signal Change'' function available in the Universal Analysis 2000 software.

Table 6: Summary of the TGA results

Binder	**Initial weight** [mg]	T_d [°C]	**Weight loss** [%]	**Loss rate peak** [°C]
CoPET	12.124	351	96.69	419
EB	23.791	250	90.44	454
PH	13.148	391	96.69	460
ME	23.089	350	101.2	462

3.4 Differential Scanning Calorimetry

Differential scanning calorimetry is widely used to identify thermal transition and chemical reaction in polymeric material like the glass transition temperature (T_g), crystallization, melting, chemical reaction like polymerization, etc. [67]. Examples of the signal associated to different thermal transition of a standard thermoplastic polymer is presented on Figure 17. A transition or reaction is considered exothermic when heat is generated by the material (heat flows out of the material). On the opposite, when the material is absorbing energy (heat flows in the sample) the occurring reaction/transition is called endothermic [68].

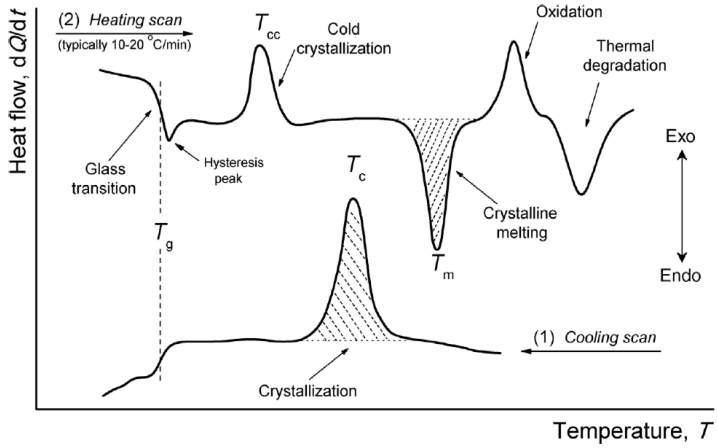

Figure 17: Schematic DSC curves of heating and cooling scans illustrating the thermal transition in a standard thermoplastic polymer [39].

3.4.1 Modulated DSC

One important limitation of standard DSC is the incapacity to identify overlapping thermal transitions which could ultimately lead to the misinterpretation of the material thermochemical behaviour. Since most of commercial polymer products such as binders are usually blends of different chemicals, it is likely that overlapping transitions will be present in such material. Nevertheless, identification of overlapping transitions is possible with modulated DSC (MDSC) as this technique allows to separate the total heat flow signal into ‘’non-reversing’’ and ‘’reversing’’ signals, provides a better definition of the material thermochemical behaviour [69-72]. This also helps for better identification of different phases in polymer blends [69] as well as reducing the risk of thermochemical behaviour misinterpretation as seen with enthalpy relaxation, for example. This thermal event, characterized by an endothermic hysteresis peak occurring on the high temperature side of the glass transition as presented in Figure 17, has sometimes been wrongly attributed as the material melting transition when using standard DSC only [38, 41, 67]. Hence, the utilization of MDSC in this thesis allows to provide a better understanding of the binder material thermochemical behaviour.

Modulated DSC experiments were performed using the same equipment as for standard DSC. The main difference is that the modulated DSC superposed sinusoidal heating rate to the standard DSC linear heating rate. The linear rate provides information related to the total heat flow (dH/dt) is equivalent to standard DSC. Then, Fourier’s transformation analysis is used to extract the fraction of the total heat flow signal caused by the oscillation applied to the linear heat rate (dT/dt), usually referred as the ‘’reversible heat flow’’. This signal indicates changes in the material heat capacity Cp associated to material transitions like the glass transition and crystalline melting. Finally, the kinetic response of the total signal, the ‘’non-reversible’’ heat flow $f(T,t)$, is obtain by subtracting the reversible heat flow to the measured total heat flow (equation (3.1)) [71, 73].

$$\frac{dH}{dt} = Cp\,\frac{dT}{dt} + f(T,t) \tag{3.1}$$

Melting transition of crystalline or semi-crystalline polymer is usually attributed to thermal transitions visible on the reversible signal. However, Sauer [72] explained why portions of the melting transition of semi-crystalline polymer can be observed on the non-reversible signals of

MDSC. Briefly, such phenomenon depends on the equilibrium between complete (non-reversible endothermic signal) and partial melting (reversible endothermic signal) behaviour of the polymer lamellae but also on the recrystallization behaviour. Also, for amorphous polymer the glass transition temperature indicates the material transition going from a solid to a liquid state [70].

3.4.2 Methodology

Standard DSC and modulated DSC experiments were performed with a TA Instrument Q100 Differential Scanning Calorimeter. Dynamic scans featuring two heating cycles were performed to simulate the thermal cycling that the binder material would see during a standard processing. The first and second heating scans are replicating the heat applied during the binder application and preforming process respectively. The materials were encapsulated using aluminum hermetic pans. Standard DSC experiments were performed at three heating ramp rates at 1, 5 and 10°C/min and the same rates were used for the cooling step. The experiments started with a temperature equilibration step at 25°C and then heated up to a safe temperature under the material degradation temperature. The MDSC were performed at 3°C/min and the temperature modulation set to +/- 0.64°C every 40 second as recommended by TA for standard T_g measurement [74]. The temperature range used for MDSC (-10°C up to 230°C) was decided based on the results obtained with the standard DSC. A summary of both test method is presented in Table 7. Any specific deviations from the two methods explained above are specified in the results section.

Table 7: DSC and MDSC Dynamic Scan Methods

Test	Segment (Ramp Rate)	Scan Range	n
DSC	1. Heat (1, 5 and 10°C/min) 2. Cool (1, 5 and 10°C/min) 3. Heat (1, 5 and 10°C/min)	25°C to $T_d - 20$°C	1 per ramp rate
MDSC	Modulate +/- 0.64°C/40 s 1. Heat (3°C/min) 2. Cool (10°C/min) 3. Heat (3°C/min)	-10°C to 230°C	2

Analysis of the thermograms was done using the TA Instrument Universal Analysis 2000 software. The glass transitions were evaluated using the midpoint temperature method as recommended by the ASTM standard D3418-12 [75]. The ‘’Glass/Step Transition’’ analysis function in the TA software with the step midpoint set to ‘’Half Height’’ was used to measure all

glass transition temperatures. The calculation for enthalpy of reaction (J/g) like fusion, crystallization, polymerization or enthalpic recovery, was done using the ‘’Integrate Peak Linear’’ analysis function. Example of T_g, reaction enthalpy (H) and peak temperature measurements are presented on Figure 18. The exothermic reactions are characterized by the enthalpy of reaction and peak temperature are noted H_r and T_r for thermoset resin (cure reaction) and H_c and T_c in the case of thermoplastic polymer (crystallization). The enthalpy of the endothermic reaction characterizing the melting transition of thermoplastic is noted H_m and the reaction peak temperature T_m which is usually identified as the melting temperature.

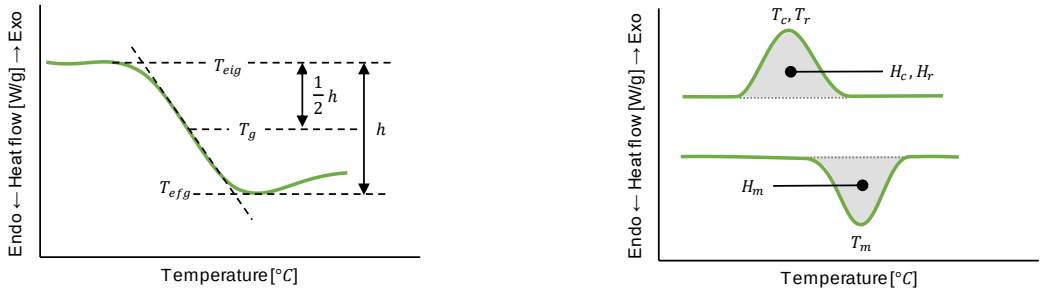

(a) (b)

Figure 18: Glass transition measurement using the half-height method (a) and reaction enthalpy (J/g) and peak temperature measurements (b) in polymer according to ASTM D3418-12 [75].

3.4.3 DSC Results

A summary of results of the DSC double scan for the 1, 5 and 10°C/min ramp rate is presented in Table 8.

Table 8: Summary of DSC double scan results for 1, 5 and 10°C/min ramp rates*

	First scan			Second scan				
Binder	T_g [°C]	H_m [J/g]	T_m [°C]	T_g [°C]	H_m [J/g]	T_m [°C]	H_c [J/g]	T_c [°C]
EB	-	10.9 (1.95)	63.2 (3.71)	56.83 (0.42)	-	-	-	-
CoPET	12.5 (NA)	20.94 (5.12)	54 – 107 (3.24 – 2.69)	15.58 (NA)	7.79 (5.21)	109.56 (8.52)	5.05 (4.20)	66.11 (12.10)
PH	66.11 (0.67)	-	-	96.33 (1.11)	-	-	-	-
ME	65.74 (5.10)	-	-	78.78 (1.41)	-	-	-	-

*The values presented in this table are averaged results ($\bar{x}$), the standard deviations (S_{n-1}) are presented in parentheses.

Thermograms of the first and second scan performed with 10°C/min heating ramp are presented on Figure 19(a) and (b) respectively. At least one example for each studied binder is presented in both figures.

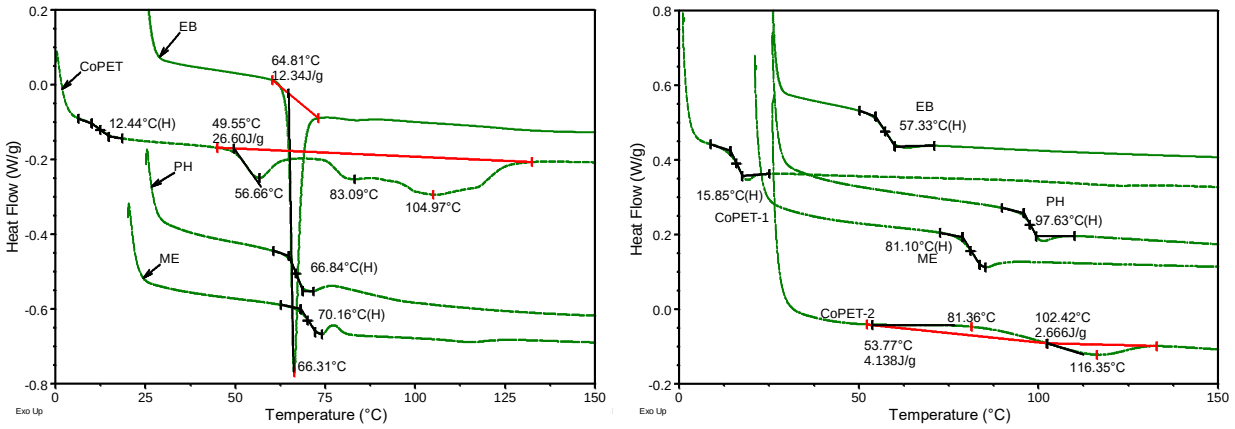

(a) (b)

Figure 19: DSC first (a) and second scan (b) thermograms performed with 10°C/min ramp rate for all binders

3.4.3.1 Results Discussion

The thermograms of the first scan presented in Figure 19(a) reveals a sharp endothermic reaction peaking at 66.31°C for the *EB* material which suggests the presence of a melting transition. The presence of a melting reaction combined to the absence of exothermic reaction indicates that this material behaves like a thermoplastic even though it is described as an ‘’epoxy based’’ by the supplier. Only a single glass transition measured at 57.33°C can be observed during the second heating scan as presented in Figure 19(b).

The *CoPET* thermogram presented on Figure 19(a) is from an additional experiment to the original test plan presented in Table 7. The temperature range of the additional DSC cycle was modified to start at 0°C instead of 25°C. This was done to validate the material glass transition temperature of 18°C claimed in the supplier’s documentation. During the first heating scan a glass transition can be observed at 12.44°C followed by a broad endothermic reaction with three distinct peak temperatures of 56.66, 83.09 and 104.97°C. Considering that this sample is a copolymer it is possible that the different observed endothermic peaks correspond to different kinetics mesophase transitions [76]. This complex phase transition process was repeated for all 4 experiments. Thermograms of the second scans for both experiments performed at 10°C are presented on Figure 19(b). A glass transition temperature measured at 15.85°C on the sample cooled down to 0°C while the experiment performed according to the initial test plan shows crystallization and melting reactions at 81.36°C and 116.35°C respectively.

The *PH* binder shows a single glass transition measured at 66.75°C during the first scan and also a single glass transition during second heating cycle but shifted to higher temperature at

97.63°C. This shift of glass transition temperature suggests that the thermal behaviour of the *PH* material seems to be significantly affected by the thermal history.

The first heating scan of the *ME* binder shows a glass transition at 70.1°C followed by what seems to be a small exothermic reaction. No exothermic reaction is observed during the second heating cycle and the measured glass transition temperature is shifted to 81.10°C. The absence of exothermic reaction during the second scan combined to the shift towards higher temperature of the glass transition suggest that the reaction observed during the first scan was a small (residual) curing reaction.

In conclusion, the DSC experiment showed that all binder materials are mostly non-reactive and they all have different thermochemical behaviour. Also, none of the binder material have shown signs of cold crystallization during the cooling scan.

3.4.4 MDSC Results and Discussion

A summary of the results of the MDSC experiments is presented in Table 9.

Table 9: Summary of MDSC double scan results*

		First scan				Second scan					
Binder	***n***	T_{g1} [°C]	T_{g2} [°C]	H_{endo} [J/g]	T_{endo} [°C]	T_{g1} [°C]	T_{g2} [°C]	H_{exo} [J/g]	T_{exo} [°C]	H_{endo} [J/g]	T_{endo} [°C]
EB	2	60.02 (1.77)	76.90 (2.36)	15.42 (2.25)	60.59 (1.54)	57.73 (1.54)	-	-	-	-	-
CoPET	3	15.44 (2.64)	118.04 (2.20)	31.41 (1.27)	52-104 (0.95-0.04)	16.77 (0.11)	120.65 (0.99)	6.66 (0.67)	79.06 (0.07)	8.23 (0.06)	114.14 (0.36)
PH	2	72.48 (1.75)	160.3 (4.2)	-	-	97.83 (1.77)	-	-	-	-	-
ME	3	79.10 (0.66)	140 (0.07)	78.98 (1.08)	15.57 (1.10)	83.87 (0.74)	-	-	-	-	-

*The values presented in this table are averaged results ($\bar{x}$), the standard deviations (S_{n-1}) are presented in parentheses.

The reversible signal of the *EB* material presented in Figure 20 shows the presence of overlapping step change and small endothermic reaction at 58.76°C followed by a second step change at 75.23°C. The first thermal transition could be attributed to the melting of the polymer crystalline portion and the second glass transition related to the softening of the amorphous portion. The sharp endothermic reaction could be attributed to mix of enthalpic relaxation and evaporation of volatile as a slight change in the weight loss at 65°C with the TGA experiment. The results presented in Table 9 suggest that the material is fully melted at temperature above 76.90 ± 2.36°C. On the second heating scan, only one glass transition temperature is visible at ≈ 58°C. Both the

sharp endothermic reaction and of T_g measured at 75.23°C of the first scan had disappeared. This indicates that some portion of this material thermochemical behaviour is not reversible.

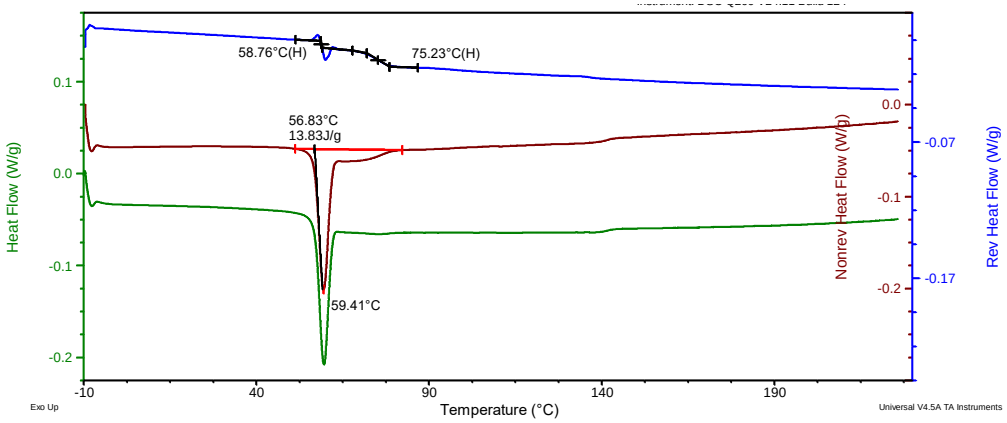

Figure 20: Example of MDSC first scan thermograms for *EB* samples

The thermograms of *CoPET* presented in Figure 21 shows that the total heat flow mostly comes from the material kinetic response. This agrees with the previous statement that theses endothermic peaks correspond to different kinetics mesophase transitions [76, 77]. Every endothermic peak on the non-reversing signal seem to be in phase with step changes of the reversible signal. The last glass transition measured at 116.81°C on Figure 21 is completed at approximately the same temperature as the endothermic reaction. Hence, this could be identified as the temperature required to complete the broad melting process of this copolymer.

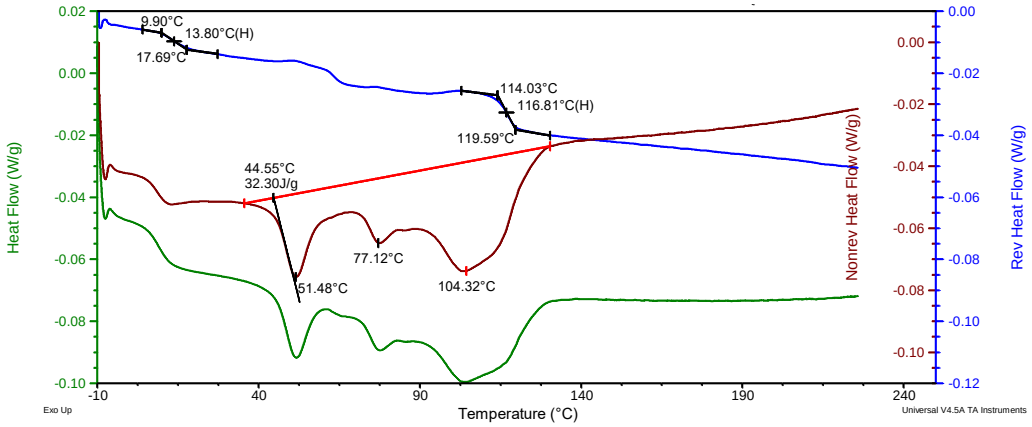

Figure 21: Example of MDSC first scan thermograms for *CoPET* samples

The reversible signal of the second scan performed with *CoPET* presented on Figure 22 revealed a first glass transition at 16.85°C. Also, the baseline of the reversible signal is much more stable compared to the first scan. The non-reversible signal shows the presence of an exothermic (crystallization) and endothermic (melting) reactions. Furthermore, a second glass transition is

visible on the reversible signal at 119.76°C suggesting that a temperature of 120°C or above should be sufficient to melt this binder during the preforming operation.

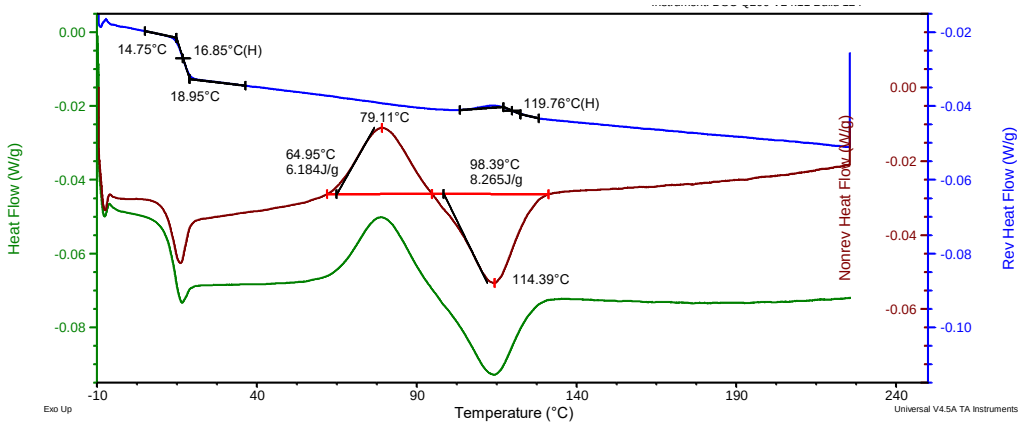

Figure 22: Example of MDSC second scan thermograms for *CoPET* samples

A complex combination of multiple glass transition is visible on the first scan reversible signal of the *ME* samples. Moreover, the observed behaviour on reversible signal is not repeatable between the three experiments performed. Both reversible and non-reversible signal of each experiment are presented on Figure 23. The measured step change in the reversible signal is presented in Table 10 shows that a thermal transition start at ≈ 79°C and ends at ≈ 140°C. In between, step changes are also measured at ≈ 93°C and ≈ 110°C. From these results we can suppose that the polymer is in a solid state below 79°C, in a rubbery or softened state between 79°C and 140°C and fully melted at temperature above 140°C. The observed thermochemical behaviour during the second scan is more stable as a single glass transition was measured at 83.87°C ($S_{n-1} = 0.74$).

Table 10: First scan T_g results for ME samples

Sample	T_{g1} [°C]	T_{g2} [°C]	T_{g3} [°C]	T_{g4} [°C]
ME1	78.63	-	110.04	140.05
ME2	-	94.15	-	-
ME3	79.57	91.59	109.56	139.95
$\bar{x}$	79.10	92.87	109.80	140.00
S_{n-1}	0.66	1.81	0.34	0.07
CV	0.84%	1.95%	0.31%	0.05%

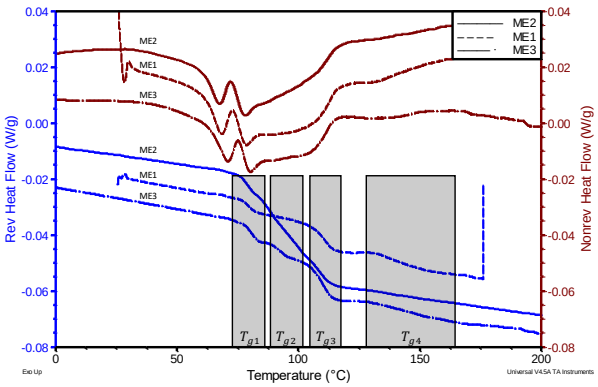

Figure 23: MDSC first scan reversible and non-reversible signals for *ME* samples

An example of the first scan for the *PH* sample is presented in Figure 24. The reversing signal shows two glass transitions at 73.48°C and 157.33°C respectively. These results suggest that the material is in a solid state under 73.48°C, fully melted above 157.33°C and in a rubbery state for in between temperatures. The second scan showed only one glass transition happening at 99.08°C.

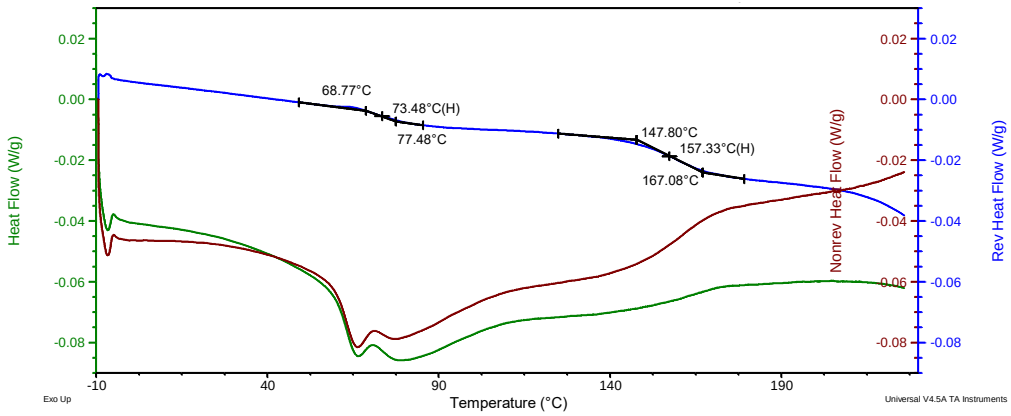

Figure 24: Example of MDSC first scan thermograms for *PH* samples

3.5 Hot-Stage Microscopy (HSM)

Differential scanning calorimetry has provided useful information regarding the binders the thermochemical. However, some binder shows complexes thermal transitions such as multiple T_g transitions or the presence of broad and complex endothermic reaction. Hence, the clear identification of binder material melting (or softening) temperature wasn't fully answered by the MDSC experiments. Hot-stage microscopy (HSM) is a technique proposed in the literature to evaluate polymer material thermal behaviour, especially to identify the melting temperature [27]. During this experiment the material is heated to specific temperatures using a heated stage while the evolution of the sample morphology is observed with a digital microscope.

3.5.1 Equipment

The pictures were captured with a handheld digital microscope from the Dino-Lite of their *Premier* series (model no. AM7013MZTS). The main specifications of this microscope are a magnification range from 10x to 240x and a 5 Megapixel camera with an image resolution of 1280 x 960. The microscope was connected to a personal computer via a USB connection. The software *DinoCapture 2.0* was used to manage, edit and proceed to the pictures acquisition.

The experimental heated stage setup used to perform this experiment is presented in Figure 25. The base of the ‘’HSM Setup’’ is a 1.27 cm flat aluminum plate supported at both ends by to aluminum I-beam. An insulating layer (0.5 cm breather cloth) was placed between the heated blanket (fibreglass reinforced silicone rubber sheet, Omegalux SRFG-808-5) and the aluminum plate. A thin steel plate (thickness of 0.815 mm) was placed over the heat source to provide a flat surface. The power supplied to the heated blanket was regulated by a heater controller (CN7800 from Omega) connected to a personal computer via a USB cable. A K-type thermocouple was positioned on top of the steel plate (as close as possible where the studied material was placed) to provide temperature feedback to the controller. A software from Omega was used to set the temperature and PID parameters of the controller.

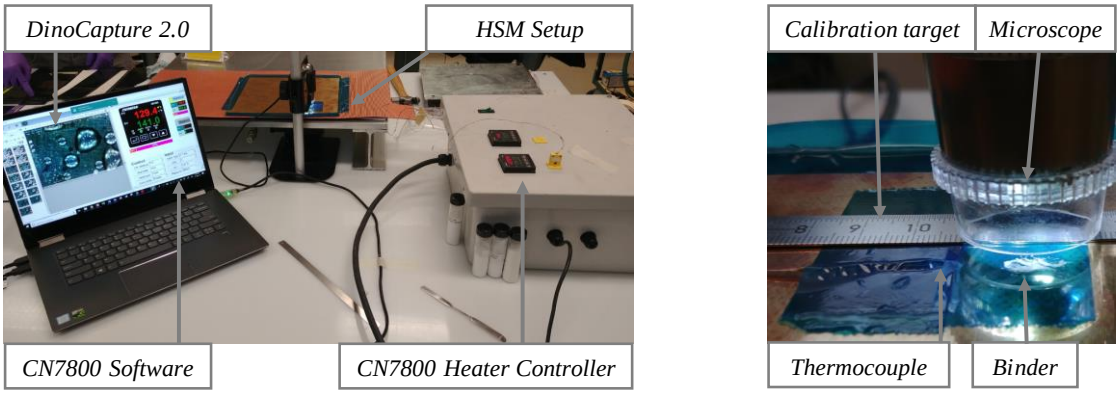

(a) (b)

Figure 25: Overall (a) and close-up view of the hot stage microscopy setup (b)

3.5.2 Method and Test Plan

Firstly, a calibration of the digital microscope image scaling was performed. The distance between the microscope and the sample as well as the focus of the image were adjusted to obtain the desired images of the binder particles. The optimal combination of sample distance and image magnification were found to be 1.25 cm and X207 respectively. Next, the image scale calibration was completed using a metallic ruler as calibration target.

All the experiments were performed following the same procedure. First a small amount of the sample material was deposited on the steel plate of the HSM setup. The powdered material was gently spread on the tool surface in order to form a thin layer of dispersed particles and avoiding material build up. Next, the digital microscope was placed over the sample material. Then the temperature of the tool was set to a series specific temperature and hold for at least 3 minutes.

Pictures of the binder sample were taken at every temperature plateau tested. The different tested temperature for the four binder chemistry are presented in Table 11. The selection of the temperature plateau for each binder chemistry was made in function of the results obtained with the MDSC experiments (Table 9). Each plateau temperature was set to be either slightly under or over the temperature of a thermal transition.

Table 11: Plateau temperature *T* for each binder chemistry

EB		***CoPET***		***ME***		***PH***	
T [°C]	Event	*T* [°C]	Event	*T* [°C]	Event	*T* [°C]	Event
< 55	Solid State	< 45	Solid State	< 60	Solid State	< 60	Solid State
60	Melting Peak	50	Melting Peak 1	70	Onset T_{g1}	68	Onset T_{g1}
65	End Endo	70	End Endo 1	80	T_{g1}	72	T_{g1}
70	Onset T_g	80	End Endo 2	95	T_{g2}	145	Onset T_{g2}
75	T_g	100	Melt Peak 3	100	Onset T_{g3}	160	T_{g2}
85	End T_g	110	Onset T_g	110	T_{g3}	> 170	Melted
> 85	Melted	120	End T_g	125	Onset T_{g4}	-	
-		>120	Melted	> 130	Melted	-	

A qualitative evaluation of the binder morphology was performed following similar criteria as those used by Wu *et al*. [52]. The particles morphology was classified in different states, solid, pre-melted, melted and fully melted (low viscosity). The material was considered in a solid state as long as the particles colour or shape have not changed. The pre-melted state was defined when some binder particles were becoming transparent. The melted state was attributed when most binder particles were completely translucid and some of them have changed shape. The fully melted state was considered when all particles have fully melted, and some have spread on the surface.

3.5.3 Results and Discussion

All the pictures presented in this section have the same scale and show an area of 1.9 mm width and 1.43 mm height. MDSC thermograms of *EB* material revealed a sharp endothermic reaction with a peak temperature around 60°C, a thermal event usually associated to a melting transition. Images from the HSM setup (Figure 26(b)) reveals that some particles start to become transparent at that same temperature. Then, at 70°C the particles start to show signs of melting (Figure 26(c)) until the fully molten state is observed at 75°C (Figure 26(d)). This confirms that

the broad thermal transition identified by MDSC (from ≈ 55°C to ≈ 75°C) is related to the melting transition of this binder material.

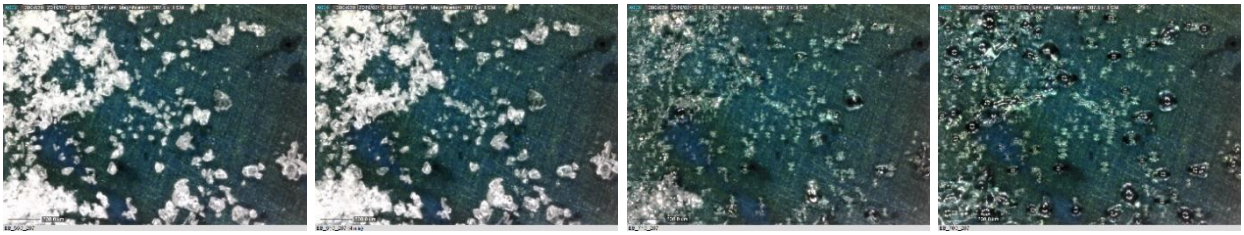

(a) Solid T = 55°C | (b) Pre-melt T = 60°C | (c) Melted T = 70°C | (d) Fully melted T = 75°C

Figure 26: *EB* hot-stage microscopy images.

The MDSC thermograms of binder *CoPET* showed a broad endothermic reaction with three distinct peaks at 52, 78 and 104°C. However, no change in the binder morphology is observed with the HSM setup (Figure 27(a)) for the first two temperatures. A subtle change in the binder morphology is visible at 100°C as some particles are becoming translucid (Figure 27(b)). Then, at 110°C (Figure 27(c)) most of the particles suddenly are molten. This rapid morphological evolution suggests that the endothermic peak temperature measured at ≈ 104°C by MDSC correspond the melting point of *CoPET* material. Next, the material shows extended molten behaviour when the temperature was brought up to 120°C as presented on Figure 27(d).

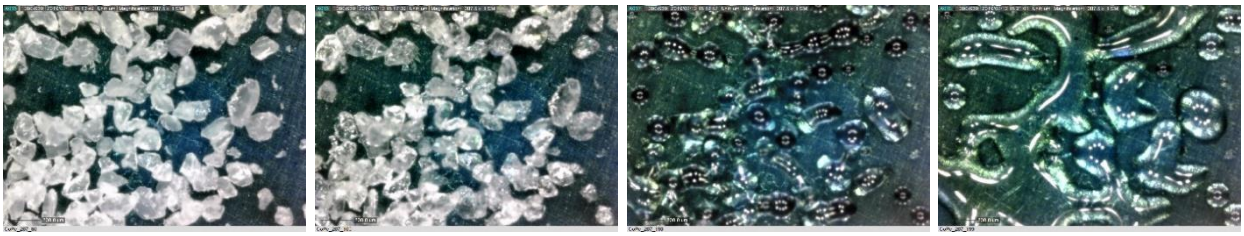

(a) Solid T = 80°C | (b) Pre-melt T = 100°C | (c) Melted T = 110°C | (d) Fully melted T = 120°C

Figure 27: *CoPET* hot-stage microscopy images.

MDSC thermograms of *PH* material have revealed two step changes in the non-reversible signal. The HSM experiment confirmed that the first one (72°C) is the material glass transition temperature as the particles shows no change of colour or shape at this temperature (Figure 28(a)). During the experiment, the material started to show unexpected signs of pre-melting (Figure 28(b)) and molten state (Figure 28(c)) when the temperature reached at 127°C and 135°C respectively. These two transitions were not identified during the MDSC experiments. The second transition

temperature measured with MDSC happening at ≈160°C corresponds to the temperature at which the material had reached a complete melted state (Figure 28(d)).

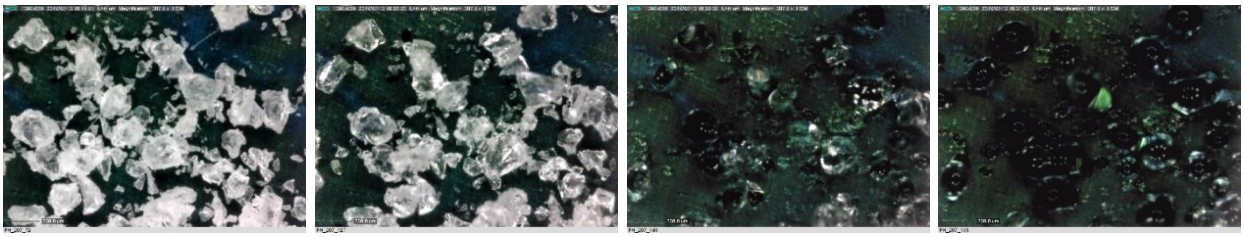

(a) Solid *T* = 72°C | (b) Pre-melt *T* =127 °C | (c) Melted *T* = 135°C | (d) Fully melted *T* = 158°C

Figure 28: *PH* hot-stage microscopy images.

MDSC thermograms of the *ME* binder have shown a first step in the reversible heat flow signal around 80°C. This is confirmed to be the material glass transition as the binder is still in a solid state at that temperature as presented in Figure 29(a). Then multiple step changes measured at ≈ 90°C and ≈ 110°C by MDSC were also investigated with the HSM. The image presented in Figure 29 (b) & (c) indicate that the material shows signs of pre-melting at 95°C and a molten state at 102°C. These observations suggest that the melting point of this material is somewhere between 95°C and 102°C.

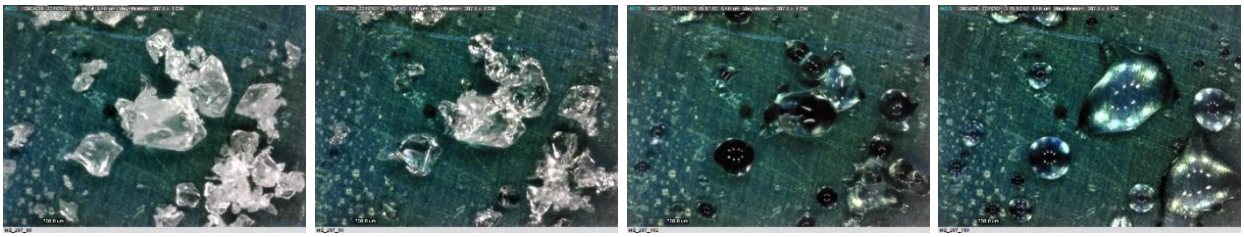

(a) Solid *T* = 80°C | (b) Pre-melt *T* = 95°C | (c) Melted *T* = 102°C | (d) Fully melted *T* = 110°C

Figure 29: *ME* hot-stage microscopy images.

3.6 Thermochemical Characterization Summary

The objective of this chapter was to characterize the thermochemical behaviour of four different binder material (one copolyester, two epoxides and one phenoxy). Four different thermal analysis techniques (TGA, DSC, MDSC and HSM) were used to identify the thermal degradation behaviour (T_d), melting/softening behaviour (T_m) and glass transition temperature (T_g). The mass loss rate curves obtained TGA was the first indicator illustrating the difference of thermochemical behaviour between the different binder. The relatively fast heating ramp (up to 10°C/min) used with Standard DSC allowed to quickly identify the binders thermochemical transition (T_g & T_m)

and confirms their non-reactive behaviour. Then, the MDSC identified the presence overlapping transitions for some materials. For the *EB* binder, a sharp endothermic reaction happening during the first scan was overlapping and hiding the material glass transition. For the other binders (*CoPET*, *ME* and *PH*), MDSC found the presence of a multiple step change in the non-reversible signal hidden by the material kinetic response (non-reversible heat flow). Comparison of results between DSC (Table 8) and MDSC (Table 9) show different results for the first scan. However, a good agreement between the results of the second scan can be observed. Hence, standard DSC seems to be good technique to rapidly get an overview of a binder thermochemical behaviour. The modulated DSC has allowed to identify the second glass transition that was not visible on the standard DSC thermograms. In general, the HSM experiments confirmed the findings of the MDSC experiments. Only with the *PH* a melting transition at a temperature that was not expected from the MDSC results was found.

3.6.1 Binder Processing Guidelines

The processing guidelines (temperature) for the coating and preforming operations for each binder material are presented in Table 12.

Table 12: Binder processing parameters recommendations

Binder	**Chemistry**	**1st heat cycle**		**HSM**	**Coating**	**2 nd heat cycle**		**Preforming**
		T_g [°C]	T_m [°C]	T_m [°C]	T_c [°C]	T_g [°C]	T_m [°C]	T_p [°C]
EB	Epoxy Based	60	61	60 – 75	≥ 80	58	-	≥ 60
CoPET	Copolyester	15	118	104 – 120	≥ 125	16	114	≥ 115
PH	Phenoxy	72	160	135 – 160	≥ 170	97	-	≥ 100
ME	Modified Epoxy	79	110	95-100	≥ 120	83	-	≥ 85

Recommendations regarding the application temperature is mainly based form the MDSC first scan and HSM conclusions. In general, the application temperature should be roughly 10 to 20°C higher than the material melting point (MDSC) to ensure that the fully molten state is reached. The recommendations for the preforming temperature are set according to the conclusions of the MDSC second scan. The material glass transition is used as the reference for minimal preforming temperature as it is in general the only transition observed during the MDSC second scans. However, the preforming temperature could be validated by measuring the resulting peel

strength of bindered preform as performed by Schmidt *et al*. [36] and Brody [50] or by characterizing its influence on the preform compaction behaviour as presented by Wu *et al*. [52].

4. Characterization of Resin-Binder Interactions

This chapter presents the compatibility evaluation between four different binder materials and one epoxy resin. Firstly, the miscibility behaviour of the studied binder in the epoxy resin is studied through rheology and microscopy experiments performed on resin-binder mixtures. Secondly, the impact of the binder materials on the resin thermochemical and mechanical properties is studied through MDSC, DMA (dynamic mechanical analysis) and mechanical tensile tests, also performed on resin-binder mixtures. Thirdly, the impact of binder material on the mechanical properties of a fibre reinforced composite laminate is assessed through the characterization of laminates short beam-strength. Finally, a summary of the resin-binder interactions is presented where the ‘’compatible’’ material concentration for each studied binder is presented as well as a discussion on the efficiency of each resin-binder evaluation strategy used.

4.1 Review of Studied Binder Material

The binders studied in the present chapter were introduced in Chapter 3 (Table 5). All the binders are described as a non-reactive polymer by their suppliers. However, it was reported in Sections 1.4.2 and 2.7 that chemical interaction between epoxy resin and non-reactive binder is possible. Lionetto *et al*. [56] have shown that the presence of the HP03 epoxide binder is needed to complete the cure of RTM6 epoxy resin system. Some epoxides binder materials like Epikote 05390 are described as a reactive thermoset without hardener component [36]. The presence of such epoxide binder (like *EB* & *ME*) material within the preform could potentially unbalance the stochiometric ratio of the injected epoxy resin thus hindering its curing process [49]. Phenoxies thermoplastic materials such as the *PH* binder are reported to have enhanced compatibility to epoxy resin due to the presence of hydroxyl reactive groups in their molecular chain [42]. A study has shown that phenoxy sizing has resulted in an increase of fatigue life of a carbon fibre vinyl ester laminate [78]. Contradictory conclusions on the compatibility of copolyester binder are reported in the literature. Tanoglu [54] and Brody [50] have reported negative impact on mechanical properties of glass/epoxy and glass/vinyl ester composite laminate respectively. On the other hand, Daelemans *et al*. [41] found that copolyester binder may increase the toughness of epoxy resin when used in appropriate concentration. In summary, these observations suggest that

every studied binder in this thesis may influence the resin thermochemical and thermo-mechanical properties of the resin.

4.2 Methodology

Different approaches for the evaluation of resin-binder compatibility were presented in Section 2.5. Potter [27] suggests that the characterization of mechanical properties of composite laminate is the best method for resin-binder compatibility validation. However, the manufacturing of bindered fabric represented a considerable technical challenge since access to industrial coating equipment was not possible in this project. Consequently, the binder material would have to be applied manually hence reducing the repeatability and reliability of the deposition process (uneven material distribution and imprecise material concentration). Hence, the fabrication of bindered preform was judged too complex considering the large number of preform combinations to be studied (12 in total, 4 different binder materials and 3 concentrations level) and the necessity of manufacturing samples with accurate resin-binder ratio.

4.2.1 Resin-Binder Samples

The evaluation of resin-binder interactions was performed on resin-binder mixtures to bypass the technical challenges of the binder application process. Accurate control of the constituent ratio, easier and faster sample fabrication are the main advantage of using resin-binder mixture samples. Furthermore, Schmidt *et al*. [36] have shown that the evaluation of resin-binder interaction is possible with resin-binder mixture samples. The evaluation process followed in the present thesis is highly inspired from [36] and can be broken down into three phases.

For the first phase, rheology and microscopy experiments were performed on resin-binder mixture with low binder concentration. Rheology quantified the influence of binder on resin initial viscosity, processing window and gel time. The solubility of the binder material in the epoxy resin was assessed through microscopy. Modulated differential scanning calorimetry was used to measure the impact of binder on resin thermochemical behaviour (cure kinetics and glass transition temperature). MDSC experiments are overlapping the first and second phases as the characterization of the glass transition is an indicator of binder miscibility and resin thermochemical behaviour. Characterization of resin-binder mixture tensile strength and glass transition temperature by dynamic mechanical analysis (DMA) concludes the second phase.

Finally, the interlaminar shear strength (ILSS) is measured on fabric reinforcement laminate made by infusion. The main objective of the last phase is to validate that the effects observed at the resin-binder mixture level are representative of effect at the full-scale level (fibre reinforced composite laminate).

4.2.2 Test Plan

The test plan followed was designed to evaluate the impact of specific characteristic of bindered preform, more precisely the binder chemical composition and material concentration (W_b). The influence of the material chemical composition is studied through the comparison of the four binder materials (*EB*, *CoPET*, *ME* & *PH*) presented in Table 5. Three levels of material concentration: low ($Aw_b = 8$ g/m^2), medium ($Aw_b = 16$ & 20 g/m^2) and high ($Aw_b = 32$ g/m^2) are evaluated. The low and medium range of binder concentration are based values recommended in the literature and representative of concentrations commonly used by fabric suppliers (Chapter 2). Samples with high concentration of binder material are included in the test plan as worst-case conditions.

The same procedure was used for all resin-binder sample fabrication (8 minutes manual mixing in preheated resin at 45°C plus 5 minutes of degassing) to minimize the influence of the processing method on the resin-binder interactions [40, 48, 54]. Two different cure cycles were used for the manufacturing of resin-binder samples. The first one is a 24-hour cure (minimal) at room temperature which is referred as the ‘’RT’’ cure cycle. The second cure cycle is the manufacturer recommended cure cycle which consists of a 16 hours (minimal) room temperature cure followed by a 4-hour cure at 100°C, referred as the ‘’Production’’ cure cycle. The binder compatibility was evaluated with a commercial epoxy resin for liquid moulding. The flow chart presented in Figure 30 shows the details of the experimental process followed for the evaluation of the resin-binder compatibility.

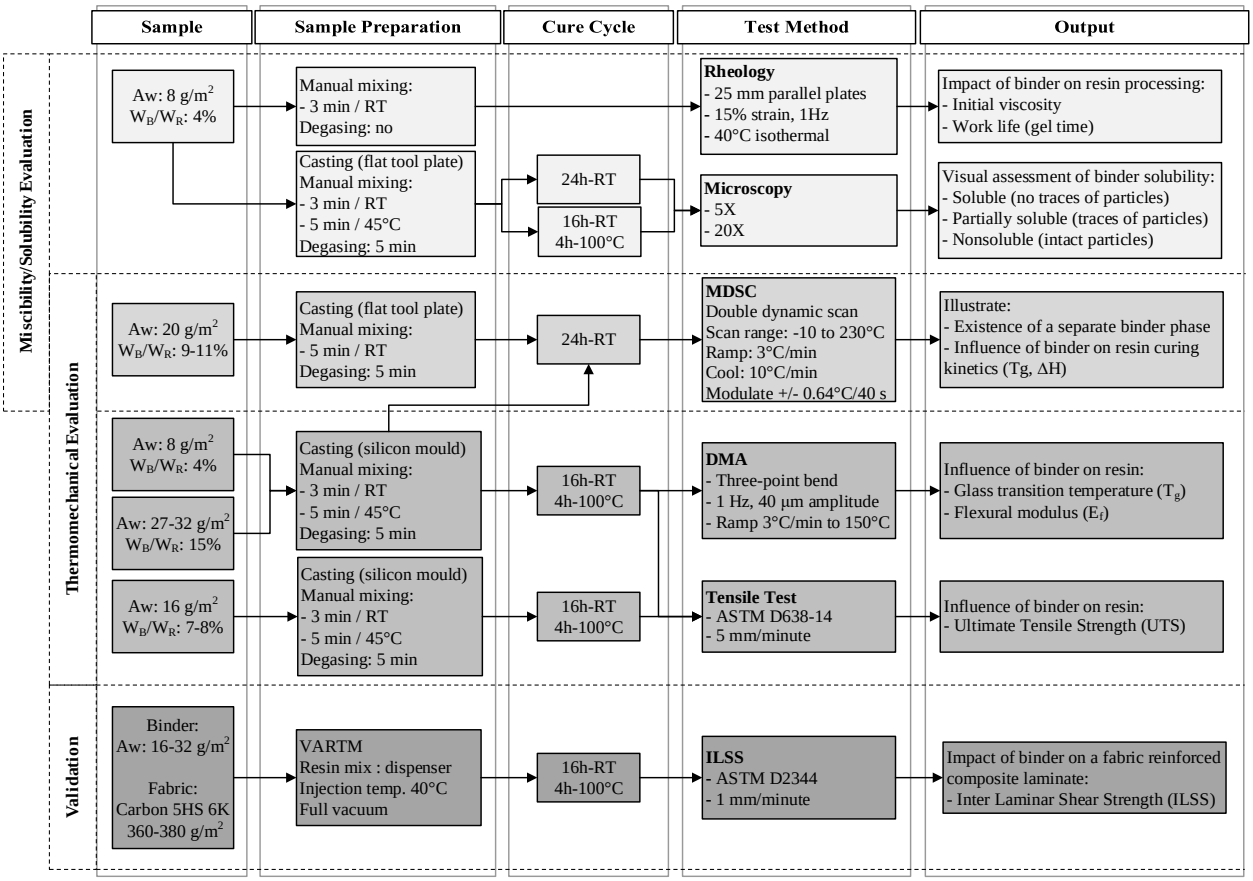

Figure 30: Flow chart of the resin-binder evaluation methodology

4.2.2.1 Samples' Formulation

The main requirement for the samples is to accurately represent the resin-binder ratio (w_b/w_r) that would be found in a generic reinforced composite laminate. This ratio depends on the amount of binder coated on top of the fabric (Aw_b) and on the quantity of resin present in the final laminate (w_r). The resin-binder ratio equivalence between a mixture sample and a generic composite laminate is presented in Figure 31.

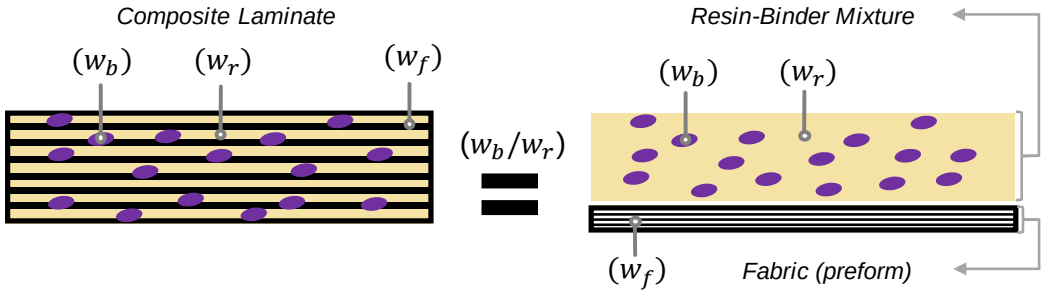

Figure 31: Constituents ratio equivalence between a composite laminate and a resin-binder mixture

The quantity of binder (w_b) in a composite laminate is relatively easy to find as the amount of material coated on the fabric (Aw_b, [g/m^2]) is usually known. The amount of binder coated on the fabric (Aw_b) is also one of the studied variables of this test plan. On the other hand, the amount of resin in the final laminate (w_r) mainly depends on the preform porosity (ϕ). During the injection process, the resin flows inside the preform filling the empty spaces which the equivalent volume usually expresses by the preform porosity. Assuming that the resin fills 100% of the empty spaces, then the resin volume ratio (V_r) of a fabric reinforced composite laminate can be considered equivalent to the preform porosity.

$$V_r = \phi \tag{4.1}$$

The concept of porosity expressed by equation (1.5) only considers the volume of the fibres. However, with bindered preforms the presence of binder material should be considered in the porosity evaluation. Hence resin volume ratio (V_r) should be evaluated using equation (4.2).

$$V_r = \phi = 1 - (V_f + V_b) \tag{4.2}$$

The laminate fibre volume fraction (V_f) can be evaluated with equation (1.6) considering the dry fabric areal weight Aw_f (weight of the fabric without binder). The binder volume fraction (V_b) can be estimated with equation (4.3), where N_L is the number of layers in the preform, A the laminate area and v_c the volume of the composite laminate.

$$V_b = \frac{(Aw_b \cdot A \cdot N_L)/\rho_b}{v_c} \tag{4.3}$$

The evaluation of the binder volume fraction (V_b) is possible when considering the following assumptions. First, the binder has the same density in solid and molten state. This allows the evaluation of the volume of binder present in the preform based on the binder total mass (w_b) and material density (ρ_b). Secondly, the binder is not absorbed within the fabric tow and it stays in the spaces described by the preform porosity. Thirdly, the binder is non-soluble and that the displacement effect is negligible, hence the binder volume will not change during the resin injection process. Finally, the weight of resin present in the final composite laminate (w_r) can be estimated using equation (4.4), where ρ_r is the resin density (mixed with the hardener component) and v_c the volume of the composite laminate.

$$w_r = \frac{v_c \cdot V_r}{\rho_r} \tag{4.4}$$

A reference composite laminate is needed to estimate the resin-binder formulations (w_b/w_r) equivalent to the binder areal weight concentrations (Aw_b) targeted in the test plan. The characteristics of the reference composite laminate used in this thesis are presented in Table 13. The materials, targeted fibre volume fraction (V_f) and laminate thickness were selected so that the laminate would be representative of semi-structural parts used in aerospace applications. The fabric used is a carbon fabric, 5 harness satin weave, 6k tow, with a dry fabric areal weight (Aw_f) of 380 g/m^2. The preform is made of 5 plies all aligned in the same direction ($[0°]_5$). The stacking sequence combined to the targeted laminate thickness of 2 mm yields a theoretical fibre volume fraction of 53.9%.

Table 13: Reference laminate characteristics

Fabric		**Matrix**		**Laminate**	
Weave: 5 harness, 6k tow, carbon fabric		Epoxy resin system		Construction:	$[0°]_5$
Fabric areal weight (Aw_f):	380 g/m^2	Mix ratio (by weight):	100R/12H	Thickness:	2 mm
Fibre density (ρ_f):	1.76 g/cm^2	Mixed density (ρ_r):	1.14 g/cm^3	Nominal V_f:	53.9%

Table 14 presents the formulations for each resin binder mixture arising from the 4 chemical compositions and 4 material concentrations evaluated in this chapter. The estimated binder volume fraction (V_b) for *EB* material turned out to be significantly different compared to all the other binder materials, especially at higher areal weight concentration. This is caused by density of the binder material *EB* being approximately twice lower compared to all the other binder materials. Hence, the targeted medium and high binder concentration (Aw_b) for material *EB* was adjusted for each binder-resin weight ratio similar values obtained with the other binders. The binder-resin weight ratio is expressed in PHR (Parts per Hundred Resin) and as the percentage of the mixture total mass (W_b) as expressed by equation (4.5). The samples binder volume ratio (V_b) and total preform volume ratio (V_{f+b}, considering both the fibres and the binder) also presented in this table.

$$W_b = \frac{w_b}{w_b + w_r} \tag{4.5}$$

Table 14: Resin-binder mixtures sample formulations

Material	Aw_b [g/m^2]	V_{f+b} [%]	V_b [%]	w_b/w_r [PHR]	W_b [%]
CoPET ρ = 1.31 g/cm^3	8	55.51	1.53	3.94	3.79
	16	57.06	3.09	8.17	7.55
	20	57.85	3.87	10.40	9.42
	32	60.22	6.24	17.64	14.99
EB ρ = 0.55 g/cm^3	8	57.67	3.69	4.14	3.98
	14.6	60.81	6.84	8.20	7.58
	20	63.40	9.42	11.98	10.70
	27	66.82	12.84	17.80	15.11
PH ρ = 1.19 g/cm^3	8	55.67	1.69	3.96	3.81
	16	57.38	3.41	8.23	7.61
	20	58.25	4.27	10.51	9.51
	32	60.88	6.91	17.94	15.21
ME ρ = 1.18 g/cm^3	8	55.68	1.71	3.96	3.81
	16	57.41	3.44	8.24	7.61
	20	58.29	4.31	10.51	9.51
	32	60.95	6.97	17.97	15.23

4.2.3 Rheology

The impact of binder material on the resin viscosity behaviour was measured using a rheometer AR 2000 from TA Instrument equipped with a parallel plate (23 mm diameters) setup. The viscosity of most thermoset resin is affected by temperature, generally reducing with the increase of temperature. However, elevated temperature also accelerates the curing process of the resin which lead to a gradual increase of the resin viscosity until it reaches the gelation point. The resin viscosity is usually modelled as a function of thermal $f(T)$ and curing $g(\alpha)$ components as expressed by the equation (4.6).

$$\eta(T, \alpha) = f(T) * g(\alpha) \tag{4.6}$$

Thus, a wide range of viscosity behaviour exist depending on the thermal conditions applied to the resin (isotherm or dynamic (ramp) and heating intensity). However, the goal of these experiment is to evaluate the impact of binder material and not the impact of the temperature. In a production context, the resin studied is injected at 40°C to reduce its viscosity and ultimately ease the injection process. Hence, the viscosity of resin binder mixtures was measured through isothermal (40°C) experiments to best represent the resin-binder interaction conditions during the injection process.

During the experiment the gap between the parallel plates, the deformation applied to sample (ε%) and the frequency of the oscillation are controlled. The characterization of the

viscosity behaviour must be performed within the Linear Viscoelastic Region (LVR) of the studied material. This region is defined by the range of strain (for a given frequency) where the storage and shear moduli (G'& G'') are stable. Hence, the strain ratio and frequency values need to be established by performing a strain sweep experiment. The results of the strain sweep performed on the virgin epoxy resin are presented in Figure 32 and show that the LVR region for this resin occurs around 10-15 strain %. All the experiments presented in this thesis were performed with controlled strain rate of 15% and an oscillation of 1 Hz.

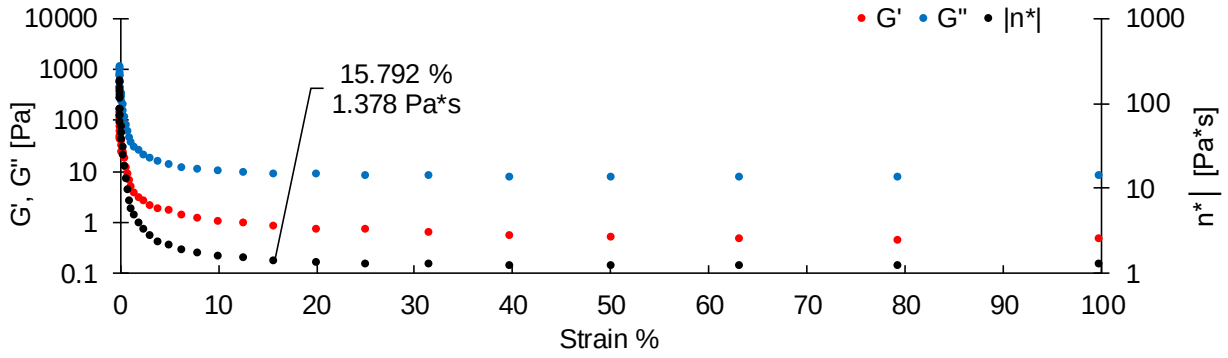

Figure 32: Viscosity curves of the strain sweep experiment performed on the neat resin

The impact of binder material was assessed based on the evaluation of three rheological characteristics of the resin-binder mixtures, the initial complex viscosity ($\eta_i{}^*$), work time (t_w) and the time to reach gelation point (t_{gel}).

4.2.4 Microscopy

The samples used for microscopy were cut from cast plates of resin-binder mixture with a binder to resin weight ratio of ≈ 4% cured using both the ‘’RT’’ and ‘’Production’’ cycles. The resin-binder mixture samples were casted using a clear casting resin (Amazing Clear Cast resin system from Alumilite) to fabricate the microscopy samples. Then, the samples were polished using an automatic polisher (FORCIPOL 1V from Metkon) until the surface have reached a mirror finish. Finally, the images of the resin-binder mixtures were captured with a Nikon ECLIPSE L150 microscope using two magnifications (5X and 20X). Schmidt *et al.* [36] have studied and categorized the solubility behaviour of different binder in an epoxy resin system. The binder was considered non-soluble if no change in the morphology particle was observed, partly soluble if the

particle morphology was modified (reduction of size, smoothing of the edges, etc.) and soluble if no particles were noticeable. The same evaluation process is used in this thesis.

4.2.5 MDSC

The *Encyclopedia of Polymer Blends. Volume 3* reports that characterization of the glass transition temperature behaviour is the most popular test for miscibility evaluation [39]. The existence of different phases in a polymer is revealed by the presence of multiple glass transitions in the material thermochemical behaviour. This method was also used in previous work to evaluate the miscibility of binder material in thermoset resin either by MDSC [36, 39, 41, 69] or DMA experiment [37, 54]. Furthermore, experimental validation is recommended since theoretical prediction of polymer miscibility is usually inaccurate [38].

The MDSC method used to assess the binder miscibility is the same as the one used for the characterization of the binder's thermochemical behaviour presented in chapter 3 (Table 7) and carried out using the same equipment (Q100 Differential Scanning Calorimeter from TA Instrument). Resin binder samples are cured for a minimum of 24 hours at room temperature were used for these experiments. This cure cycle was selected to ensure the gelation of the resin while minimizing the thermal energy applied to the binder material. The first scan performed during the MDSC experiments allows to measure the residual heat of reaction (H_r) of the resin-binder mixture to evaluate if the presence of binder material hindered the resin cure kinetics. Moreover, the first scan acts as a cure cycle and will complete the cure of the resin-binder mixture. Hence, the second heating scan analyzes the resin-binder interactions in a completely cured resin conditions (usually confirmed by the absence of heat of reaction during the second scan). The behaviour of the reversible signal should be the main indicator of dual material phase. If two or more glass transition are measured and that one of them can be attributed to the binder thermochemical behaviour, this will confirm the presence of physical phase of binder within the resin. A binder concentration will be considered incompatible if the second glass transition temperature (caused by the presence of the binder) is lower than the resin glass transition temperature. However, the analysis of the MDSC thermograms is not limited to the evaluation of the reversible signal. The analysis is carried out with a special attention to identify any signs of binder material in both the reversible and non-reversible signal at any point of the MDSC run.

4.2.6 Tensile Mechanical Testing

The influence of binder material on the resin mechanical properties is evaluated by measuring the ultimate tensile strength (UTS) of resin-binder samples. The tests were performed on a universal testing machine (300 Series Universal Test Machine, from TestResource) equipped with a 30kN load cell (TCTN-9110, from TestResources). The speed of testing (5 mm/min) and sample dimensions (Specimen Type I) were selected accordingly to the ASTM standard test method for tensile properties of plastics D638-14 [79]. The sample formulations ($Aw_b = 8, 16$ & $32\ g/m^2$) and preparation method used for these tests are presented in Figure 30. Silicone moulds were used to cast the testing sample according to the dimensions and shape of Specimen Type I. The ‘’Production’’ cure cycle is used to reach the highest mechanical and thermochemical properties.

4.2.7 Dynamic Mechanical Analysis

The dynamic mechanical analysis (DMA) experiments were performed on a DMA Q800 from TA Instrument. The samples were fabricated (mixing and curing operation) simultaneously with the tensile test samples, the only difference being the mould used to cast the samples into the desired shapes and dimensions. Only the low and high binder areal weight concentration ($Aw_b = 8$ & $32\ g/m^2$) were tested in this experiment. The geometry of the DMA samples were set to meet the requirements of the ASTM standard method D7028-07 for the three-point bend flexural loading mode with a span of 50 mm (65 mm length, 12.5 mm wide and 2.0 ± 0.5 mm thick) [80]. The test method was set to apply a controlled displacement amplitude of 40 μm at 1 Hz. The amplitude value was selected by performing a strain sweep experiment on the studied epoxy matrix. The initial test temperature set to 30°C (or below) and ramped up to 130°C at a rate of 3°C per minute. The glass transition ($T_{g(DMA)}$) was evaluated following the guidelines of ASTM standard test method D7028-07. The ‘’Onset Point’’ analysis function available in the TA Instrument Universal Analysis 2000 software was used to measure the glass transition temperature value from the storage modulus (E') signal. The temperature of the tan delta ($T_{E''}$) and loss modulus (T_{δ}) peak signals were also measured for comparison purposes. The flexural modulus was measured (E_F) was measured at 30°C for each tested sample. Examples of signals and different measurements are presented in Figure 33.

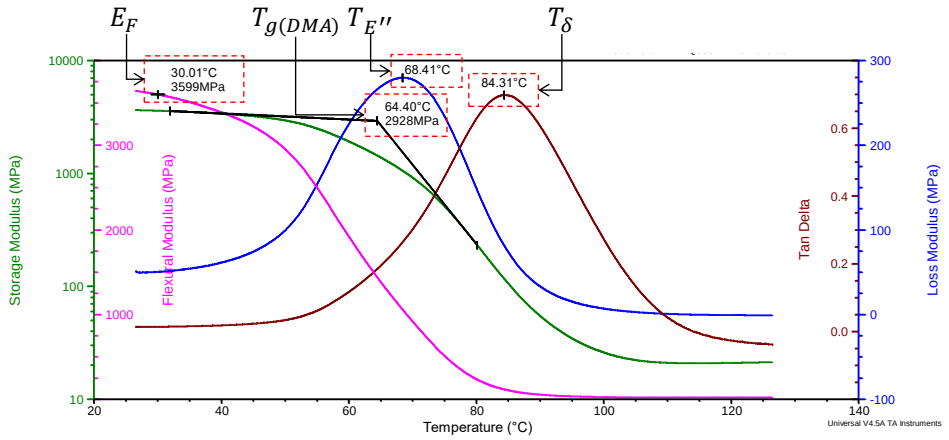

Figure 33: Example of signals and measurements for a DMA experiments performed on a neat resin sample

4.2.8 Interlaminar Shear Strength

Several published papers present the characterization of the interlaminar shear strength (ILSS) of fibre-reinforced composite as a method to evaluate the impact of binder material [42, 43, 50, 54, 55, 78]. In this thesis the ILSS (also referred as short-beam strength) is evaluated for a small number of preform configurations, mainly to avoid the intensive workload associated to the manufacturing of bindered fabric as previously mentioned in this chapter. The definition of the studied variables (binder material type and concentration) was decided with the intention to validate the conclusions obtained from the tensile mechanical testing and DMA presented in the results Section (4.3.4) of this chapter.

The characteristics of the studied preforms combination are presented in Table 15. All preforms are made using the same type of reinforcement textile material (carbon fabric, 5 harness 6k weave, areal weight (Aw_f) of ≈ 360-380 g/m^2) and stacking sequence of $[(0/90)_2]_s$. These characteristics describe the construction of the reference laminate (*SB_REF)* which will provide the baseline to quantify the impact of binder material on ILSS

Table 15: Preform configurations for ILSS evaluation

Sample ID	**Fabric**		**Binder**			
	ID	Aw_f [g/m^2]	**Material**	Aw_b [g/m^2]	**Application**	
SB_REF	A	≈ 378*	NA	NA	NA	NA
SB_EP	B	368**	*EP*	≈ 14	2 sides	Industrial
SB_ME	C	≈ 355*	*ME*	≈ 19	1 side	Industrial
SB_CoPET	A	≈ 378*	*CoPET*	≈ 35	1 side	Manual
SB_PH	A	≈ 378*	*PH*	≈ 18	1 side	Manual

*Evaluation from experimental data
**Value from product certificate of conformance

4.2.8.1 Sample fabrication

For some preform configuration (*SB_EP* & *SB_ME*), precoated bindered fabrics meeting the required specifications (similar fabric, specific commercial binder and material concentration) were available. Configuration *SB_EP* is made with a reinforcement textile precoated on both sides with a powdered epoxide binder (*EP*) representing a material concentration of ≈ 14 g/m^2.Since this binder was not available in powder form, it could not be evaluated using the resin-binder mixture methodology. However, it is still pertinent to include this bindered fabric in the evaluation process as it is the only fabric that is coated on both faces (by an industrial, hence assumed repeatable, process) and aerospace approved. Sample *SB_ME* is made with different commercial bindered fabric (fabric *B*) precoated with binder *ME* on one side for a material concentration of ≈ 19 g/m^2.

The *SB_CoPET* and SB_PH configuration are included in the test matrix to validate the negative (CoPET) and positive (PH) impact on the mechanical properties observed on the resin-binder mixture sample (UTS). For these two samples the binder was manually scattered on the surface (one side) of the fabric using a manual sieve device. The amount of material deposed was measured with a precision scale to ensure that the concentration of binder material was within the range studied in this thesis ($8\ g/m^2 \leq Aw_b \leq 32\ g/m^2$). Next the surface of the fabric was heated using an infrared lamp (2600 W carbon infrared emitter) until the binder material particles have melted and bonded to the fabric. The plies were stacked ensuring that all the bindered side of the layers are facing the symmetry of the stack up. Then all the preforms were consolidated using the same thermoforming process (vacuum bag, full vacuum, 130°C for 60 minutes). All the preforms were infused with the same epoxy resin as used for the resin-binder sample fabrication. The mould was placed on a heated table so that the resin could be heated to 40°C during the infusion process. The laminates were cured following the ‘’Production’’ cure cycle. Finally, the short beam samples were cut from the laminates and the samples final dimensions were achieved by milling operations.

4.2.8.2 Test Method

The dimensions of the samples (40 mm X 9.45 mm X 3 mm) and experimental method (span-to-measured thickness ratio of 4.0, speed of testing of 1.0 mm/min, diameters of the loading nose and supports of 6.00 mm and 3.00 mm respectively) were selected to meet the requirements

of ASTM Standard D2344 [81]. The calculation of the short-beam strength F^{sbs} (MPa) was carried out accordingly to the ASTM standard using equation (4.7)

$$F^{sbs} = 0.75 \times \frac{P_m}{b \times h} \tag{4.7}$$

where P_m is the maximum load (N) measured during the test, b the measured specimen width (mm) and h the measured specimen thickness (mm). The tests were carried out with the same universal testing machine and 30kN load cell used for the tensile mechanical testing (300 Series Universal Test Machine and TCTN-9110 from TestResource). All specimen failure areas were inspected using a digital microscope (Dino-Lite model no. AM7013MZTS) to confirm that the samples have failed in proper mode according to the D2344 ASTM standard.

4.3 Results and discussions

4.3.1 Resin Viscosity

First the complex viscosity (η^*) and temperature recorded in function of time is plotted for each experiment to find that the longest stabilization time (to reach 40°C) of all the experiments was 8 minutes. The measure of initial complex viscosity ($\eta_i{}^*$) of each sample are evaluated at that time. Next, the average viscosity of each sample configuration is evaluated at every two-minute intervals starting from the fifth minute of the experiments. The Figure 34 illustrates the averaged complex viscosity curves in isothermal conditions the different tested sample configurations.

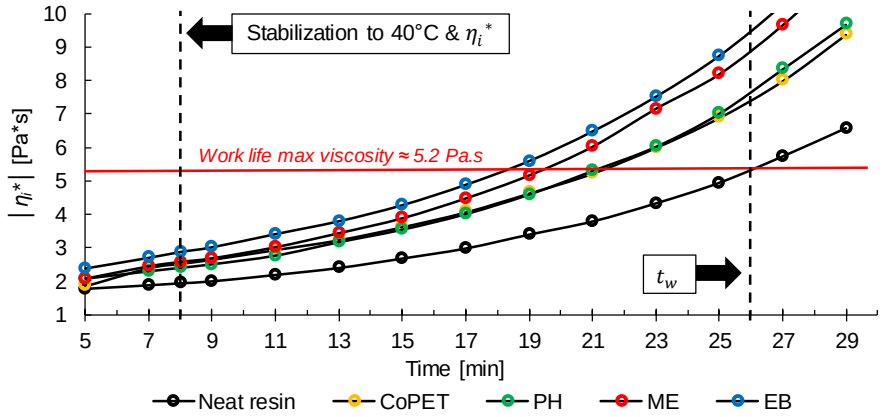

Figure 34: Averaged viscosity behaviour of resin binder mixtures with binder concentration of $W_b \approx 4\%$ ($Aw_b \approx 8\ g/m^2$) in isothermal condition (40°C)

Next the viscosity value indicating the end of the available resin work time (t_w) is empirically defined in function of the value stated in the resin technical documentation (36 minutes) and the measured viscosity behaviour for the neat resin samples. Hence, the work time of resin-binder mixture is taken when the sample complex viscosity reaches a value of $\eta_i^* = 5.2\ \text{Pa} \cdot \text{s}$. The gel point ($t_{gel}$) is taken when the inverse of the complex viscosity ($1/\eta_i^*$) reaches a value of $0.0001(\text{Pa} \cdot \text{s})^{-1}$. The summary of the average measured rheological characteristics of the resin-binder mixtures is presented in Table 16. The time required for the sample preparation (resin mixing) and experiment setup, a total of 10 minutes, is included in the presented results.

Table 16: Summary of the average measured rheological characteristics of the resin-binder mixtures

Sample	n	$\lvert\eta_i^*\rvert$ [Pa.s]			**Gel time* (t_{gel})** [min]			**Work life* (t_w)** [min]		
		$\bar{x}$	CV	Δ_{REF}	$\bar{x}$	CV	Δ_{REF}	$\bar{x}$	CV	Δ_{REF}
Neat resin	3	1.925	18.9%	-	110.33	2.0%	-	35.13	1.8%	-
CoPET	3	2.531	8.6%	32%	111.49	4.6%	1.15%	31.21	11.3%	-16%
EB	3	2.862	9.1%	49%	107.10	5.5%	-3.22%	27.95	8.2%	-29%
ME	4	2.564	13.7%	33%	107.08	7.0%	-3.25%	30.61	8.2%	-18%
PH	3	2.384	12.5%	24%	107.50	4.2%	-2.83%	31.15	10.3%	-16%

*All results include an additional 10 minutes for sample mixing and experiment setup time

The results show that a binder concentration of $W_b \approx 4\%$ lead to an increase of the resin initial viscosity (η_i^*). The highest increase of viscosity is measured with the EB binder represents a 49% increase of the neat resin property (Δ_{REF}). The viscosity behaviour characterization alone does not help to clearly identify if the impact on the resin viscosity is caused by either the modification of the resin cure kinetic as suggested by Lionetto *et al*. [56] or by the dissolution of the binder material as suggested by Schmidt *et al*. [36]. The absence of a significant impact in the measured gel time presented in Table 16 suggests that the binder does not influence the resin cure kinetics. The increase of resin initial viscosity shown in Table 16 could be the results of binder dissolution or just caused by the presence of solid binder particles. The results do not indicate which of the binder miscibility behaviour, particle size or processing condition (temperature and mixing intensity) had the most significant impact on initial viscosity. In conclusion, these experiments showed that the *EB* binder is the most susceptible to significantly influence the resin viscosity. However, the physical interaction between the resin and the binder during the rheology experiment is not representative of the interaction from the resin flowing inside a bindered preform during the injection process.

4.3.2 Binder Solubility Behaviour

This section presents the results of the microscopy experiments. Examples of images of samples cured with the ‘’RT’’ and ‘’Production’’ cycles are presented in Figure 35 and Figure 36 respectively. Only the image captured with the 5X objective is presented in this thesis, as the 20X magnification hasn’t led to additional conclusion. The presence of particles in all resin-binder mixture indicates that none of binder material is completely soluble in the epoxy resin for the processing condition described in Section 4.2.2. Images of the room temperature cured samples presented on Figure 35 shows that only the EB binder can be classified as partly soluble as the edges of the particles seem smoothed. The other three binder (*CoPET, ME* and *PH*) shows no clear signs of dissolution.

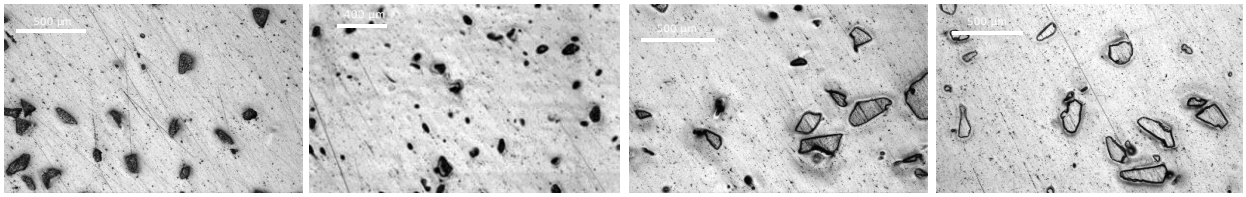

(a)*CoPET* (b)*EB* (c)*ME* (d)*PH*

Figure 35: Examples of resin binder mixture sample cured with the ‘’RT’’ cycle

The images of the samples cured with the ‘’Production’’ cycle presented in Figure 36 show the influenced of the cure cycle on the solubility behaviour of certain binder. The blurry area around the particles of the *EB* sample has expanded suggesting that the dissolution state of this material was increased by the cure cycle. Changes of the particle morphology is also visible with the *ME* (blurred edges) and *PH* (blurred edges and shrunk particles) suggesting that these materials might be partly soluble when cured at high (100°C) temperature. Only the *CoPET* binder has showed no change in the particle morphology suggesting that this material is non-or very slightly soluble in the epoxy resin.

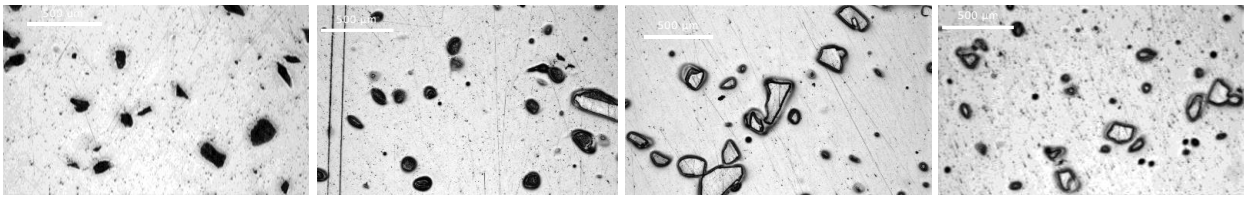

(a)*CoPET* (b)*EB* (c)*ME* (d)*PH*

Figure 36: Examples of resin binder mixture sample cured with the ‘’Production’’ cycle

In conclusion, this experiment allowed to rank the different binder in terms of solubility behaviour. *EB* binder material is the strongest partly soluble binder of all studied binder as it showed signs of solubility even with the room temperature cure. The *ME* and *PH* binder can be considered partly soluble as they have shown signs of solubility with the ‘’Production’’ cured samples. The *CoPET* binder is insoluble in the epoxy resin. But mostly, this experiment confirmed that binder particles are still present in the resin-binder mixtures when mixed following the procedure described in Section 4.2.2 and for all studied binder material. Since this observation was made with the lowest concentration evaluated in this test plan ($W_b \approx 4$ %, 8 g/m^2) it is acceptable to assume that binder particles will also be present in mixture with higher binder concentration.

4.3.3 Thermochemical Behaviour of Resin-Binder Mixtures

4.3.3.1 Neat Resin

This section presents the results of the MDSC experiments. Firstly, the neat resin thermochemical behaviour is characterized to identify a baseline to evaluate the influence of binder materials. The results presented in Table 17 show that residual heat of reaction (H_r) measured with the 24h RT cured samples (9.48 J/g) represents only 2.9% of the total heat of reaction measured from the liquid sample (326.2 J/g). The ‘’Production’’ cycle reaches a higher degree of cure but the presence of residual heat (H_r= 1.62 J/g) suggests that the cure is not complete. This results in a 10°C increase of the T_g (61.42°C) compared to the ‘’RT’’ cure but is still significantly lower than the ‘’infinite’’ glass transition $T_g\infty$ measured for all samples (92.9°C for liquid samples and ≈ 102°C for gelled samples).

Table 17: Neat resin MDSC results summary*

Sample type	Cure cycle	n	H_r [J/g]	T_g [°C]	$T_g\infty$[°C]
Liquid	230°C at 3°C/min	3	326.2 (15.98)	-	92.9 (0.71)
Gelled sample	‘’RT’’	3	9.48 (3.45)	51.55 (4.42)	102.79 (1.28)
Gelled sample	‘’Production’’	3	1.62 (1.00)	61.42 (0.55)	102.28 (1.23)

*The values presented are averaged results ($\bar{x}$) and the standard deviations (S_{n-1}) are presented in parentheses.

4.3.3.2 *CoPET* resin-binder mixtures

A summary of the results for the *CoPET* mixtures is presented in Table 18. The heat of reaction measured during the first scan performed on high binder ratio samples ($H_r = 17.01\,J/g$) is significantly higher compared to the neat resin samples ($H_r = 9.48\,J/g$). Hence, this

observation suggests that the binder have hindered the resin cure kinetic as all the MDSC samples were cured in the same conditions.

Table 18: MDSC results of *CoPET* mixtures first and second heating scan*

Binder ratio (W_b)		n	First scan H_r [J/g]	First scan $T_{g(r)}$ [°C]	First scan $T_{g(b)}$ [°C]	Second scan $T_{g^\infty(r)}$ [°C]	Second scan $T_{g^\infty(b)}$ [°C]
Low	3.79%	3	4.44 (1.43)	55.71 (4.15)	-	102.44 (3.93)	-
Medium	9.42%	3	4.50 (1.43)	54.27 (6.26)	-	107.25 (1.94)	9.39 (0.85)
High	14.99%	3	17.01 (0.81)	48.99 (1.10)	18.14 (0.73)	113.14 (1.41)	9.49 (0.21)

*The values presented are averaged results ($\bar{x}$) and the standard deviations (S_{n-1}) are presented in parentheses.

Examples of non-reversible signals from the first scan for each concentration of *CoPET* resin-binder mixture, the neat resin and the *CoPET* binder are presented in Figure 37. The thermograms show a significant increase of residual heat observed with the high binder ratio samples ($W_b = 14.99\%$). The increased residual heat of reaction measured is represented in Figure 37 by the red area. Furthermore, two glass transitions are measured during the first scan, again with the highly binder-loaded samples. The first transition is measured at 18.14°C which is much lower than the neat resin glass transition evaluated at ≈51°C indicating the presence of a distinct binder material phase ($T_{g(b)}$) as it corresponds to the binder material thermochemical behaviour.

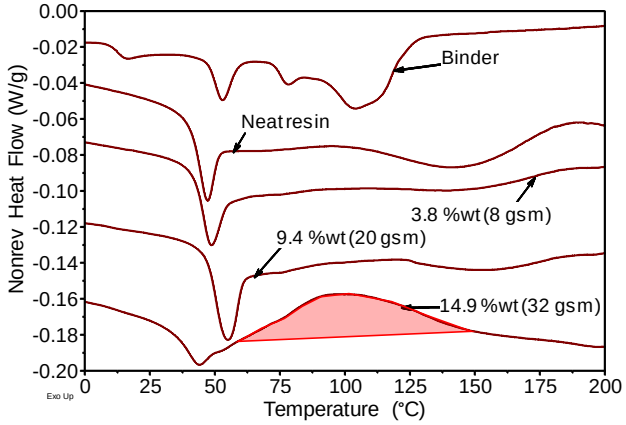

Figure 37: Examples of 1st scan non-reversible thermograms for *CoPET* samples.

The thermograms for the second scan presented in Figure 38(a) reveals the presence of two glass transitions are with the samples with binder weight ratio of 9.42% & 14.99%. Even if the lowest measured $T_{g^\infty(b)}$ (9.39 & 9.49°C) does not correspond exactly to the binder characteristic

behaviour, these transitions are likely the result of the interaction between the resin and the binder. The curves of the non-reversible signals presented in Figure 38(b) show the traces of binder as the exothermic and endothermic reactions (represented by the red areas) of the binder is visible in the resin-binder mixture with binder concentration of 9.42% and 14.99%.

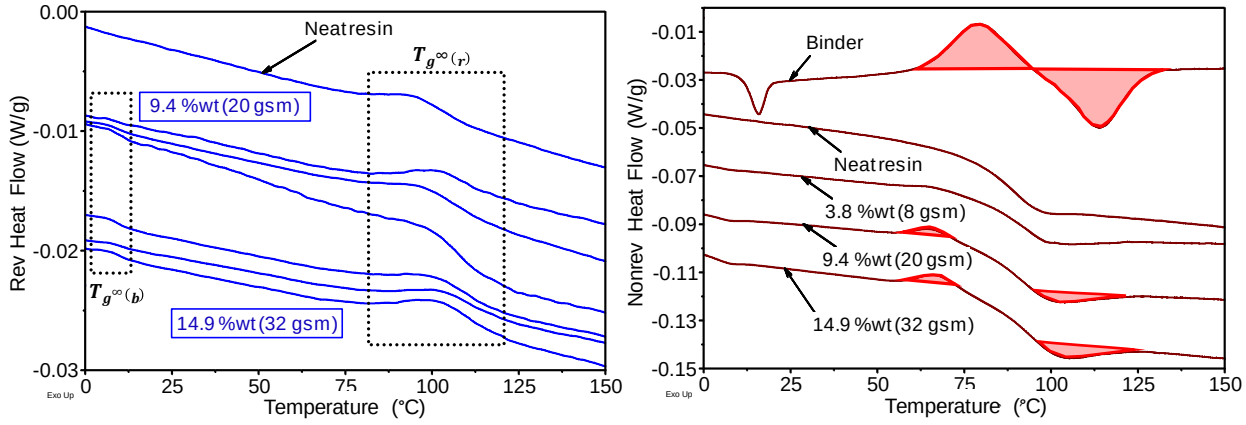

(a) (b)

Figure 38: Examples of 2nd scan reversible (a) and non-reversible (b) thermograms for *CoPET* samples.

In conclusion, the results suggest that the presence of *CoPET* binder material may impact the resin thermo-mechanical properties if the binder weight ratio is above 9.42%. The results show that a binder concentration of 3.79 % could be acceptable as no significant impact on the resin curing process or thermo-mechanical properties was noticed. Hence, the precise limit for acceptable resin to *CoPET* binder ratio (W_b) lies somewhere between 3.79% (8 g/m^2) and 9.42% (20 g/m^2).

4.3.3.3 *EB* resin-binder mixtures

A summary of the results for the *EB* mixtures is presented in Table 19. Thermograms for the first scan reveals many thermochemical events indicating the presence of *EB* binder phases within the mixture samples. Samples with a binder loading of 15.11% shows significant increase of the residual heat of reaction ($H_r = 25.64\, J/g$) compared to lower binder concentration and neat resin samples ($H_r = 9.48\, J/g$).

Table 19: MDSC results of *EB* mixtures first and second heating scan*

Binder ratio (W_b)		n	First scan H_r [J/g]	First scan H_m [J/g]	First scan $T_{g(r)}$ [°C]	First scan $T_{g(b)}$ [°C]	Second scan $T_{g^\infty(r)}$ [°C]
Low	(3.98)	3	9.62 (0.58)	0.06 (0.02)	53.07 (0.12)	-	103.08 (3.71)
Medium	(10.70)	3	8.23 (5.09)	0.25 (0.08)	50.19 (1.57)	61.39 (0.98)	107.18 (1.93)
High	(15.11)	3	25.64 (4.34)	0.32 (0.05)	46.66 (1.54)	63.27 (1.71)	107.64 (0.67)

*The values presented in this table are averaged results ($\bar{x}$), the standard deviations (S_{n-1}) are presented in parentheses.

Furthermore, the presence of binder material is noticeable for all tested concentration on the first scan non-reversible signals. The endothermic peak from the melting reaction of the binder is clearly visible in the curves presented in Figure 39(a) and highlighted by red circles. The enthalpy of melting reaction (H_m) increases accordingly to the binder to resin weight ratio increase as demonstrated by the results presented in Table 19 and Figure 39(a). The binder glass transition temperature was also noticeable during the first scan for the medium and high binder concentration samples. The absence of signs of binder during the second scan (Figure 39(b)) suggest that the cure cycle may influence the material interactions and reducing the effects of the binder material *EB* on the matrix thermo-mechanical properties. Thus, from a thermochemical perspective the allowable binder to resin weight ratio could potentially reach 15.11% (32 g/m^2). However, the cure cycle resulting from the first scan (3°C/ min temperature ramp to 230°C) is not representative of the ‘’Production’’ cure cycle used for this resin. Hence, the influence of a realistic cure cycle should be investigated in future work to validate if identified allowable binder concentration could be used in a production context.

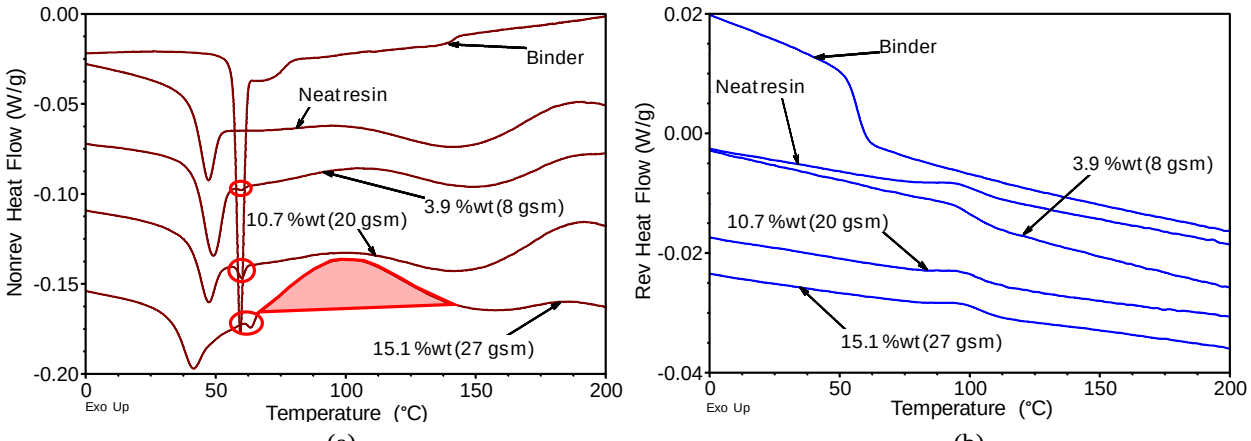

Figure 39: Examples of 1st scan non-reversible signals (a) and 2nd scan reversible signals (b) thermograms of EB samples.

4.3.3.4 *PH* resin-binder mixtures

A summary of the results for the *PH* binder samples is presented in Table 20. As seen with the *CoPET* and *EB* resin-binder mixtures, the measured heat of reaction ($H_r = 15.79\,J/g$) for the sample with high (*PH*) binder concentration is significantly higher compared to the neat resin and lower concentration samples.

Table 20: MDSC results of *PH* mixtures

Binder ratio (W_b)		n	First scan H_r [J/g]	First scan $T_{g(r)}$ [°C]	First scan $T_{g(b)}$ [°C]	Second scan $T_{g^\infty(r)}$ [°C]	Second scan $T_{g^\infty(b)}$ [°C]
Low	(3.81)	3	6.32 (4.40)	54.84 (1.46)	83.04*	105.13 (3.83)	-
Medium	(9.51)	3	4.94 (2.13)	52.77 (6.27)	77.44*	103.57 (2.71)	73.21*
High	(15.21)	3	15.79 (1.21)	50.20 (0.66)	78.02 (0.15)	106.55 (0.92)	74.77 (1.14)

*The values presented in this table are averaged results ($\bar{x}$), the standard deviations (S_{n-1}) are presented in parentheses.
** One of three trials have shown a T_g

Examples of first scan non-reversible signals illustrating the increase of residual heat of reaction (represented by the red area) for high concentration sample is presented in Figure 40(a). The presence of a second glass transition attributable to the binder material is noticed with all binder concentration on both the first ($T_{g(b)}$) and second scan ($T_{g^\infty(b)}$). However, this observation is repeated only for the sample at high concentration ($W_b = 15.21\%$) and is observed in singular case for the low and medium binder concentration. Examples of the second scan reversible signals are presented in Figure 40(b) and shows the presence of a second glass transition ($T_{g^\infty(b)}$). A deeper investigation of the low and medium concentration is required to confirm the impact of this binder. However, considering the present results the *PH* binder show a compatible behaviour for weight ratio of 9.51% (20 g/m^2) and under. Hence, the acceptable limit of resin-binder ratio would lie somewhere between 9.51% (20 g/m^2) and 15.21% (32 g/m^2).

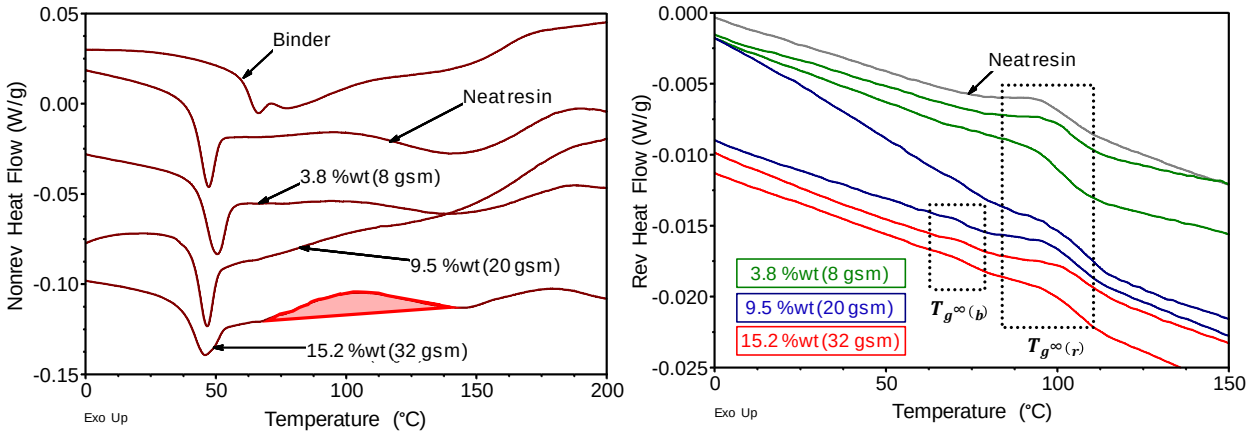

(a) (b)

Figure 40: Examples of 1st scan non-reversible signal (a) and 2nd scan reversible signal (b) thermograms of PH samples.

4.3.3.5 *ME* resin-binder mixtures

A summary of the results for the *ME* mixtures is presented in Table 21. The results presented in Figure 41(a) reveal that the sample with high binder concentration ($W_b = 15.23\%$) shows a relatively high residual heat of reaction ($H_r = 15.17\ J/g$) compared to the neat resin samples ($H_r = 9.48\ J/g$). The same observation was made with all the other binder chemistries.

Table 21: MDSC results of ME mixtures

Binder ratio (W_b)		n	First scan H_r [J/g]	First scan $T_{g(r)}$ [°C]	First scan $T_{g(b)}$ [°C]	Second scan $T_{g^\infty(r)}$ [°C]	Second scan $T_{g^\infty(b)}$ [°C]
Low	(3.81)	3	5.79 (2.45)	54.68 (3.24)	-	102.42 (0.5)	-
Medium	(9.51)	3	5.46 (0.60)	49.82 (3.49)	-	104.63 (1.77)	-
High	(15.23)	3	15.17 (5.93)	51.09 (2.43)	86.44 (6.27)	108.67 (2.24)	77.52 (0.78)

*The values presented in this table are averaged results ($\bar{x}$), the standard deviations (S_{n-1}) are presented in parentheses.

Furthermore, a second glass transitions ($T_{g(b)}$) is measured at 86.44°C during the first scan for samples with high binder concentration. The thermochemical characterization of this binder presented in Section 3 revealed a complex glass transition behaviour made of a combination of multiple glass transitions happening at T≈ 79, 93, 110 and 140°C. Thus, the relatively high variation observed in the $T_{g(b)}$ measurements (S_{n-1} of 6.27) could be caused by the binder intrinsic material variability. Thermograms of the second scan presented in Figure 41(b) illustrate the presence of a second glass transition for the sample with high binder concentration (15.21%).

Hence, the limit of allowable resin-binder ratio lies between 15.21% (32 g/m^2) and 9.51% (20 g/m^2), the last one being the highest acceptable known concentration.

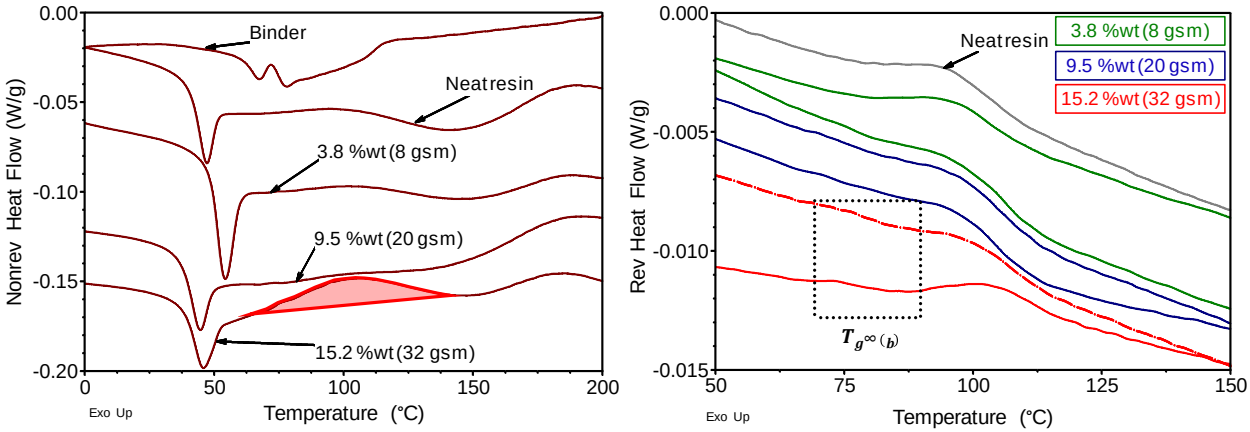

(a) (b)

Figure 41: Examples of 1st scan non-reversible signals (a) and 2nd scan reversible signals (b) thermograms of ME samples.

4.3.3.6 Discussion

The main conclusion of the MDSC experiment is that different binder chemistry will yield different impact on the resin thermochemical behaviour, hence each chemistry has a different ‘’compatible’’ concentration. Furthermore, the observation of higher residual heat of reaction with high binder concentration ($Aw_b = 32\ g/m^2$) suggests that the binder might influence the resin cure kinetics. Hence, the impact of high binder concentration on the cure kinetics needs to be verified with samples cured with a cycle representative of the production condition. Also, this effect was observed with the four binder chemistries hence suggesting that the main factor would be the high the amount of binder instead of material chemistry.

The results of the second was used to define the ‘’compatible’’ binder to resin ratio for each chemistry. The results obtained with the *EB* binder showed that the cure cycle might influence the resin-binder interactions as no trace of the binder could be found in the second scan thermograms. For the *ME*, *PH* and *CoPET* binders the presence of a second glass transition indicated the existence of a binder phase in the resin and was used to set the binder to resin compatible ratio. However, only the *CoPET* binder showed a T_g lower than the neat resin cured with the ‘’Production’’ cycle. Hence, in a production only the *CoPET* binder would represent a risk as it is the only binder with a T_g lower than the resin. The limits of compatible material concentration for each binder are presented in Table 22. A binder concentration is considered

‘’compatible’’ when no alteration of the resin thermochemical behaviour was observed. The values of material concentration expressed in binder to resin weight ratio (W_b) and binder areal weight (Aw_b) are evaluated considering the characteristic of the composite laminate presented in Table 13.

Table 22: Summary of compatible resin-binder concentration

Binder material	Maximal compatible binder concentration	
	W_b[%]	Aw_b[g/m^2]
CoPET	≤ 3.79%	8
EB	≥ 15.11%	27
PH	≤ 9.51%	20
ME	≤ 9.51%	20

4.3.4 Resin-Binder Mixture Ultimate Tensile Strength

Summary of results for the resin-binder mixtures tensile property characterization is presented in Figure 42. At least 6 samples were tested per configuration. The samples ultimate tensile strength (UTS) is the main characteristic evaluated with this experiment. Detailed results are presented in Appendix A.

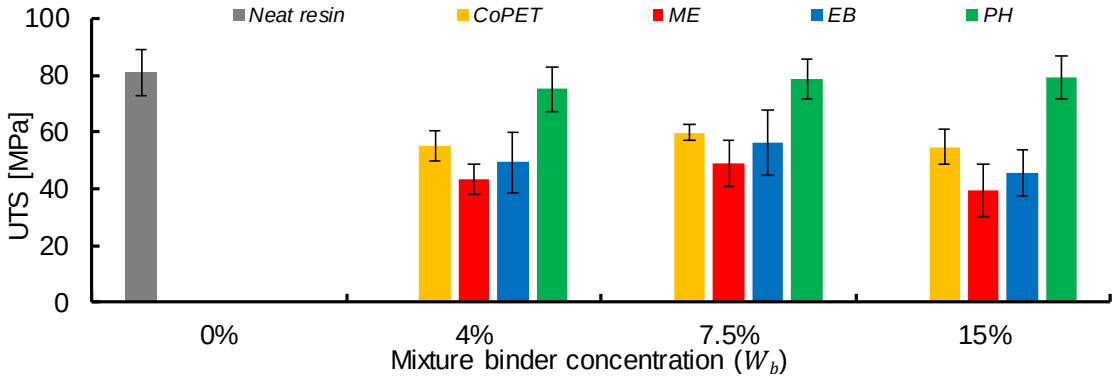

Figure 42: Results summary of resin-binder mixtures tensile property characterization. The error bars represent the standard deviation (S_{n-1})

The results indicate that the presence of binder lead to a reduction of the UTS for all resin-binder formulations tested and suggests that the material product (chemical composition) is the main determinant factor. The results show that the *PH* binder material has the lowest impact on the resin mechanical properties of all the evaluated binder material. The influence of the *PH* binder results in a reduction of 2.03 to 7.03% of the neat resin UTS (Δ_{REF}). More significant reduction ranging from 26.14% to 51.21% is observed with *CoPET*, *ME* and *EB* binder inclusively. The

binder particle size and morphology may have influenced the impact of the binder on the resin mechanical properties as some resin-binder interactions, like mechanical interlocking adhesive mechanism or binder solubility rate, are affected by these two characteristics. However, the review of the resin-binder interaction presented in Section 2.5 suggested that chemical interactions such as polymer miscibility or chemical bonding provides the strongest interfacial adhesion. The analysis of the UTS results agrees with this statement as the chemical composition of the binder material is a key factor determining the impact of binder material on the resin ultimate tensile strength. Furthermore, the graph presented in Figure 42 shows no upward or downward trend in the samples UTS suggesting that mixture concentration of binder material (W_b) is not a determinant factor for the resulting UTS properties.

4.3.5 DMA - Glass Transition Temperature and Flexural Modulus

MDSC experiments have shown that a high concentration of binder may influence the resin cure kinetics (increased of residual heat (H_r)) and that the cure cycle influences the outcomes of the resin-binder interactions. Hence, the evaluation of samples cured with the ‘’Production’’ cycle should indicate if this a high binder concentration may influence the resin thermo-mechanical properties in a production context. The results of the DMA characterization are presented in Figure 43. Detailed results are presented in Appendix A.

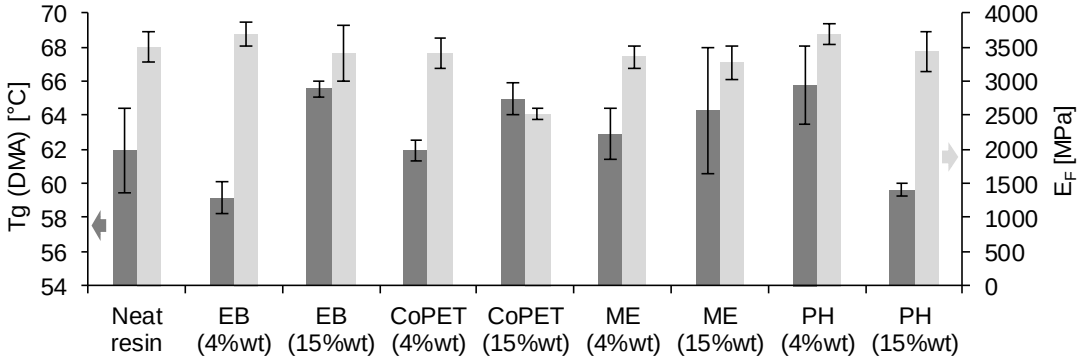

Figure 43: Average measured T_g*(DMA)* and flexural modulus (E_F), the error bars represent the standard deviation (S_{n-1}).

A glass transition temperature of 61.42°C was measured by MDSC with the neat resin sample cure with the ‘’Production’’ cycle (Section 4.3.3) which agrees with the values of 61.94°C measured by DMA. All the T_g measured with the resin-binder mixtures fits more or less within the variations observed with the neat resin samples. This suggests that the neither the chemical

composition nor the material concentration seems to have a significant effect on the resin apparent glass transition temperature. The thermochemical characterization of the binder material (Section 3.4.4) showed that the *ME* and *PH* binder have a higher T_g than the neat resin and that *EB* binder. Thus, no sign of these three binders was expected with the DMA experiments. However, even the *CoPET* binder with a significantly lower glass transition compared to the resin (15-16°C) did significantly affect the resin-binder mixture T_g measured by DMA. Hence, the T_g results suggest that the ''Production'' cure cycle was enough to eliminate the residual heat of reaction (H_r) caused by the high binder concentration since the measured T_g of all resin-binder samples are within the range of the resin properties.

The analysis of the flexural modulus (E_F) of the resin-binder sample shows that a high concentration of *CoPET* binder results in a diminution of the matrix properties. A flexural modulus of 3503.2 MPa was measured for the neat resin while 2528 MPa was measured with *CoPET* samples (W_b= 15.11%) representing a 27.83% reduction of the neat resin properties. This result suggests that a binder concentration identified incompatible with the MDSC methodology could potentially lead to a decrease of the resin thermo-mechanical properties when the T_g of resin is higher than the binder one.

4.3.6 Mechanical Behaviour of Composite Made with Bindered Fabrics

The chart presented in Figure 44 shows the averaged maximum load measured during the experiment (P_m) and the short-beam strength (F^{sbs}). Detailed results are presented in Appendix A. Results suggest that the presence of binder materials *ME* and *PH* have limited impact on the short beam strength as a slight reduction of -13.8% is observed with the *ME* chemistry and no significant impact for the *PH* binder. However, significant reduction of the short-beam strength is observed with the *SB_CoPET* (-53.3%) and *SB_EP* (-49.9%) samples.

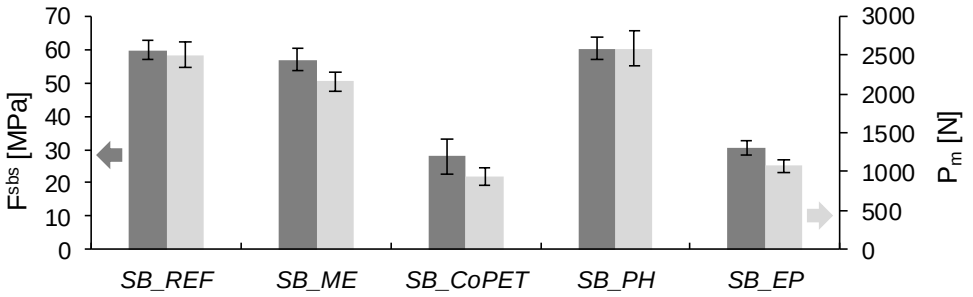

Figure 44: Averaged maximum load measured during the experiment (P_m) and the short-beam strength (F^{sbs}). The error bars represent the standard deviations (S_{n-1})

A correlation seems to exist between the samples short-beam strength and failure mode observed during the tests. The *SB_REF*, *SB_ME* and *SB_PH* samples failed by interlaminar shear-stress according to the D2344 standard guidelines (presence of crack in the resin between and absence of other damage mode). Furthermore, the standard states that the test should be terminated when the measured load reach a drop-off of 30%. These characteristics were observed with the *SB_REF*, *SB_ME* and *SB_PH* samples which also present the highest short-beam strength. An example of the curves obtained, and typical failure damage observed with these two configurations are presented in Figure 45 and Figure 47 respectively.

On the other hand, the *SB_CoPET* and *SB_EP* samples show a plastic deformation failure mode as well as the most important reduction of short-beam strength of 53.3% and 49.0% respectively. Example of the curves obtained with the *Co_PET* sample presented in Figure 46 (also representative of the *SB_EP* samples behaviour) illustrates the plastic deformation behaviour and the absence of load drop-off in the measured load. The calculation of the short-beam strength F^{sbs} (equation(4.7)) recommended by the ASTM standard had to be slightly modified as the measured load never reach the 30% drop-off of which normally signifies the end of the experiment. Instead, the experiments were stopped when the head travel exceeded the specimen nominal thickness. Hence, the maximum load P_m value used for these two sample was taken when the curves showed a drop off of the sample stiffness as presented in Figure 46. However, such failure mode (Figure 48) could be considered the result of interlaminar shear stress since there were no signs of compressive or tensile failure damage and that the presence of interlayers cracks was the main observed failure damage.

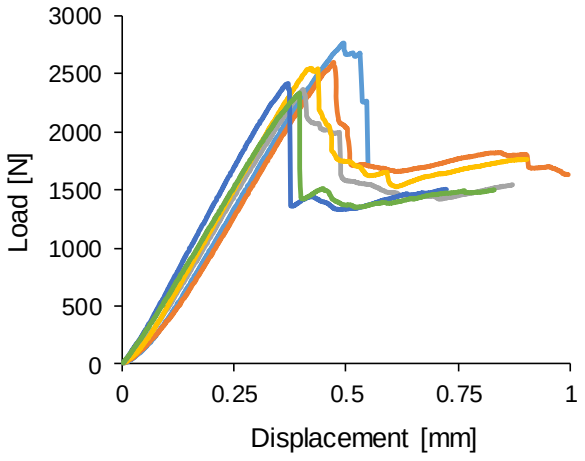

Figure 45: Measured load in function of crosshead displacement for the *SB_REF* samples.

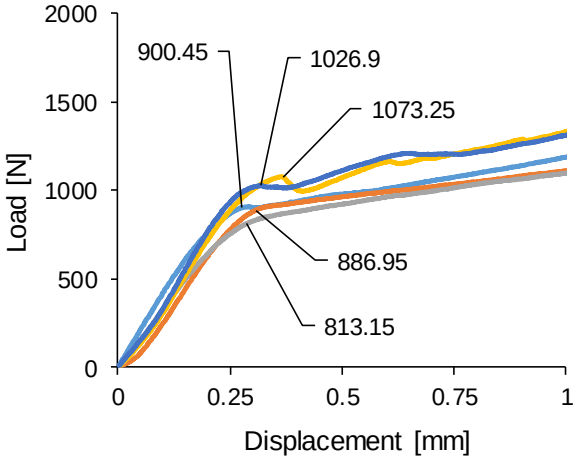

Figure 46: Measured load in function of crosshead displacement for the *SB_CoPET* samples.

Figure 47: Typical interlaminar shear failure mode observed with *SB_REF* and *SB_ME* samples

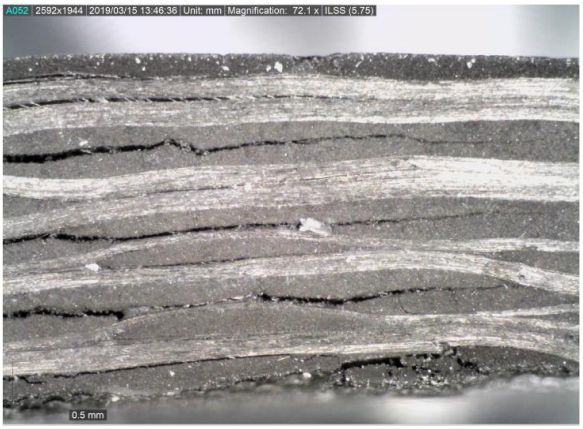

Figure 48: Typical extended plastic deformation failure mode observed with *SB_CoPET* and *SB_EP* samples

4.3.6.1 Discussion

Analysis of results showed that the short-beam strength of a composite material could be significantly influenced by the preforming process. However, it is not obvious which of the preforms characteristic (binder chemical composition, material concentration or the consolidation process itself) have the greatest impact on the laminate mechanical properties.

The reduction of the *SB_CoPET* sample short-beam properties was expected as the presence of *CoPET* binder material led to a reduction of resin ultimate tensile strength and flexural modulus. However, the reduction of the ILSS properties measured for the *SB_EP* sample was not expected as the binder material (*EP*) is claimed epoxy compatible, applied in controlled low concentration and approved for aerospace applications. These two samples have not only presented

lowest short-beam strength and plastic deformation failure mode but have also shown the highest V_f estimations (58.2% and 59.6% respectively) of all tested samples. This is the only similarity between these two samples as the other preform characteristic such as binder chemistry (copolyester versus epoxy based), application processes (manual on one face versus industrial on both side) and material concentration (34.96 g/m^2 versus 11.17 g/m^2) are significantly different. Wu *et al*. [52] showed that the presence of binder material combined to the application of high temperature during the preform consolidation process may enhance the compaction behaviour, ultimately resulting in higher fibre volume fraction. S. van Oosterom *et al*. [53] have shown that the influence of binder material on the preform compaction behaviour may lead to modifications of the flow behaviour during the injection process. Hence, the comparison between the *SB_CoPET* and *SB_EP* preforms characteristics suggest that the short-beam strength reduction could be potentially caused by an inefficient wetting of the reinforcement fabric layers. Furthermore, an increase of fibre volume fraction (V_f) would result in a reduction of the resin volume fraction (V_r) and to an increase of binder to resin ratio (V_b) of the composite (equation (4.2)). Hence this would be increasing the risk of reaching an incompatible binder concentration. The estimated resin weight ratio (W_b) of sample *SB_CoPET* presented in Table illustrate that the resulting binder concentration (19.4%) is incompatible according to the conclusions of previous evaluation method (MDSC and DMA.).

The results of *SB_ME* tends to confirm that the reduction of the ILSS properties is caused by a combination of incompatible binder to resin ratios and potential poor fibre wetting. The tensile mechanical characterization experiments (4.3.4) revealed that the *ME* binder may reduce the resin properties independently of the concentration used. However, the binder to resin ratio of sample *SB_ME* (9.36%) was judged compatible by the MDSC characterization experiments. Hence, the slight reduction of the sample short-beam strength might be caused by the negative impact of the binder on the resin mechanical properties but haven't led to severe reduction of the laminate properties because the concentration used is considered compatible at the thermo-mechanical level (MDSC). The results of the *SB_PH* samples agree with this conclusion as the results shows that *PH* binder leads to no reduction of the short-beam properties (+0.09%), which is coherent with the resin-binder mixture tensile mechanical conclusions obtained with this binder.

In conclusion, the evaluation the short-beam strength helped to better understand the impact of bindered preforms on the mechanical properties of fabric reinforced composite laminates. The results showed that over compaction of the preform that may result in severe reduction of the laminate short-beam strength (potential poor fibre wetting, increased binder to resin ratio). Hence, this indicates that the compaction behaviour of preform in function of temperature and binder concentration should be investigated. The good short-beam strength properties of *SB_ME* and *SB_PH* samples shows that used in proper conditions (compatible binder concentration, proper preforming process) binder material might lead to minimal or no impact on the composite laminate mechanical properties (short-beam strength). Also, the small difference observed between the *SB_ME* and *SB_PH* samples suggest that the conclusions of the resin-binder tensile mechanical properties evaluation had forecast the slight reduction of the short-beam strength properties.

4.4 Summary and Recommendations

4.4.1 Discussion on Evaluation Methods

Rheology:

This method did not provide any clear information on the binder solubility behaviour or on the impact of binder on the resin cure behaviour. However, it revealed that the binder *EB* ($W_b = 4.14\%$) yielded the highest increase of resin initial viscosity (η_i^*). Furthermore, it is suspected that the binder-resin interaction of the small-scale (rheometer sample) probably lacks representativeness of the large scale (resin flow behaviour during injection).

Microscopy:

This method allowed to categorize the binder solubility behaviour using qualitative criteria (non-soluble, partly soluble and soluble). One key finding of this experiment is the assessment of binder material phase for all low concentration samples, hence allow to evaluate the efficiency of MDSC to identify separate binder phase.

MDSC:

The presence of binder phases in some of the low and medium concentration sample was no assessed while it has been confirmed with the microscopy experiments. However, this may suggest that the presence of such separate binder phases is not enough to affect the resin thermo-chemical

properties. In general, the MDSC experiments have provided useful information on many aspects of the resin thermochemical behaviour such as the glass transition temperature and resin cure kinetics.

UTS:

These experiments led to the conclusion that the resin tensile behaviour is mostly influenced by the binder chemical composition and less sensitive to the material concentration (at least for the concentration tested).

DMA:

These experiments revealed the extent of the impacts of binder materials on the resin thermo-chemical properties. The results suggested that a separate binder material phase does not influence the resin apparent glass transition temperature behaviour if the binder transition is higher than the resin. This method also revealed that a high concentration ($W_b \approx 15\%$, 32 g/m^2) the *CoPET* binder may significantly reduce the resin flexural modulus.

ILSS:

This experiment showed that the preforming process might influence the resulting mechanical behaviour of the composite. Over compacted preforms have presented severe reduction of the laminate short-beam strength. It also showed the influence of binder to resin ratios and suggest that the MDSC is an acceptable technique for the determination of compatible binder ratio. This experiment also revealed that the negative effect of binder on the resin ultimate tensile strength could translate into a slight reduction of the laminate short-beam strength.

4.4.2 Binder Material Recommendation Based on the Thermo-Mechanical Properties

A results summary of the resin-binder interactions evaluations is presented in Table 23. The impact of binder (average for all tested conditions) on the resin initial viscosity ($\eta_i{}^*$), resin ultimate tensile strength (UTS) and resin flexural modulus (E_f) is presented in terms of percentage of reduction or increase a reference material property value (matrix, fabric reinforced polymer etc.). The solubility behaviour categorization from the microscopy experiments and the compatible binder concentration identified by MDSC are also presented. Finally, the overall compatibility categorization of the binder material is also presented in this table.

Table 23: Summary of resin-binder interaction characterization

Material	**Phase 1**		**Phase 2**			**Phase 3**	**Compatibility**
	η_i^*	Solubility	MDSC	UTS	DMA (E_f)	ILSS	
CoPET	+32%	No	$\boldsymbol{W_b = 3.79\%\ (8\ g/m^2)}$	-30%	-28%	-53%	Low
EB	+49%	Partly	$\boldsymbol{W_b > 15.11\%(27\ g/m^2)}$	-38%	-	NA	Acceptable
ME	+33%	Partly	$\boldsymbol{W_b = 9.51\%\ (20\ g/m^2)}$	-46%	-	-5%	Acceptable
PH	+24%	Partly	$\boldsymbol{W_b = 9.51\%\ (20\ g/m^2)}$	-4%	-	+0.1%	Good

The *EB* binder is considered to have a best compatibility with the epoxy resin of all studied binder for binder to resin weight ratio (W_b) up to 15.11% and areal weight of 27 g/m^2. The EB binder has shown to have a negative impact on the resin tensile properties (UTS). However, the ILSS characterization suggested that negative effect of binder on the resin ultimate tensile strength (UTS) results to a slight reduction of the laminate short-beam strength. Unfortunately, not enough material was available to confirm this hypothesis with this specific binder. MDSC experiments have revealed that the effect of this binder on the resin thermo-mechanical could be ‘’erased’’ by the cure cycle. The results of the DMA experiments suggest that the ‘’Production’’ cure cycle is enough to eliminate the residual heat of reaction (H_r) caused by the high binder concentration. This binder also showed the highest impact on the resin viscosity, but because of the suspected non-representativeness of this experiment its conclusions are not considered.

The *PH* binder would be the second recommended material as it showed to have an acceptable compatibility behaviour with the epoxy resin. This material showed almost no impact on the resin-binder mixture UTS. This absence of impact on mechanical properties was validated with the evaluation of composite laminate short-beam strength. This binder revealed to have no impact on the resin thermo-mechanical properties at the medium concentration and no impact on the resin flexural modulus at high concentration. This binder is judged compatible for binder to resin weight ratio (W_b) of 9.51% and areal weight of 20 g/m^2.

The *ME* binder was also attributed an acceptable compatibility behaviour with the epoxy resin for binder to resin weight ratio (W_b) of 9.51% and areal weight of 20 g/m^2. Even if this binder showed a significant reduction of the resin UTS (-46%) properties, it showed only a slight reduction of the composite laminate short-beam strength (-5%). It also showed no influence on resin thermophysical properties (MDCS) at the medium concentration and no significant influence on thermo-mechanical properties (DMA) at high concentration.

The *CoPET* revealed the lowest compatibility behaviour of all material tested, showing a compatible behaviour only for the lowest binder concentration evaluated ($W_b = 3.79\%$, $Aw_b = 8\ g/m^2$). This binder revealed to cause a significant reduction of the resin tensile properties and to influence the resin thermochemical behaviour for binder to resin concentration of 9.42%. Furthermore, this is the only binder who led to a reduction of the resin flexural modulus.

5. Experimental Permeability Evaluation of Bindered Preform

This chapter presents the experimental work done to investigate the influence of different preforming methods on in-plane and out-of-plane preform permeability. Seven preforming processes with four different binder materials are evaluated. First the material used, and details of the studied preforming process are described. Next, the test bench and experimental procedures used are detailed followed by the presentation and analysis of the results. Finally, guidelines for preforming process development and optimization to achieve best mould filling results are presented.

5.1 Material

5.1.1 Fabrics

Two 5 harness satin weaves with the same amount of yarn/inch in the warp and weft direction were used for the sample fabrication. Fabric *D* and *B* areal weight are 380 g/m² and 368 g/m² respectively. Fabric *B*, already introduced in Chapter 4, was supplied with 14 g/m² of epoxy powder coated on both sides. Hence, the total areal weight of fabric *B* including the weight of the binder material was 382 g/m².

Table 24: Fabric Characteristics

Fabric	Fibre type	Weave	Areal weight [g/m²]	Warp [yarns/inch]	Weft [yarns/inch]	Tow Count	Other
D	Carbon	5 Harness	380	12	12	6K	
B	Carbon	5 Harness	368 (382*)	12	12	6K	*Binder concentration ≈ $14\ g/m^2$

5.1.2 Binder Material

Four different binder materials are studied in this chapter. The binder material precoated on fabric *B* by the fabric supplier is an epoxy powder (*EP)*. Manufacturing of precoated fabric involve the utilisation of industrial coating processes (e.g. Hot-melt adhesive application [82]) to apply the binder material. The second studied epoxy power is the binder material *EB* which was already introduced in Chapters 2, 3 and 4. This binder was supplied in powder form thus had to be manually scattered on the surface of the fabrics. Binder material *CoPA12* and *CoPA40* are

thermoplastic copolyamide adhesive webs. Copolyamide adhesives web a commonly used because of their cost effectiveness and relatively easy processing. Table 25 presents the binder material studied in the present chapter.

Table 25: Binder Material

Binder	Chemistry	Density	Melting Temperature	Physical form
EP	Modified epoxy	Unknown	ca. 60°C	Powder precoated on Fabric B
EB	Epoxy-based	550±50 kg/m³	90±15 °C	Powder
CoPA40	Copolyamide	40 g/m²	82-112 °C	Adhesive web
CoPA12	Copolyamide	12 g/m²	82-112 °C	Adhesive web

5.1.3 Test Fluid

The test fluid used for the permeability measurements is the XIAMETER PMX-200 silicone oil. Technical properties of the silicone fluid are presented in Table 26. A test fluid is used instead of an actual resin to have a stable fluid viscosity during the entire injection process. The viscosity of a thermoset resin will increase accordingly to the evolution of the degree of cure and may cause problems for the permeability evaluation. Ideally, the selected test fluid should have similar viscosity properties to resin intended to be used in the actual manufacturing process. Viscosity values of some commercial resin designed for LCM presented in Table 27 shows that the XIAMETER PMX-200 is an acceptable test fluid in terms of viscosity properties.

Table 26: XIAMETER PMX-200 technical specification

Appearance	Viscosity [cP]	Specific Gravity at 25°C
Crystal clear	96.4	0.964

Table 27: Commercial resin viscosity

Resin	Injection Temperature	Viscosity
EPIKOTE Resin System 600	80°C – 120°C	300 cP – 50 cP
Cycom 890 RTM	80°C – 120°C	250 cP – 50 cP
Resin XB 3585 /Aradur®3486	30°C	208 cP – 380 cP

5.2 Sample Fabrication

5.2.1 Cutting Process

All plies for the sample fabrication were cut using a 2D CNC cutting table to assure maximum level of accuracy and repeatability. The cutting dimensions for each experiment are

shown in Figure 49. All the in-plane permeability samples were cut making sure that the length *L* was aligned with the warp (0°) direction of the original fabric roll.

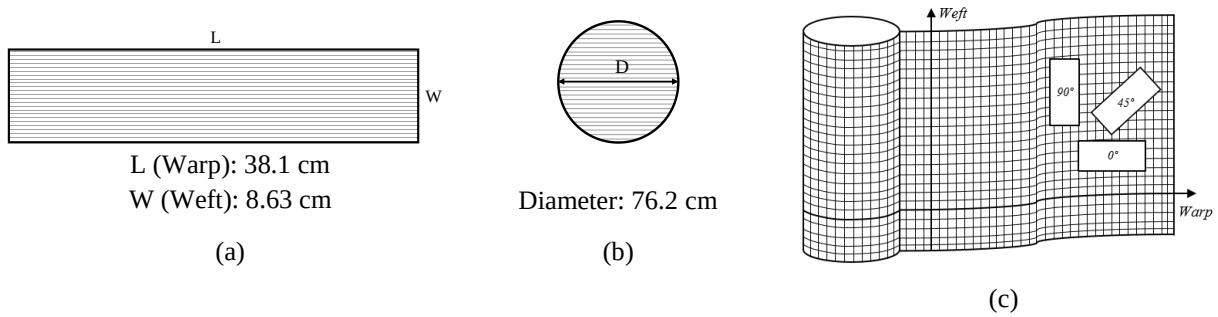

Figure 49: Schematization of (a) in-plane permeability sample, (b) out-of-plane permeability sample and (c) fabric roll versus sample orientations

5.2.2 Preforming Process

The preforms construction parameters that are non-related to the preforming process were fixed for all studied configurations to minimize their impact on the mould filling behaviour. The same reinforcement material and stacking sequence were used for the fabrication of all preform samples. Combined with the fixed geometry of the test bench injection cavity, all samples have the same theoretical fibre volume fraction (V_f) of 55% when the volume of the binder is not considered. The details of the preforms fixed parameters are presented in Table 28.

Table 28: Preforms fixed construction parameters

Fabric	Stacking Sequence	Targeted V_f
5HS / 6K / 368-380 g/m^2	$[0°]_5$	≈55%

Different factors related to the binder application process are studied with this test plan. The type of binder material is examined through the comparison of bindered fabric coated with powder and adhesive web binders. The impacts of binder application process parameters such as the temperature, pressure, time and material concentration are also studied. Different binder application techniques like industrial coating process, manual powder sifting and local powder application are also covered by this test plan. The influence of the preforming process is assessed by comparing two sample configurations made with the same fabric and binder material. The first one is a stack of bindered fabrics and the other a 3D preform. All information related to the fabrication of the seven studied preform combinations is shown in Table 29.

Table 29: Preform Fabrication Process Parameters

Preform sample	Fabric	Binder (g/m^2 | wt%*)	Preforming Parameters	
			Binder Application	Preforming
REF	*D*	None	NA	None
P1-3D	*B*	*EP* (≈ 14 | ≈ 4%)	Industrial process	Thermoforming: (-47.5 kPa | 60 min | 65°C)
P1	*B*	*EP* (≈ 14 | ≈ 4%)	Industrial process	None
P2	*D*	*EB* (≈ 19 | ≈ 5%)	Manual powder scattering (full) Thermoforming (-98.2 kPa | 85°C | 45 s)	None
P2-L	*D*	*EB* (≈ 19 | ≈ 5%)	Manual powder scattering (local) Thermoforming (-98.2 kPa | 85°C | 45 s)	None
W1	*D*	*CoPA40* (≈ 40 | ≈ 10.5%)	Industrial Pressure Laminating (344 kPa | 126°C | 4.57 m/min)	None
W2	*D*	*CoPA12* (≈ 12 | ≈ 3.4%)	Industrial Pressure Laminating (344 kPa | 93°C | 3.05 m/min)	None

* $wt\ \% = binder\ weight$ \| fabric weight

Dry fabric preform (*REF*):

The sample *REF* is the only preform combination that is free of binder material. This sample is intended to measure the reference permeability behaviour to assess the impact of the studied preforming technique.

Precoated fabric and 3D preform (*P1* & *P1-3D*):

The *P1-3D* configuration was made with the fabric *B* precoated with the epoxy powder *EP*. It has been presented in Section 2.7 that different compaction levels of bindered preforms can be achieved by varying the preforming process parameters. Process parameters used for preforming of the samples *P1-3D* to achieve the desired thickness of 2.1 mm (height of the injection cavity being 1.95 mm) are presented in Table 29.

The *P1* configuration was also made with fabric *B* precoated with modified epoxy binder *EP*. However, no preforming process was performed for this configuration. Hence, *P1* is actually a stack of non-consolidate bindered fabric. Comparison of the results between samples *P1-3D* and *P1* should demonstrate the impact of the preforming process on the mould filling behaviour. The areal weight of precoated binder *EP* reported in Table 24 (≈ 14 g/m^2, ≈ 4 wt%) was evaluated from the measured total areal weight of preforms made with fabric *B* during the experiments. The procedure to measure the experimental areal weight of a fabric is presented in the further Section 5.6.

Manual powder application (*P2 & P2-L*):

Powder binder *EB* was manually scattered on top face of fabric *D* to make the bindered fabrics for the preform samples *P2* and *P2-L*. First, the binder was deposed using a lab sieve device, then the material was consolidated by a heated vacuum process for each layer. Parameters of the coating process are presented in Table 29. As presented in Section 2.3, the standard concentration of binder used by suppliers for the manufacturing of bindered fabric varies between 2 and 10% of the fabric areal weight. For the present study the targeted binder concentration was fixed at 5% of fabric *D* areal weight representing 19 g/m^2 in equivalent areal weight. For preform samples *P2* the powder was scattered over all the surface of the fabric. For *P2-L* stencils were used to limit the material deposition to specific areas of the fabric. Linear application of binder material was simulated as presented in Figure 50.

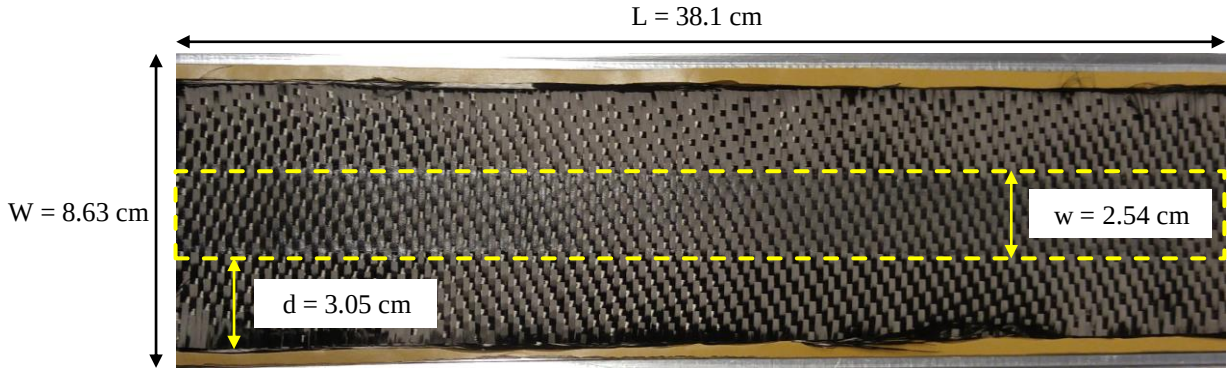

Figure 50: Local binder application (*P2-L*). The binder application limits represented by the dash lines

Adhesive webs (*W1 & W2*):

Preform samples *W1* and *W2* were coated using an industrial pressure laminating process performed by the binder material supplier. The difference between these two samples is not only density of the binder material used (40 g/m² and 12.9 g/m²) but also the intensity of the coating process. The coating parameters used for the fabrication of these bindered fabrics are presented in Table 29. The process temperature for the manufacturing of bindered fabric *W1* was set to 126°C which is above the binder material melting range of 82-112 °C leading to an increased spread of the material on the fabric surface. On the other hand, the lower temperature used for the manufacturing of *W2* bindered fabric has resulted in a lower spread of the material on the fabric surface. The pictures presented on Figure 51 shows the impact of the preforming parameters on the binder morphology.

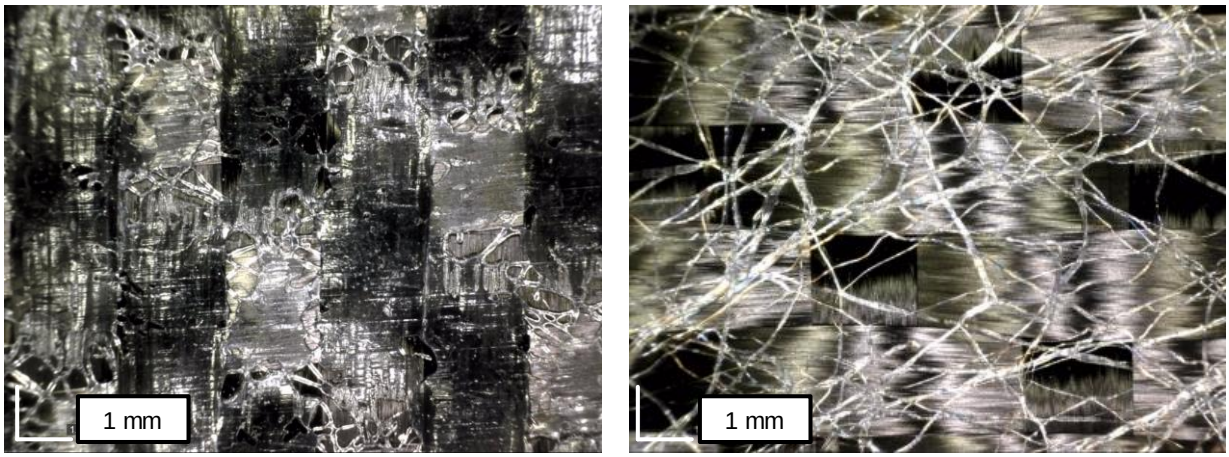

(a) (b)

Figure 51: Binder morphology of *W1*(a) and *W2*(b) bindered fabric

5.3 Test Plan

The unsaturated in-plane permeability was measured from longitudinal injections at constant injection pressure following the standard method proposed by Alms *et al*. [83]. The main reason why unsaturated in-plane permeability is measured instead of saturated permeability is that numerical filling simulations are using unsaturated values [84]. Preform samples *P2-L* and *P2* were excluded from the out-of-plane (transverse) permeability measurement. The test plan followed for the evaluation of the permeability is presented in Table 30.

Table 30: Permeability evaluation test plan

Permeability	**Samples**
In-plane (K_x)	*REF, P1, P1-3D, P2-L, P2, W1, W2*
Out-of-plane (K_z)	*REF, P1, P1-3D, W1, W2*

5.4 Test Bench

5.4.1 In-Plane Permeability Test Bench

The in-plane permeability test bench was designed to perform longitudinal injection at constant pressure following the guidelines proposed by Alms *et al*. [83]. The test bench design requirements are presented in Table 31.

Table 31: In-plane permeability test bench design requirements

Requirements	Values
Cavity dimensions	100 mm by 400 mm
Cavity thickness	1.95 mm
Injection pressure	207 kPa (liquid tight up to 310 kPa)
Injection strategy	Longitudinal injections, linear resin inlet and outlet VARTM injection system (pressure pot and vacuum assistance)
Clamping system	Out of press, must support injection pressure
Dimensional tolerance	Max mould deflection during injection: 2% of the nominal thickness
Special feature	See-through top mould surface for data acquisitions and observed flow behaviour

The test bench is made from a 25.4 mm thick aluminum machined plate as a bottom mould. The top surface of the mould is a 50.8 mm thick acrylic bloc. A silicone flat gasket (1.59 mm thickness, 60A hardness) provides the sealing of the bench. The clamping system is assured by 14 bolts directly fastened into the aluminum bottom mould. A general view of the test bench is presented in Figure 52. The cavity thickness is assured by the design of the sealing system. The sealing gasket is compressed between the top and bottom mould until the top mould get in contact as shown in Figure 53. The design also respects the recommended preform aspect ratio of L:W>3. The cavity thickness is slightly lower than the recommended value of 2.5 mm to 10 mm. The actual cavity thickness of 1.95 mm was chosen to be more representative of the overall part thickness moulded by Hutchinson. The maximum mould deflection was evaluated using the finite element analysis software Abaqus. For a 207 kPa injection pressure the estimated mould deflection was 2.25% of its nominal thickness which is slightly higher than the recommended value of 2% but acceptable for this situation.

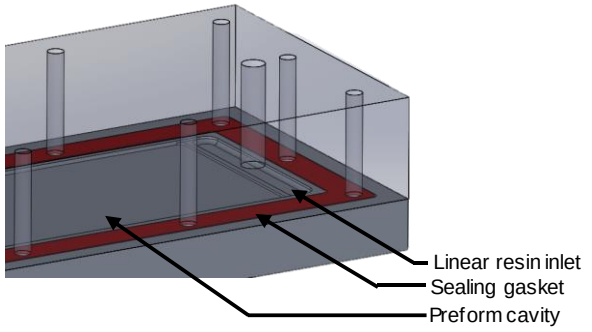

Figure 52: In-plane permeability test bench

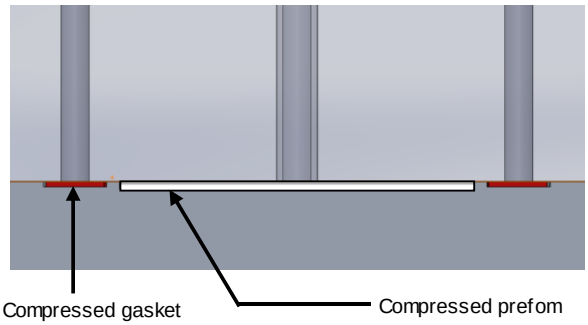

Figure 53: In-plane permeability test bench cross section

5.4.2 Out-of-Plane Permeability Test Bench

This bench was designed and fabricated by the McGill Structures and Composite Materials Laboratory. Through the thickness (or out-of-plane) injection can be performed on this test bench to measure the transverse permeability of a stack of fabric. An exploded view showing all the different part of the test bench is presented in Figure 54. The diameter of the injection cavity is fixed at 7.62 cm while the height of the cavity needs to be manually adjusted. When the mould is assembled, the sample to be measured sits between the base of the test bench and the perforated closing plate. Then, the bolt place in the centre of the test bench is used to adjust the height of the cavity. Changing the height of the cavity allows to control the compaction level of the sample hence to reach the desired volume fraction V_f for the studied preform. This bench is designed to work for standard resin transfer moulding (RTM) injection strategy. The injection pressure required to perform the injection was provided by a pressure pot. Two pressure sensors are installed on this bench. The first one is placed in the bottom part of the bench to measure the inlet injection pressure. The second is placed in the closing plate to measure the outlet pressure. The injected fluid is collected in a recipient from the outlet of the test bench. The same recipient is placed on a scale to measure the fluid flow rate of the injection. A data acquisition system (DAQ) is used to record both pressure and the weight measured with the scale as a function of time. A LabView script is used to display the sensors signals on a monitor. The complete out-of-plane injection setup is presented in Figure 55.

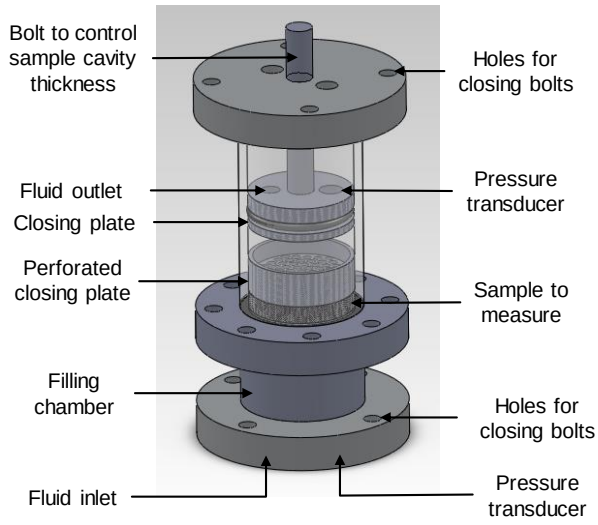

Figure 54: Transverse permeability test bench

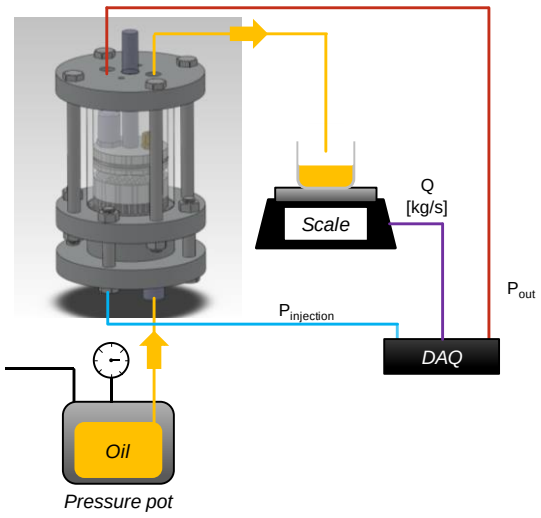

Figure 55: Out of-plane injection setup

5.5 Experimental test procedure

5.5.1 Injection Procedure for Measurement of In-Plane Permeability K_x

The following steps describe the experimental procedure for the longitudinal injections at constant pressure performed to measure the in-plan permeability. A simplified representation of in-plane permeability measurement experimental setup is shown in Figure 56.

1. Check and note room temperature before each injection.
2. Measure and note the following preform characteristics:
    a. The mass M_f, the thickness $h_\circ$, length L and width W
3. Place two strips of damming material (Airdam 1) on both side edges of the bottom mould
4. Place the preform inside bottom mould cavity so it is flush with the resin outlet
    a. Careful manipulation of the layers is required to minimize fabric fraying and keep fibre alignment
5. Assemble top mould (including bolts and gaskets) and bottom part of the mould
6. Tighten of all bolts and assure the compaction of the material inside the cavity. For the tightening of the bolt follow the bolt numbering identified on the test bench.
7. Connect the vacuum line and verify that a minimum vacuum of -98.2 kPa is achieved
8. Pressurize the pressure pot to desired injection pressure (207 kPa)
9. Connect oil line to the inlet fluid fitting on the test bench (oil line valve most be closed)

10. Start the video and time recording to record the flow front position in function of the time (X_{ff}, *time*)
11. Open valve on oil line to start injection
12. Note the injection initial pressure on the pressure pot analogical gauge ($P_{inj,ini}$) and on the digital manometer connect to the vacuum at the outlet ($P_{vac,ini}$)
13. Wait for the fluid to flow out from the outlet, then measure the end of injection pressures ($P_{inj,end}$ & $P_{vac,end}$).
14. Close the oil line valve and disconnect all tubes from the test bench
15. Disassemble the test bench, dispose of the fabric properly and wash all parts of the test bench that have been in contact with the oil.

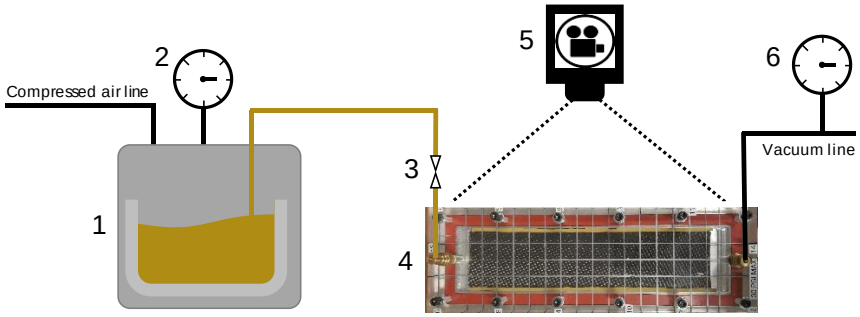

Figure 56: Simplified representation of in-plane permeability measurement experimental setup

The flow front position in function of the time ($X_{ff,i}$, t_i) is the main information to collect during these experiments. All the other variables needed for the permeability evaluation using equation (5.2) can be estimated using theoretical relations or found in technical documentation. However, some parameters are measured to increase the representativeness of the experiments. This is the case of the mass of the preform M_f that needs to be measured to latter evaluate the preform porosity ϕ. In theory the injection process must be proceeded at constant pressure. However, but for many reasons the pressure values set initially may vary slightly during the injection process. Hence, to consider this variation, the pressure was measured at the inlet and the outlet of the mould at the very beginning of the injection and right before ending the injection. An

average value for the pressure gradient ΔP is estimated with equation (5.1) and later used for the evaluation of the preform permeability (K_{exp}).

$$\Delta P = \frac{(P_{inj,ini} + P_{inj,end})}{2} - \frac{(P_{vac,ini} + P_{vac,end})}{2} \quad (5.1)$$

5.5.2 Injection procedure for measurement of out-of-plane permeability K_z

The following steps described the experimental procedure to measure the out-of-plane permeability using the out-of-plane test bench presented in Section 5.4.2.

1. Place the preform on the perforated section of the bottom part of mould
2. Place the perforated closing on the preform followed by the upper part of the bench
3. Tight the four closing bolts to make sure that all sealing gaskets are firmly compressed
4. Adjust the height of the injection cavity with the central bolt to obtain the desired sample compaction level
5. Make sure that the data acquisition system and the monitoring equipment (pressure sensors and scale) are all turned on and functioning
6. Start data acquisition, then start injection process
7. Set a given injection pressure and wait for the stabilization of the measured flow rate and pressures signals. An example of injection procedure is presented in Figure 57.
    a. Test at least five different injection pressures between 69 and 310 kPa in one experiment

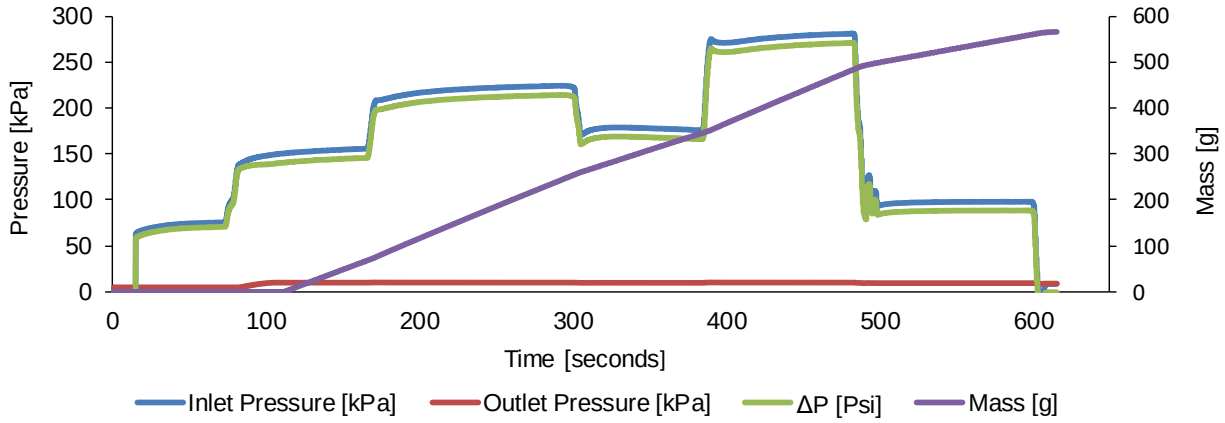

Figure 57: Example of recorded data of transverse permeability measurement

Some details of the transverse permeability injection required more attention. The cavity height needs to be carefully verified to assure the right compaction level of the preform. The

pressure dwells need to be held until the measured pressure gradient and scale flow rate appeared to be stable. The measured pressure at the outlet should always be close to zero (≈ 7 kPa or less). If higher pressures are measured at the outlet (over ≈ 20 kPa), this is a sign of race tracking somewhere in the cavity, thus invalidating the measured permeability values.

5.6 Experimental Permeability Evaluation Procedure

5.6.1 In-Plane Permeability

Alms *et al*. [83] have proposed a standardized procedure to measure experimental unsaturated permeability K_{exp} based on equation (5.2) derived from Darcy's Law (equation (1.1)).

$$K_{exp} = \frac{x_{ff}^2 \cdot \phi \cdot \mu}{2 \cdot \Delta P \cdot t} \tag{5.2}$$

This method uses the inlet injection pressure P_I for the evaluation of the experimental permeability. However, in the present work, the vacuum has been applied during the injection, hence the total pressure gradient ΔP (equation (5.1)) is considered instead. The preform areal weight A_w is evaluated with equation (5.3) where M_f is the mass, L the length , W the width and N_L the number of layers of the preform.

$$A_w = \frac{M_f}{L\,W\,N_L} \tag{5.3}$$

The concept fabric porosity ϕ and fibre volume fraction V_f were both introduce in Section 1.3.1.1 and are evaluated using equation (1.5) and (1.6) respectively. It is important to mention that the binder was considered in the evaluation of the fibre volume fraction in this chapter. Hence, the volume fraction V_f represent the volume of both the fibres and the binder material. The flow front positions x_{ff} are measured from the recorded video of the injection. Each time the flow front is crossing a measuring point x_{ff}, i the time t is noted. Then, the series of paired data are plotted on a graph to show the evolution of the flow front position over time as presented in Figure 58(a).

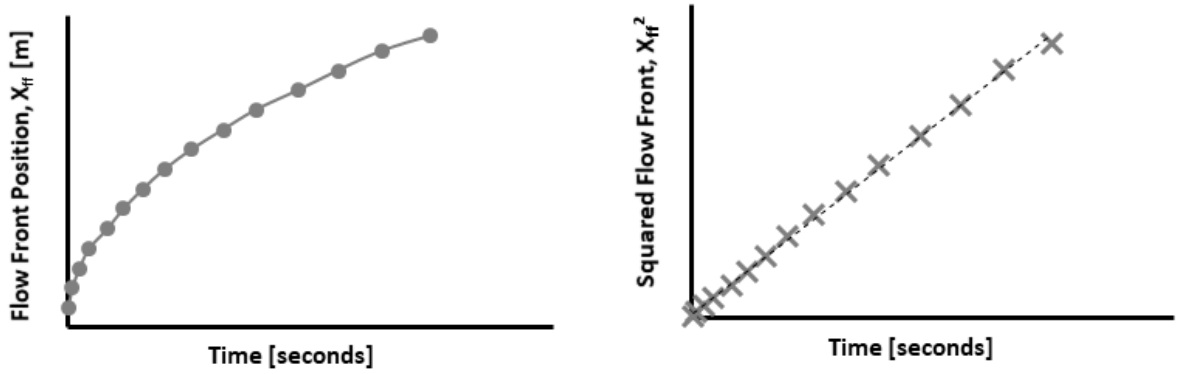

(a) (b)

Figure 58: Example of (a) flow front position as a function of time and (b) squared flow front position as a function of time

Next, the squared flow front x_{ff}^2 is computed and plotted as a function of time on a graph from which a linear trend can be obtained. Equation (5.1) can be derived to include the parameter m which is the slope of the linear trend obtain from the squared front flow data presented in Figure 58(b). Then, equation (5.4) can be used to compute the experimental permeability.

$$K_{exp} = \frac{\phi\,\mu}{2P_I} m \tag{5.4}$$

5.6.1.1 Error of Measure

The error of measure for in-plane permeability measurements is evaluated with the following equation, as recommended by the procedure proposed by Alms *et al*. [83]

$$\epsilon = 100 \times \sqrt{\frac{1}{n}\sum_{i=1}^{n}\left(x_{ff,i} - \sqrt{m\,t_i}\right)^2} \tag{5.5}$$

5.6.2 Out-of-plane Permeability

At the time of doing these experiments, there was no official standard method proposed for the measurement of the out-of-plane permeability like the one proposed for the in-plane measurement. However, out-of-plane permeability is generally measured following similar procedures [16, 84]. The first step is to evaluate the ratios of measured injection mass flow rates Q_m over the applied pressure gradients ΔP. In this thesis the average value of measured flow rate Q_m is evaluated from a linear approximation of the measured data. An example is presented on Figure 59.

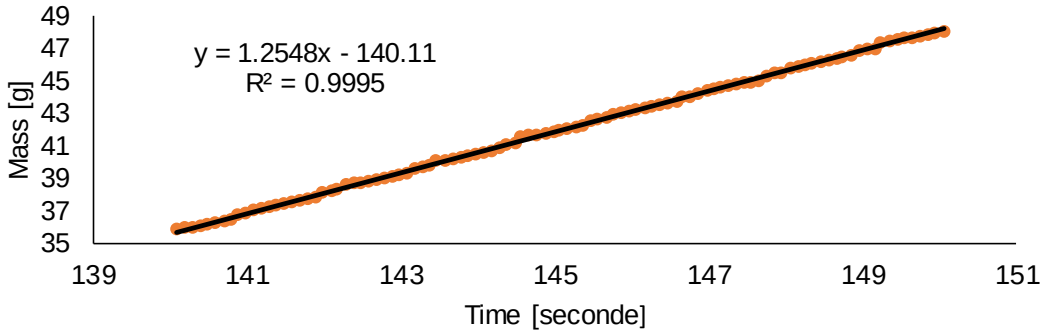

Figure 59: Example of Q_m measurement at 152 kPa injection pressure plateau (*REF* 3rd trial).

Then the mass injection flow rate Q_m is converted into volumetric flow rate Q. By plotting these combinations of $Q/\Delta P$ a linear correlation can be found and the slope m_z evaluated. For certain experiments some $Q/\Delta P$ data points seemed to deviate from the general linear trend and were then excluded from the linear correlation evaluation. Figure 60 shows an example of linear correlation of $Q/\Delta P$ data points with one discarded value identified by the red x marker.

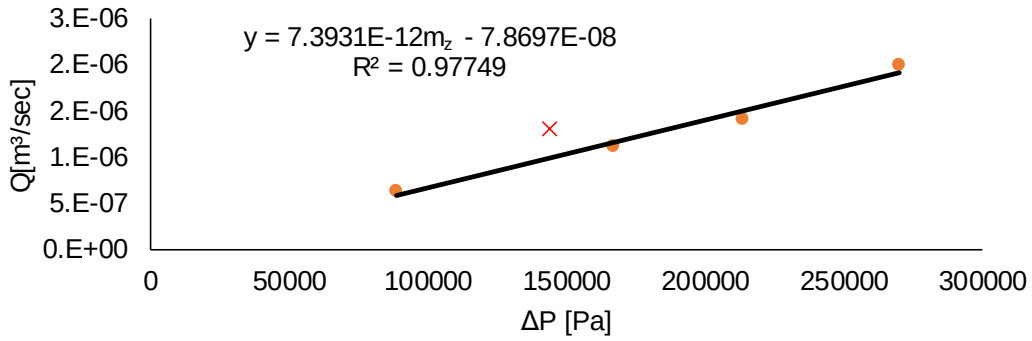

Figure 60: Evaluation of the variable m_z by linear correlation (*REF* 3rd trial)

Then, the out-of-plane permeability can be evaluated using equation (5.6) where μ is the dynamic viscosity of the fluid, h is the height of the test bench cavity where the fluid flow through the porous media. A is the area of the open holes of the perforated sections of the test bench ($A = 0.001932\ m^2$) and m_z is the slope of the linear trend obtained from the ratios of the volumetric flow rate as a function of the measured pressure gradient ($Q/\Delta P$).

$$K_z = \frac{u\,h}{A} m_z \tag{5.6}$$

5.7 Results

A summary of the results for the in-plane permeability measurements for each set of experiments are presented in Table 32 and Figure 61. Measured out-of-plane permeability values are presented in Table 33 and Figure 62.

Table 32: Summary of measured in-plane permeability $\bar{K}_x$

Sample	**Number of experiments** n	**K_x** $\bar{x}$ [m²]	S_{n-1} [m²]	CV [%]	$\bar{\epsilon}$ [%]	V_f	$\bar{A}_w$ [g/m²]
REF	4	5.98E-11	6.02E-12	10.06	2.00	0.5472	375.6
P1	4	3.11E-11	1.96E-12	6.31	0.62	0.5590	383.7
P1-3D	3	2.03E-11	3.15E-12	15.55	0.57	0.5614	385.4
P2	6	4.99E-11	8.11E-12	16.27	0.74	0.5746	394.4
P2-L	4	4.30E-11	6.83E-12	15.88	1.10	0.5484	376.4
W1	3	3.59E-11	3.07E-12	8.56	1.14	0.6090	417.9
W2	3	3.72E-11	3.04E-12	8.17	0.65	0.5756	395.1

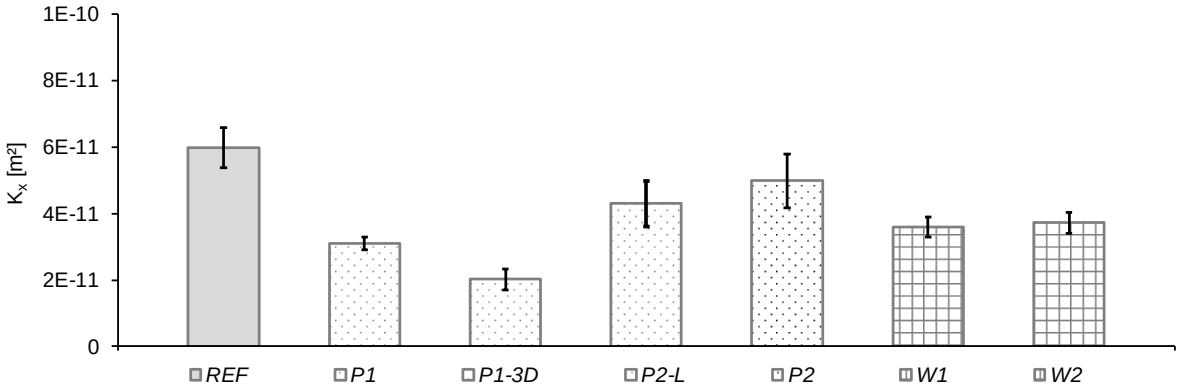

Figure 61: Summary of measured in-plane permeability $\bar{K}_x$. The error bars represent the standard deviation (S_{n-1})

Table 33: Summary of measured out-of-plane permeability $\bar{K}_z$

Sample	**Number of experiments** n	**K_z** $\bar{x}$ [m²]	S_{n-1} [m²]	CV [%]	V_f	$\bar{A}_w$ [g/m²]
REF	3	4.66E-13	2.90E-13	62.15	0.5309	369.9
P1	3	7.53E-13	1.98E-13	26.28	0.5392	374.2
P1-3D	3	4.81E-13	1.85E-13	38.35	0.5775	384.4
W1	2	2.78E-13	8.39E-14	30.22	0.6218	421
W2	3	3.13E-13	7.07E-14	22.57	0.5838	396.2

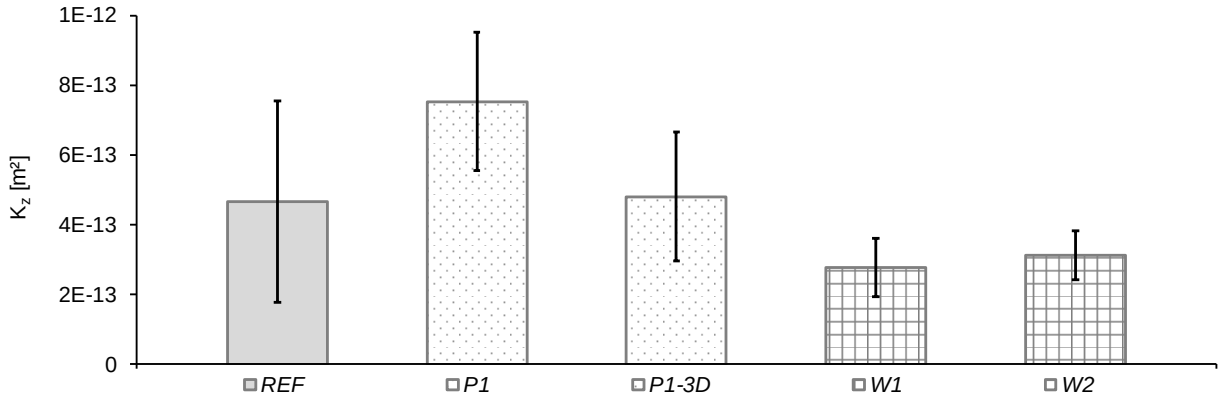

Figure 62: Summary of measured out-of-plane permeability $\bar{K}_z$. The error bars represent the standard deviation (S_{n-1}).

5.7.1 Impact of Preforming Processes on In-Plane Mould Filling Process

5.7.1.1 In-Plane Bulk Permeability

The averaged permeability values presented Table 32 shows that the preforming process has an impact on the permeability behaviour of a preform. The results are spread over a relatively broad range starting 6E-11 m² up to 2E-11 m². The highest permeability value (5.98E-11 m²) is obtained with the reference samples *REF*, the only preform without binder material. This was the expected result since most of the results published in literature presented in Section 2.9 have reported a diminution of the permeability values when binder material is used.

Averaged measured permeability values for preform samples *P2* and *P2-L* is 4.99E-11 m² and 4.30E-11 m² respectively. The difference between these two samples is relatively low (13.8%). Hence, we can conclude that local binder application (parallel to the fluid flow as presented in Figure 50) has minimal impact on the flow behaviour. Preform *P1* & *P2* are both combination of bindered fabric coated with epoxy powders *EP* and *EB* respectively. The measured permeability of configurations *P2* is 1.6 (60%) times higher compared to the value evaluated for *P1* preforms (3.1E-11 m²). The difference between these two sets of preform is mainly the binder application process. For preforms *P2* the binder powder was manual scattered while an industrial process was used in the cases of *P1* samples. One side of the fabric was coated for the preforms *P2* while two sides were coated for the *P1* preforms. Even if the amount of binder material was similar for both combinations (*P2* ≈ 19 g/m^2, 5 wt% of fabric *A* and *P1* ≈ 14 g/m^2, 4 wt% of fabric *B*) it could have impacted the porosity of the preforms, hence influencing the permeability behaviour. Binder

material *EP* and *EB* are not identical and their application process was different, thus their respective final location in the fabric (intra-layer or inter-layer, Figure 11) could be different. Figure 63 shows the different binder dispersion on *P1* and *P2* bindered fabric. It is difficult to identify from the results which of these factors have the greatest impact on the permeability behaviour. However, the comparison of these two configurations shows that the permeability behaviour is influenced by the binder application process.

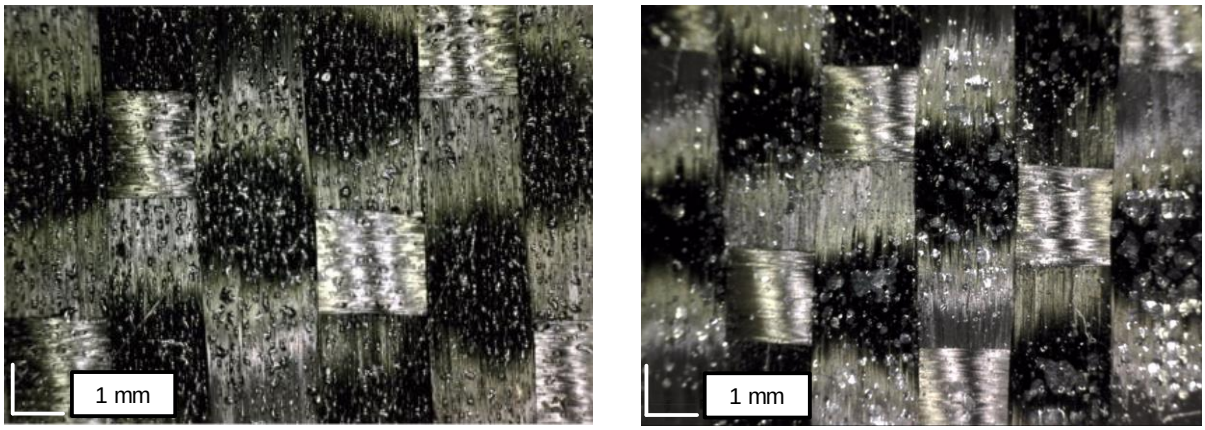

(a) (b)

Figure 63: Binder dispersion on binder fabric *P1*(a) and *P2*(b)

The lowest permeability value (2.03E-11 m²) of all studied preforming technique was measured for the sample *P1-3D*. It is the only sample for which a thermoforming process was performed on the stack of bindered fabric to produce a 3D preform. Preform *P1-3D* and *P1* were made with the exact same fabric, binder material and binder coating process, hence the only difference is the preforming process. Theoretical estimation of the porosity of these two sets of preform using equation (1.5) & (1.6) give the same value. The experimental fibre volume fraction evaluations of *P1-3D* and *P1* samples have shown equivalent fibre volume fractions of 55.90% and 56.14% respectively thus leading similar porosity value estimations. The diminution of the permeability compared to the *P1* sample suggests that the preforming process influence the in-plane permeability characteristic of a preform. This could be caused by the difference of binder final location within the preform, inter-layer vs. intra-layer binder location as previously presented on Figure 11. The modification of the preform compaction behaviour generated by the addition of the binder material (bindered plies preform samples) but mostly by the preforming process (3D preform) could also explain the difference in the permeability behaviour. Some findings in the literature presented in Section 2.9 are in agreements with the last statement. S. van Oosterom *et al*.

[53] reported that the permeability behaviour of a preform is highly affected by its compaction behaviour which is greatly influence the preforming process. Wu *et al*. [52] have reported that the compaction behaviour of a stack of fabric is influenced by the presence of binder material and by the preforming process used. Ultimately, the preform fibre volume fraction is influenced by its compaction behaviour, hence the properties that depends on the fibre volume fraction like permeability behaviour. Grujicic *et al*. [61] have reported that many physical changes in the preform may occur due to the application of pressure during the closing of RTM moulds. These changes are fibre tow flattening, reduction of pores and gaps in the inter and intra-layer region, elastic deformation of the fibre tow and inter-layer shifting (nesting). Thus, after the preforming process, during which the stack of plies is consolidated, the inter-layer shifting, or the layer nesting effect is no longer possible, leading to an increase in preform compaction resistance and finally to a reduction of the preform permeability.

Results for the two sets of preform made with the copolyamide (*W*1 & *W*2) adhesive web show similar averaged permeability even if their preforming process was quite different in terms of application temperature and areal weight. This difference is clearly visible on Figure 51 where the adhesive web appears highly melted for the preforms *W*1 and that the web doesn't seem to have melted for preform *W2*.

One of the principal impacts of preform permeability value of the manufacturing process is the total filling time of a given geometry. The curves presented in Figure 64 represent the theoretical flow front position obtained with the averaged permeability and porosity values measured for each preform samples. These filling times were calculated considering same geometry (38.1 cm longitudinal injection, 1.95 mm cavity thickness) and injection parameters (fixed injection pressure and fluid viscosity) used during the experimental injection presented in Sections 5.4.1 and 5.5.1. Results show that the preforming process has an impact on the mould filling time of a cavity and that the impact depends on the preforming configuration. Compared to the dry fabric configuration (*REF)* the evaluated filling time for a 3D preform is 2.86 times higher.

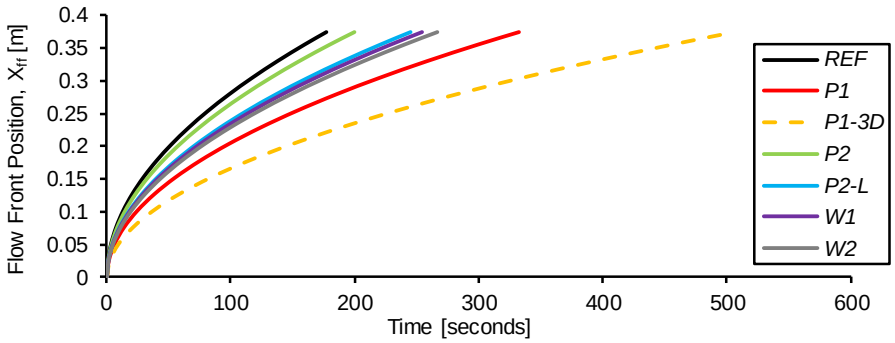

Figure 64: Averaged filling time of different preform configurations for a 38.1 cm longitudinal injection performed at constant pressure

Another important aspect other than the averaged permeability value measured is the variation observed in the results. The standard deviation (S_{n-1}) of the results presented in Figure 61 shows higher levels of variation for some samples while others seem to have more repeatable behaviour. The high variability observed for some samples is the reason why some sets of experiments were repeated more than three times. A minimal target value was fixed for the results coefficient of variation *CV* to assure a certain level of trust in the measured permeability values. The goal was to perform experiments until the *CV* would be under, or close as possible, 15%. This targeted value was selected considering the results of the second experimental determination of permeability of engineering textiles benchmark showing that the *CV* of every participant was varying between 15% and 20% [85]. The standard deviation of each set of experiments is also a good insight of the stability of the sample's permeability behaviour. In general, the samples which the binder was coated by the supplier (*P1*, *P1-3D*, *W1*, *W2*) shows lower variation with standard deviation ranging from 1.95E-12 to 3.72E-11. Samples *P2-F* & *P2-L*, which the binder was applied manually, show higher standard deviation values, respectively 4.99E-12 and 4.30E-12. Even if the amount of powder coated on the fabrics has seemed to respect the targeted values during their fabrications, it doesn't mean it was applied evenly on all the fabric surface. The lack of repeatability of the method for powder application may be the cause of the higher variation observed with these preforms. Higher standard deviation has also been observed with the reference set of preform (sample *REF*). Dry fabrics are sensitive to manipulation, they can be sheared easily and cause fibre misalignment. Fraying of the fabric is also a recurrent problem faced with the manipulation of dry fabrics. These phenomena could be the cause of the higher variation observed with the dry fabric preform. The lower variation observed for samples *P1* and *P1-3D* compared to

samples *REF* suggest that the presence of binder material could help to reduce the variation of permeability behaviour. Knowing that the objective of the project COMP1601 is to manufacture complex geometries by liquid composite moulding, hence minimizing the permeability variation of the preform is something desired. This would increase the mould filling simulation accuracy and improve the robustness of the manufacturing process.

5.7.1.2 Flow Front Stability

The transparent surface of the mould has allowed to make interesting observation on the flow front shape of certain preform samples. In general, preform *REF*, *P1* and *P1-3D* have shown stable straight-line flow front. The filling behaviour observed with the *P1-3D* suggests that the presence of consolidated binder could help impede the distortion of the flow front. However, other preform combinations like *P2*, *P2-F* but particularly *W1* and *W2* have shown different levels of flow front instability. The presence of coated adhesive film on preforms *W2* & *W2* increased the fabric shear stiffness. Copolyamide webs are often used as fabric ‘’stabilizer’’ because of their ability to limit the deformation (shearing) of the fabric. The high-nesting resistance of these preforms led to channels creation on the top of the preform after being compressed during the mould closure [57]. These channels have generated flow front instabilities like a racetracking effect. Examples of different type flow front observed during the experiments are presented in Figure 65.

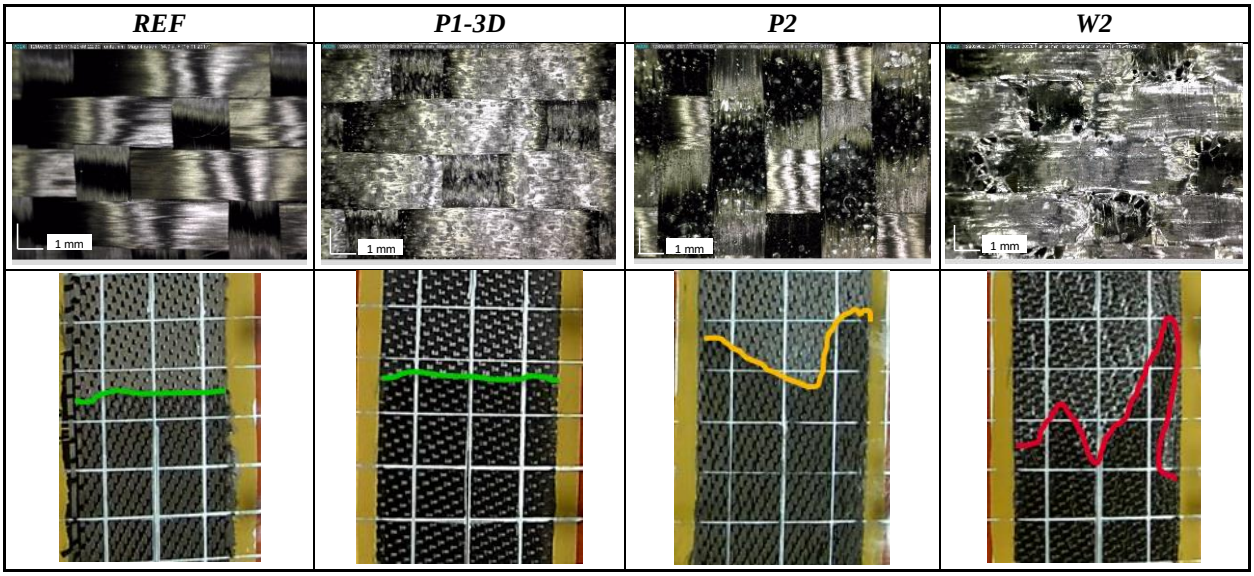

Figure 65: Example of flow front instabilities. The dimensions of the squares of the grid pattern of the see-through surface are 2.54 cm per 2.54 cm

The relation between the fabric ability to be deformed or sheared and the compaction behaviour reported by Grujicic *et al*. could explain the phenomena observe (channel formation) with the *W1* & *W2* sample [61]. S. van Oosterom *et al*. have also stated that the compaction behaviour of a preform can have a significant impact on the filling behaviour [53]. Gokce and Advani [60] have stated that ‘*’in general, compaction affects the preform permeability globally, hence it may affect the fill time but not the flow pattern.*’’ The present results show that a high restriction of nesting behaviour of the fabric could lead to severe negative impact on the flow front shape and consequently on the mould filling patterns.

5.7.2 Impact of Preforming Processes on Out-of-Plane Permeability

The coefficients of variation evaluated ranges from 5% to 15 % and 20% to 30% for the in-plane and out-of-plane permeability respectively. The experimental process for measuring the out-of-plane permeability was more challenging as the process of adjusting precisely the cavity height was inaccurate, thus potentially impacting the sample fibre volume fraction. Nevertheless, the results obtained confirmed previous findings on the impact of the preforming process on transverse permeability.

Becker and Mitschang [16] have studied the influence of thermoplastic adhesive web (Spunfab, 12 g/m^2) on out-of-plane permeability and on the hydrodynamic compaction behaviour of textiles. They showed that for low injection pressure the non-activated binder only influence was the addition of volume to the preform hence reducing the flow space. However, they also observed an increase of the compaction resistance and a reduction of the variation in the hydrodynamic compaction of the textile which helped to preserve the flow channel at high injection pressure. The activated bindered sample (30 minutes at 90°C and compacted to the cavity initial height) led to a reduction of the permeability caused by the increased molten area hence blocking more flow channels. However, lower variation compared to the non-activated sample was observed suggesting that the distribution of the molten binder material led to more homogenize size of the flow channels, hence leading to a more stable behaviour. In summary, they showed that preform with high compaction resistance are less sensitive to hydrodynamic compaction, hence limiting the increase of the apparent fibre volume fraction causing the reduction of the permeability during the injection.

High variation (62.15% *CV*) has been observed in the permeability results (Table 33) of the non-bindered sample *REF*. The manipulation of the layers during the layup of the dry fabric of *REF* samples was challenging. Dry fabric, especially 5 harness satin, can easily be deformed and sheared during the layup process and fibre alignment may be difficult to preserve. Deformation of the fabric modifies the geometry of the gap between the fabric tows and may reduce the permeability of the fabric [16, 86]. The compaction-relaxation process seen by the preform from the low pressure (69 kPa) to the high-pressure plateau (310 kPa) have probably led to a random rearrangement of the textile layers during the injections hence explaining the high variability observed for this sample. However, lower coefficient of variation was observed with the bindered fabric (22.57% to 38.35%) suggesting that the binder is likely to reduce the variation of the out-of-plane permeability.

The non-activated powdered preform *P1* has shown higher results than the reference sample *REF* and compared to its consolidated version *P1-3D,* which is likely to be partly caused by the resulting different locations of the binder within the preform. Also, non-activated binder was probably enough to stabilize the layers and minimize the shear deformation of the fabric thus keeping the inter-roving gap open facilitating the transverse flow. The different compaction and nesting behaviour between these two samples could also explain the difference in the out-of-plane permeability behaviour. These observations somehow agree with the conclusion of Becker and Mitschang [16] regarding the influence of non-activated and activated binder on the permeability value. The presence of binder material combined with the preforming process performed of sample *P1-3D* is likely to have increased the nesting effect (molten binder lubrication effect) of the fibre bed during the 3D preform fabrication, as previously reported in Section 2.7. The impact of the preforming process on the nesting behaviour which also impacts the morphology of the transverse flow channel could explain why the *P1* sample has shown better out-of-plane permeability than the *P1-3D* samples.

The preforms made with the copolyamide adhesive webs *W1* & *W2* has presented lower permeability value than the reference and both powdered preform (*P1-3D* & *P1*). The difference in the morphology of powdered and webs binder coated on the surface of the fabric may be the reason for the difference in permeability values. Coated binder morphology has already presented

in Figure 51 Figure 63 for powdered and webs binder respectively. Comparison of these two figures shows that web binder seems to cover more fabric surface than the powder one.

5.7.3 Summary

The goal of this investigation was to understand the impact on preforming technologies on the mould filling process to guide the development and optimization of the tailored preforming process. Technologies minimizing the impact or improving the in-plane and out-of-plane permeability behaviour (bulk property and variation) should be preferred. Figure 66 present the normalized in-plane and out-of-plane permeability values of the studied preforming technologies. Based on the needs of the industrial partner, a tailored application of binder of powder binder would be the recommended. Preforms *P2* and *P2-L* showed minimal impact on the in-plane permeability of all preforming technologies. The results also showed that the modifications of binder application parameters like physical form, material concentration or applied temperature and pressure could be used to tailor in-plane permeability behaviour. The out-of-plane permeability results obtained with the preforms *P1* & *P1-3D* suggests that improvement of the transverse permeability could be achieved by using powder binder materials.

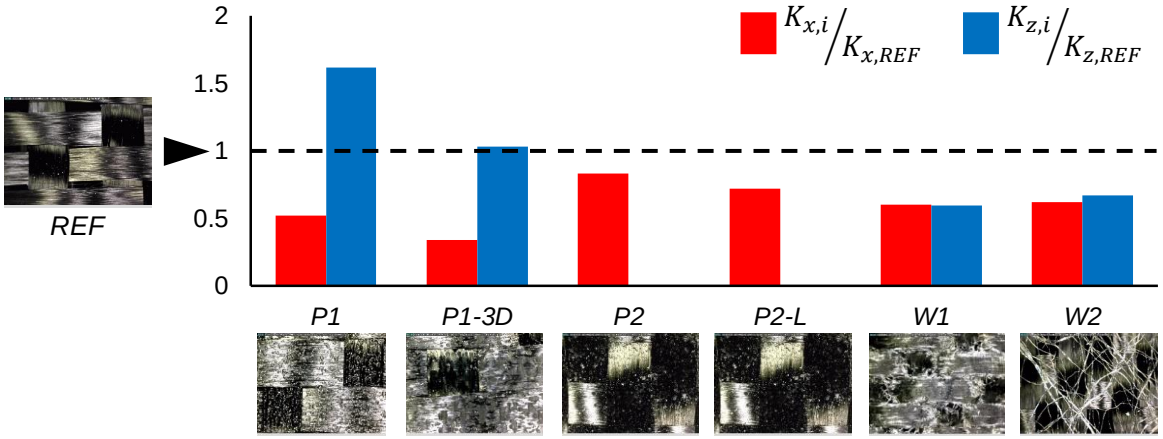

Figure 66: Bulk permeability summary

However, the in-plane permeability results have shown that the quality of the binder application process may influence the stability of the preform permeability behaviour. Manual powder application (*P2*) have generated higher variation of the in-plane permeability behaviour compared to the preform which the powder binder was applied by an industrial process (*P1*). Hence, this observation suggests that the developed tailored preforming process should assure a

relatively tight control of the binder material deposed in terms of material concentration and uniformity.

Adhesive web binder was an interesting solution because of their relatively easy processing and low material cost. However, the observed permeability behaviour of samples *W1* and *W2* have shown that thermoplastic web adhesives would not be a suitable solution for the application considered in this project. The main problem noticed with this technology is the negative impact on the filling behaviour during the injection. Both samples made with adhesive webs showed severe flow front distortion during the in-plane injections. Such process variation would need to be avoided for the manufacturing of complex geometries. However, no 3D preforms made with adhesive web were studied. Maybe the activation of the binder material during the preforming process would help to minimize the compaction issues observed with these preforms that cause the flow front distortion.

For further analysis it would be pertinent study more in detail the mechanism governing the final location of the binder in the fabric. Investigating the wettability behaviour between the binder material and the fabric would be a good way to better understand what determines the final location of the binder material. The sample P1-3D has also shown that the preforming process (consolidation of the bindered fabric layers) influence the permeability behaviour. Further investigation of 3D preforms made from different process should be performed to better understand the influence of the preforming operation. Regarding the transverse permeability measurement, improving the test bench to ensure the fibre volume fraction of the measured preform would help have more accurate results. Characterization of the compaction and hydrodynamic compaction behaviour of the preforms should also be studied to better understand the impact of preforming technologies on the out-of-plane permeability.

6. Conclusion

The experimental work presented in this thesis has demonstrated the effects of different binder material on LCM processing and on the thermo-mechanical properties of reinforced composite laminates. The conclusions of each characterization process are used to provide guidelines for the development, optimization and evaluation processes of the tailored binder application preforming process. The key parameters of the tailored binder application preforming process were identified:

- **Material chemical composition**: The binder material thermochemical behaviour (T_m and Tg) guide the definition of both the application and preforming processes temperature. The *EB* (epoxide) and *PH* (phenoxy) binders had the lowest and highest melting point:61°C and 135-160°C respectively. The binder chemistry has a significant influence on the resin tensile (UTS) and thermo-mechanical properties ($T_{g(\mathrm{DSC})}$ and $E_{f(DMA)}$). The *PH* binder had almost no impact on the resin-binder mixture tensile properties (-4% of UTS) while the other studied binder led in a significant reduction of the properties (-26% to -51% of UTS). Furthermore, all the binders, except the *EB* material, affected the thermochemical behaviour of the cured epoxy resin.
- **Material concentration** (W_b): The binders investigated in this work had different levels of compatible concentration. The thermochemical characterization of resin-binder mixtures suggested that the *CoPET* binder is compatible when the binder to resin weight ratio is W_b < 3.79%, that *PH* and *ME* are compatible for W_b<9.51% and that *EB* binder is compatibility up to W_b = 15.11%. Furthermore, fluctuation in the amount of binder material coated on the fabric (Aw_b) may generate variation in the preform permeability behaviour.
- **Preforming (consolidation) process**: The preform consolidation level directly influences the preform in-plane and transverse permeability behaviour, most likely to cause a reduction of the permeability behaviour as the preform compaction is increased. Also, the characterization of short-beam strength of composite laminate revealed that over compaction of the preform may result in a significant degradation of the mechanical properties. The compaction behaviour of the preform depends on the preforming process and the binder thermochemical behaviour.

Furthermore, general recommendations can be formulated from the observations made in this thesis:

- **Evaluation method for resin-binder compatibility**: The thermochemical characterization (MDSC) of resin-binder mixtures allowed to identify a compatible binder to resin weight ratio for each studied binder. From tensile property characterization, binder chemistry like *PH* is more likely to have minimal impact on the composite mechanical properties (-4% of resin UTS) which was confirmed with the characterization of composite laminate ILSS (+0.1%). *ME* binder showed only a slight reduction of the laminate ILSS (-5%) while it has significantly reduced the resin UTS (-46%). This suggests that the evaluation resin-binder UTS allow to foresee small reduction of composite laminate properties (when the binder is processed in the right conditions). Hence, relying only on this method could lead to false negative conclusion. The thermochemical (MDSC) and tensile strength (UTS) and tensile strength characterization of resin-binder mixture provides a rapid estimation of the resin-binder compatibility. However, since the preforming process highly influences the compaction level of the preform (also the resulting fibre volume fraction), the compatibility of the binder material should always be validated through the characterization of reinforced composite laminate mechanical properties.
- **Material selection:** Overall, the *EB* binder stands out as it had the lowest melting temperature which would facilitate the application and preforming process and had the best thermochemical compatibility. Furthermore, the work presented in this thesis suggest that all binder evaluated in this thesis can be considered ‘’compatible’’ if the right material concentration and preforming process (preform compaction) are used. However, other binder materials like *CoPET* had low compatible ratio (W_b<3.79%) or required more intense processing parameters like PH (T_m = 135-160°C) may be less interesting for final selection.
- **Processing recommendation:** The development of the localized binder application process should focus on achieving a uniform and accurately controlled material quantity deposition. Otherwise, even a binder material evaluated ‘’compatible’’ could become a contaminant if the concentration deposed on the fabric is too important.

6.1 Future Work

Many aspects could be addressed to optimize the tailored binder application process. Here are a few suggestions:

- **Resin-binder interaction:** First, the evaluation of the ILSS properties of laminate made with the EB binder material should be performed. Also, further thermochemical characterization would be required to better understand the impact of binder material on resin curing process. Secondly, pursue the investigation to better understand if the impact on the resin T_g is either the results of mixed properties from the separates material phases (rule of mixture), the result of the incomplete cure of the resin cause by the presence of binder or a mix of both phenomena.
- **Impact of binder material on fabric drapeability:** Experimental characterization should be performed to identify which parameter between the binder chemistry, material concentration or application parameter have the most influence on the fabric fraying. Fabric drapeability characterization experiments (e.g. measure of fabric locking angle and bending stiffness) should be performed to identify the optimal binder application parameter (areal weight concentration (Aw_b) and coating temperature) to obtain the desired drapeability behaviour.
- **Influence of preforming parameters of bindered preform:** The consolidation operation could be optimized by measuring the preform peel strength in function of the preforming temperature, binder chemistry and material concentration (Aw_b) as performed by Schmidt *et al*. [36], Tanoglu [54] and Brody [50]. The compaction behaviour of the preform could be characterized as a function of the preforming temperature, binder chemistry and material concentration as presented by Wu *et al*. [52]. Results of this characterization would allow to tailor the final fibre volume fraction of the preform hence avoiding the reduction of preform permeability behaviour and laminate mechanical properties.

References

1. *Research Proposal "Complex composite structure multifunction for aerospace".* Hutchinson Aerospace & Industry (Canada), 2016.
2. Wang, J., R. Paton, and J.R. Page, *The draping of woven fabric preforms and prepregs for production of polymer composite components.* Composites Part A: Applied Science and Manufacturing, 1999. **30**(6): p. 757-765.
3. Rohatgi, V., L.J. Lee, and A. Melton, *Overview of fibre preforming*, in *Resin Transfer Moulding for Aerospace Structures*, T.M. Kruckenberg and R. Paton, Editors. 1998, Springer Netherlands: Dordrecht. p. 148-176.
4. GARDINER, G., *Preforming goes industrial: Part 1*, in *CompositesWorld*. 2017, Gardner Business Media, Inc. : 6915 Valley Ave., Cincinnati OH.
5. GARDINER, G., *Preforming goes industrial: Part 2*, in *CompositesWorld*. 2017, Gardner Business Media, Inc. : 6915 Valley Ave., Cincinnati OH.
6. Campbell, F.C., *5. Thermoset Composite Fabrication Processes*, in *Structural Composite Materials*. ASM International.
7. Christ, M., A. Miene, and U. Mörschel, *Measurement and Analysis of Drapeability Effects of Warp-Knit NCF with a Standardised, Automated Testing Device.* Applied Composite Materials, 2017. **24**(4): p. 803-820.
8. Potter, K., *Reinforcement manipulation and preforming*, in *Resin Transfer Moulding*. 1997, Springer Netherlands: Dordrecht. p. 52-73.
9. Prodromou, A.G. and J. Chen, *On the relationship between shear angle and wrinkling of textile composite preforms.* Composites Part a-Applied Science and Manufacturing, 1997. **28**(5): p. 491-503.
10. Alice E Snape, J.L.T., Hassan M El-Dessouky, Mohamed N Saleh, Hannah Tew, Richard J Scaife, *Stabilising and Trimming 3D Woven Fabrics for Composite Preforming Applications.* Proceedings of the 8th World Conference on 3D Fabrics and Their Applications, 2018.
11. Bickerton, S., et al., *Investigation of draping and its effects on the mold filling process during manufacturing of a compound curved composite part.* Composites Part A: Applied Science and Manufacturing, 1997. **28**(9-10): p. 801-816.
12. Jones, I.A. and A.K. Pickett, *8 - Mechanical properties of textile composites A2 - Long, A.C*, in *Design and Manufacture of Textile Composites*. 2005, Woodhead Publishing. p. 292-329.
13. Long, A.C. and I. Textile, *Design and manufacture of textile composites.* 2005.
14. Dominy, J. and C. Rudd, *5 - Manufacturing with thermosets A2 - Long, A.C*, in *Design and Manufacture of Textile Composites*. 2005, Woodhead Publishing. p. 181-196.
15. Rudd, C.D., et al., *2 - Process fundamentals*, in *Liquid Moulding Technologies*, C.D. Rudd, et al., Editors. 1997, Woodhead Publishing. p. 38-64.
16. Becker, D. and P. Mitschang, *Influence of preforming technology on the out-of-plane impregnation behavior of textiles.* Composites Part A: Applied Science and Manufacturing, 2015. **77**: p. 248-256.

17. Darcy, H., *Les fontaines publiques de la ville de Dijon: exposition et application*. 1856: Victor Dalmont.
18. RUIZ, E.-A.-J., *Analysis of reinforcement impregnation by liquid injection*, in *MEC6318 Fabrication des composites par injection*, É.p.d. Montréal, Editor. 2012.
19. Potter, K., *RTM theory*, in *Resin Transfer Moulding*. 1997, Springer Netherlands: Dordrecht. p. 1-27.
20. LeBel, F., et al., *Prediction of optimal flow front velocity to minimize void formation in dual scale fibrous reinforcements.* International Journal of Material Forming, 2014. **7**(1): p. 93-116.
21. Puckett, M. and M. Petervary, *Materials*, in *Resin Transfer Moulding for Aerospace Structures*, T.M. Kruckenberg and R. Paton, Editors. 1998, Springer Netherlands: Dordrecht. p. 42-82.
22. Lomov, S. and I. Verpoest, *1 - Manufacturing and internal geometry of textiles A2 - Long, A.C*, in *Design and Manufacture of Textile Composites*. 2005, Woodhead Publishing. p. 1-61.
23. De Bilbao, E., et al., *Experimental study of bending behaviour of reinforcements.* Experimental Mechanics, 2010. **50**(3): p. 333-351.
24. Bannister, M. and I. Herszberg, *Advanced reinforcements*, in *Resin Transfer Moulding for Aerospace Structures*, T.M. Kruckenberg and R. Paton, Editors. 1998, Springer Netherlands: Dordrecht. p. 83-111.
25. Tong, L., A.P. Mouritz, and M.K. Bannister, *Chapter 2 - Manufacture of 3D Fibre Preforms*, in *3D Fibre Reinforced Polymer Composites*. 2002, Elsevier Science: Oxford. p. 13-46.
26. Wambua, P. and R. Anandjiwala, *A review of preforms for the composites industry.* Journal of Industrial Textiles, 2011. **40**(4): p. 310-333.
27. Potter, K., *Materials for RTM*, in *Resin Transfer Moulding*. 1997, Springer Netherlands: Dordrecht. p. 28-51.
28. *EPIKOTE™ Resin Preform Binder Systems for Mass Production of Composite Parts.* Hexion Inc., 2016.
29. Räckers, B., *Introduction to resin transfer moulding*, in *Resin Transfer Moulding for Aerospace Structures*, T.M. Kruckenberg and R. Paton, Editors. 1998, Springer Netherlands: Dordrecht. p. 1-24.
30. Rudd, C.D., et al., *6 - Preform design and manufacture*, in *Liquid Moulding Technologies*, C.D. Rudd, et al., Editors. 1997, Woodhead Publishing. p. 151-202.
31. Potter, K., *Resin Transfer Moulding.* 1997.
32. Kruckenberg, T.M. and R. Paton, *Resin transfer moulding for aerospace structures.* 1998.
33. Giessmann, A., *Basic Elements of Coating Systems*, in *Coating Substrates and Textiles: A Practical Guide to Coating and Laminating Technologies*. 2012, Springer Berlin Heidelberg: Berlin, Heidelberg. p. 23-76.
34. *Application Methods*, in *Organic Coatings*.
35. Rudd, C.D., et al., *4 - Reinforcement materials*, in *Liquid Moulding Technologies*, C.D. Rudd, et al., Editors. 1997, Woodhead Publishing. p. 100-123.
36. Schmidt, S., et al., *Powder binders used for the manufacturing of wind turbine rotor blades. Part 1. Characterization of resin-binder interaction and preform properties.* Polymer Composites, 2018. **39**(3): p. 708-717.

37. Guo, Q., *Effect of curing agent on the phase behaviour of epoxy resin/phenoxy blends.* Polymer, 1995. **36**(25): p. 4753-4760.
38. Isayev, A.I., *Encyclopedia of polymer blends. Volume 3.* 2016.
39. Isayev, A.I., *Glass-Transition Phenomena in Polymer Blends*, in *Encyclopedia of polymer blends. Volume 3*. 2016.
40. Isayev, A.I., *Crystallization and Melting Behavior in Polymer Blends*, in *Encyclopedia of polymer blends. Volume 3*. 2016.
41. Daelemans, L., et al., *Bisphenol A based polyester binder as an effective interlaminar toughener.* Composites Part B: Engineering, 2015. **80**: p. 145-153.
42. Velthem, P.V., *Comparative Study of High Performance Epoxy Based Composites Modified with Different Tougheners*. UCL - Université catholique de Louvain.
43. Henne, M., *Improvement of Thoughness of Epoxy Resin Systems Using thermoplastic Binders.* Institue for Materials Technology and Plastics Processing, 2012.
44. Hedrick, J.L., *Chemical modification of matrix resin networks with engineering thermoplastics. 1. Synthesis, morphology, physical behaviour and toughening mechanisms of poly(arylene ether sulphone) modified epoxy networks.* Polymer, 1991. **32**(11): p. 2020-2032.
45. Constantin, F. and ois, *Blends of a new thermoplastic in a thermoset epoxy matrix.* Macromolecular Symposia, 2003. **198**: p. 335-344.
46. Hodgkin, J.H., *Thermoplastic toughening of epoxy resins: A critical review.* Polymers for Advanced Technologies, 1998. **9**(1): p. 3-10.
47. Deng, S., et al., *Thermoplastic–epoxy interactions and their potential applications in joining composite structures–A review.* Composites Part A: Applied Science and Manufacturing, 2015. **68**: p. 121-132.
48. Chen, J., *Dynamics of binder displacement in liquid molding.* Polymer Composites, 1996. **17**(1): p. 23-33.
49. Potter, K., *Troubleshooting RTM processing problems*, in *Resin Transfer Moulding*. 1997, Springer Netherlands: Dordrecht. p. 188-199.
50. Brody, J.C., *Reactive and non-reactive binders in glass/vinyl ester composites.* Polymer Composites, 2005. **26**(3): p. 377-387.
51. Potter, K., *Quality control/assurance*, in *Resin Transfer Moulding*. 1997, Springer Netherlands: Dordrecht. p. 211-230.
52. Wu, W., et al., *Effect of Compaction and Preforming Parameters on the Compaction Behavior of Bindered Textile Preforms for Automated Composite Manufacturing.* Applied Composite Materials, 2013. **20**(5): p. 907-926.
53. S. van Oosterom, S.B., J. Applegate, D. Young, *Effects of Variability in Carbon Fibre Preforms on Resin Transfer Moulding Filling Behaviour*, in *Processing and Fabrication of Advanced Materials XXV*. 2017: University of Auckland, Auckland, New Zealand,.
54. Tanoglu, M., *Effects of thermoplastic preforming binder on the properties of S2-glass fabric reinforced epoxy composites.* International Journal of Adhesion and Adhesives, 2001. **21**(3): p. 187-195.
55. Beier, U., *Mechanical performance of carbon fibre-reinforced composites based on stitched and bindered preforms.* Composites Part A: Applied Science and Manufacturing, 2009. **40**(11): p. 1756-1763.

56. Lionetto, F., A. Moscatello, and A. Maffezzoli, *Effect of binder powders added to carbon fiber reinforcements on the chemoreology of an epoxy resin for composites.* Composites Part B: Engineering, 2017. **112**: p. 243-250.
57. George, A., *Optimization of resin infusion processing for composite materials: simulation and characterization strategies.* 2011.
58. Estrada, G., *Experimental characterization of the influence of tackifier material on preform permeability.* Journal of Composite Materials, 2002. **36**(19): p. 2297-2310.
59. Sommerlot, S., *The effects of a low areal weight inter-layer tackifier on saturated permeability of carbon fabrics.* Proceedings of the American Society for Composites - 31st Technical Conference, ASC 2016, 2016.
60. Gokce, A. and S.G. Advani, *7 - Modeling, optimization and control of resin flow during manufacturing of textile composites with liquid molding A2 - Long, A.C*, in *Design and Manufacture of Textile Composites*. 2005, Woodhead Publishing. p. 242-291.
61. Grujicic, M., K.M. Chittajallu, and S. Walsh, *Effect of shear, compaction and nesting on permeability of the orthogonal plain-weave fabric preforms.* Materials Chemistry and Physics, 2004. **86**(2): p. 358-369.
62. Lomov, S.V., et al., *Nesting in textile laminates: geometrical modelling of the laminate.* Composites Science and Technology, 2003. **63**(7): p. 993-1007.
63. Steenkamer, D., D. Wilkins, and V. Karbhari, *The influence of preform joints on the processing of RTM composites.* Composites Manufacturing, 1995. **6**(1): p. 23-34.
64. Magagnato, D., *Experimental characterization to determine the influence of different binder systems on the preform permeability during RTM manufacturing* Zeitschrift Kunststofftechnik, 2015. **2015**(4): p. 256-270.
65. Rudd, C.D., et al., *Liquid moulding technologies: Resin transfer moulding, structural reaction injection moulding and related processing techniques*. 1997: Elsevier.
66. Rohatgi, V., *Moldability of tackified fiber preforms in liquid composite molding.* Journal of Composite Materials, 1997. **31**(7): p. 720-744.
67. Gabbott, P., *Principles and applications of thermal analysis*. 2008: John Wiley & Sons.
68. Hubert, P., *Module 2.1 Resin Types Resin, Cure Kinetics and Glass Temperature.* PROCESSING OF COMPOSITE MATERIALS – MECH 544, 2018.
69. Lundgren, C.J., *Determination of the Glass Transition Temperatures of a Polymer (Polyamide) Blend using MDSC.* TA Instruments Technol. Pap.
70. Wunderlich, B., *The contributions of MDSC to the understanding of the thermodynamics of polymers.* Journal of Thermal Analysis and Calorimetry, 2006. **85**(1): p. 179-187.
71. Thomas, L.C., *Modulated DSC® Paper# 1 Why Modulated DSC®?; An Overview and Summary of Advantages and Disadvantages Relative to Traditional DSC.* TA Instruments Technol. Pap, 2005.
72. Sauer, B.B., *Temperature modulated DSC studies of melting and recrystallization in polymers exhibiting multiple endotherms.* Polymer, 2000. **41**(3): p. 1099-1108.
73. Thomas, L.C., *MDSC Paper #2, Modulated DSC® Basics: Calculation and Calibration of MDSC Signals.* TA Instruments Technol. Pap, 2005.
74. Thomas, L.C., *Modulated DSC® Paper# 3 Modulated DSC® Basics; Optimization of MDSC® Experimental Conditions*. 2005, Technical report, TA Instruments.
75. International, A., *ASTM D3418-12, Standard Test Method for Transition Temperatures and Enthalpies of Fusion and Crystallization of Polymers by Differential Scanning Calorimetry*. 2012, West Conshohocken, PA: ASTM International.

76. Cheng Stephen, Z.D., *Kinetics of mesophase transitionsin thermotropic copolyesters. 1. Calorimetric study.* Macromolecules, 1988. **21**(8): p. 2475-2484.
77. Bernstein, J., *Polymorphism in Molecular Crystals*. 2002, Oxford, UNITED KINGDOM: Oxford University Press USA - OSO.
78. Broyles, N., et al., *Fatigue performance of carbon fibre/vinyl ester composites: the effect of two dissimilar polymeric sizing agents.* Polymer, 1998. **39**(15): p. 3417-3424.
79. International, A., *ASTM D638-14, Standard Test Method for Tensile Properties of Plastics*. 2015, West Conshohocken, PA: ASTM International.
80. International, A., *ASTM D7028-07(2015), Standard Test Method for Glass Transition Temperature (DMA Tg) of Polymer Matrix Composites by Dynamic Mechanical Analysis (DMA).* 2015, West Conshohocken, PA: ASTM International.
81. International, A., *ASTM D2344 / D2344M-16, Standard Test Method for Short-Beam Strength of Polymer Matrix Composite Materials and Their Laminates*. 2016, West Conshohocken, PA: ASTM International.
82. Giessmann, A., *Coating substrates and textiles : a practical guide to coating and laminating technologies.* 2012.
83. Alms, J.B., et al., *Experimental procedures to run longitudinal injections to measure unsaturated permeability of LCM reinforcements.* FCPM Collaboration, 2010.
84. Ruiz, E., *Note De Cours : MEC6318 - Fabrication Des Composites Par Injection*. 2017.
85. Vernet, N., et al., *Experimental determination of the permeability of engineering textiles: Benchmark II.* Composites Part A: Applied Science and Manufacturing, 2014. **61**: p. 172-184.
86. Demaria, C., E. Ruiz, and F. Trochu, *In-plane anisotropic permeability characterization of deformed woven fabrics by unidirectional injection. Part I: Experimental results.* Polymer Composites, 2007. **28**(6): p. 797-811.

Appendix A: Resin-Binder Interactions Characterization Results

The detailed results of some experiments performed to characterize the resin-binder interactions are presented in the following subsections of this Appendix.

A.1 Resin-Binder Mixture Ultimate Tensile Strength

Table A.1: Results summary of resin-binder mixtures tensile property characterization

Material	$\boldsymbol{W_b}$ [%]	$\boldsymbol{Aw_b}$ [g/m^2]	**UTS** [MPa]			
			$\bar{x}$	S_{n-1}	*CV*	Δ_{REF}
Neat resin	0%	0	81.0	8.37	10.33%	-
CoPET	3.79%	8	55.2	5.08	9.21%	-31.83%
	7.55%	16	59.8	2.67	4.46%	-26.14%
	14.99%	32	54.8	6.33	11.55%	-32.31%
ME	3.81%	8	43.3	5.49	12.67%	-46.51%
	7.61%	16	49.0	7.93	16.18%	-39.48%
	15.23%	32	39.5	9.31	23.56%	-51.21%
EB	3.98%	8	49.5	10.66	21.53%	-38.86%
	7.58%	15	56.4	11.63	20.63%	-30.33%
	15.11%	27	45.6	8.11	17.79%	-43.72%
PH	3.81%	8	75.27	7.91	10.50%	-7.03%
	7.61%	16	78.75	6.81	8.64%	-2.74%
	15.21%	32	79.32	7.79	9.82%	-2.03%

A.2 DMA - Glass Transition Temperature and Flexural Modulus

Table A.2: Results summary of resin-binder mixtures dynamic mechanical analysis characterization

	Material	**Resin**	***EB***		***CoPET***		***ME***		***PH***	
	$\boldsymbol{W_b}$[%]	0%	3.98%	15.11%	3.79%	14.99%	3.81%	15.23%	3.81%	15.21%
	$\boldsymbol{n}$	6	3	4	3	3	3	5	4	3
$\boldsymbol{T_g}$ [°C]	$\bar{x}$	61.94	59.13	65.54	61.94	64.97	62.91	64.30	65.77	59.62
	S_{n-1}	2.50	0.93	0.49	0.61	0.92	1.49	3.69	2.30	0.34
	CV	4.03%	1.57%	0.74%	0.98%	1.42%	2.37%	5.74%	3.50%	0.57%
$\boldsymbol{E_F}$ [MPa]	$\bar{x}$	3503.2	3691.3	3414.0	3416.3	2528.0	3360.7	3279.8	3694.5	3441.0
	S_{n-1}	216.6	184.7	416.6	218.9	79.7	164.0	244.1	149.5	294.1
	CV	6.2%	5.0%	12.2%	6.4%	3.2%	4.9%	7.4%	4.0%	8.5%

A.3 Mechanical Behaviour of Composite Made with Bindered Fabrics

Table A.3 presents the averaged results $\bar{x}$ and coefficient of variation *CV* for the short-beam strength (F^{sbs}) calculated using equation (4.7) as well as the identified failure mode for each sample. Some of the laminate characteristics are also presented such as the measured binder areal

weight Aw_b, fibre volume fraction V_f evaluated using equation (1.6), the laminate binder-resin weight ratio (W_b) and binder volume ratio (V_b).

Table A.3: ILSS summary of results

Sample		**Laminate Characteristics**				**F^{sbs}** [MPa]			**Failure mode**
ID	n	Aw_b $[g/m^2]$	V_f	W_b	V_b	$\bar{x}$	*CV*	Δ_{REF}	
SB_REF	6	-	51.5%	-	-	59.7	4.9%	-	Interlaminar shear
SB_ME	6	18.70	53.6%	9.36%	4.21%	56.8	5.8%	-4.8%	Interlaminar shear
SB_CoPET	5	34.96	58.2%	19.4%	7.23%	27.9	19.4%	-53.3%	Plastic deformation
SB_PH	6	17.48	50.9%	7.2%	2.35%	60.25	5.5%	0.09%	Interlaminar shear
SB_EP	6	11.17	59.6%	NA	NA	30.4	7.3%	-49.0%	Plastic deformation